Muhammad Razin Abdullah

# The Fracturing Behavior in Layered Rocks: Modeling and Analyses of Fractured Samples

TU Delft

# The Fracturing Behavior in Layered Rocks: Modeling and Analyses of Fractured Samples

By

Muhammad Razin Abdullah

in partial fulfilment of the requirements for the degree of

**Master of Science**
in Applied Earth Sciences

at the Delft University of Technology,
to be defended publicly on Monday November 26, 2018 at 10:00 AM.

| | |
|---|---|
| Supervisor: | Dr. A. Barnhoorn |
| Thesis committee: | Prof. Dr. G. Bertotti |
| | Dr. J.E.A. Storms |
| | L.A.N.R. Douma, MSc. |



TU Delft

# Abstract

Hydrocarbon or geothermal reservoir often consists of several rock layers from different lithology. The various lithologies have their own number of mechanical properties and the layering effect introduced the term of mechanical contrast, which represents the ratio of rock strength between adjacent layers. Mechanical contrast and confining pressure highly influence the fracture behavior in the layered rocks.

In this study, fractures in layered rocks are investigated, starting with its geometry and also the stress field contributed to the fracture generation and development. The fracture geometry such as fracture length, average aperture, aperture distribution and orientation are quantified in a two dimension slice image. The study focused on comparing the fracture behavior when (a) the layered rock compositions are the same between samples with increasing confining pressure or (b) the different compositions of layered rocks (different mechanical contrast) between samples in the same confining pressure.

The results show that fracture tends to propagate through layer interface when the mechanical contrast between adjacent layers and the confining pressure are low. The fracture in the weak layer developed at a gentler dip (shear fracture) with higher fracture aperture compared to the ones in the strong layer which almost vertical (tensile fracture). In addition, the shear fracture in the weak layer usually accompanied by the zone of cataclastic flow while the tensile fracture has a more clear pathway for fluid flow.

However, mode I opening/tensile fractures are less likely to affect fluid flow in the reservoir because their aperture is insignificant at depth. While in mode II sliding/shear fractures, only several parts along the fracture that can provide the open space, which depend on the presence of jogs and irregularities on the fracture surfaces.

The results from fracture measurements show that in the weak layer, average aperture and aperture distribution will reduce with the increasing of confining pressure, but increased with the increasing of mechanical contrast. Average fracture aperture and distribution have a significant role in capillary pressure. The higher average aperture will reduce the amount of pressure needed to flow the fluid, while a higher number of aperture standard deviation (aperture distribution) has a contrasting effect. The average aperture has a bigger impact on capillary pressure compare to aperture distribution. Thus, by increasing the confining pressure or decreasing the mechanical contrast, the required pressure for fluid to flow is increasing.

Furthermore, the numerical modeling is performed by imitating the rock mechanical properties and the fracturing conditions from the laboratory experiment. The results show that under compressive stresses, the layered rocks still generate tensile stresses around the interface within the strong layer. The tensile stresses occur because of the stress transfer between adjacent stiff and soft layer with a bonded interface. The presence of tensile stress and the crack-tip stress are responsible for the generation of the tensile fracture in the strong layer for all samples.

The effect of varying the number of confining pressure, Poisson's ratio and Young's modulus on the tensile stresses distribution are also performed. The sensitivity study shows that Poisson's ratio has a more significant impact compared to Young's modulus on both maximum tensile stress and thickness of tensile region. Higher Poisson's ratio resulting in higher tensile stresses, while on Young's modulus it depends on the contrast between adjacent layers rather than the magnitudes.

Understanding the fracture behavior in layered rocks is beneficial for reservoir characterization, as fractures can enhance the permeability and providing vertical connectivity between isolated reservoirs. Accurately interpret 3D natural fracture distribution can help the estimation of the resource and recoverable potential early in field life. It will also contribute to optimizing the well placement and completion design for efficient production planning.

# Acknowledgments

In this very special page, I would like to express my gratitude for God and everyone involved, so that I can finish my study at TU Delft. In particular, I want to thanks my supervisor Dr. Auke Barnhoorn for all your time, support and brainstorming sessions. Thank you for letting me work with you, I learn a lot from you in the last 12 months.

Next, I really appreciate the help from Lisanne and Quinten. Thank you for reviewing my writings and help me with the software works. Without your help, I would lose my mind coping with all the software and writing tasks.

My infinite gratitude for Indonesia Endowment Fund for Education (LPDP) as the sponsor for my study in TU Delft. They not only give me the opportunity to study in one of the best university but also to learn so much else about the world and broaden my perspective as a human being.

Also, cheers to all my friends from PEG track for all the fun and team works, I learned so much from everything we did. Last but not least, thanks to my family for the endless prayer and supports, especially to my parents who have been through a lot, guiding me in the very best way, so I can achieve things that I never dared to dream before.

And dear mom, I owe the world to you and I dedicate this works for you, the very least I can do. Thank you for everything.

# Table of Contents

# Table of Figures

# List of Tables

# 1. Introduction

Reservoir characterization is one of the most fundamental steps in evaluating the conditions of a reservoir rock. A decent understanding of the reservoir rock is needed in order to perform a better field performance. It is very useful for planning the production phase, such as well placement, modeling the flow, determined the facility and also optimizing the economics. Reservoir characterization involves many branches of studies, including geology, geomechanics, geophysics, petrophysics and reservoir engineering. Those studies complement each other to generate accurate conditions of a reservoir. Basic works such as structural modeling, sedimentary modeling, petrophysical modeling and flow simulation are essential in reservoir characterization.

## 1.1. Problem Statement

Heterogeneity is one of the main challenges in reservoir characterization as it will greatly influence the fluid flow and control the production of the reservoir (Grammer, Harris and Eberli, 2004). Reservoir heterogeneity refers to the distribution of porosity or permeability within the reservoir due to the lithologic variation (Bonnell and Hurich, 2008) and a layered reservoir is a perfect example of a heterogeneous succession. Layered rocks may separate the reservoir into several compartments, as some layers might be impermeable and limit the fluid flow between two or more reservoir prospects. Nevertheless, the presence of fractures may provide the vertical connectivity between the reservoir layers and also greatly enhance the reservoir permeability.

Therefore, the fracture network becomes important to consider in reservoir characterization, as it may also alter the fluid flow in the reservoir target and influenced the reservoir performance. A better understanding of fracture characteristics between adjacent layers is a must in order to interpret the subsurface fracture network. This includes the mechanism of fracture propagation or arrest at the layer interface, fracture aperture, aperture variation and orientation.

One of the main factors that influences the fracture growth in brittle rocks is the strain. Different level of strain will result in different fracture geometry. Field study shows that there are three fracture types that can be generated depends on the amount of strain they experienced, namely incipient (arrested), throughgoing (propagating) and throughgoing with aperture (Gross and Eyal, 2007). The foundings from the field study executed by Gross and Eyal (2007) are simplified and illustrated in Figure 1.

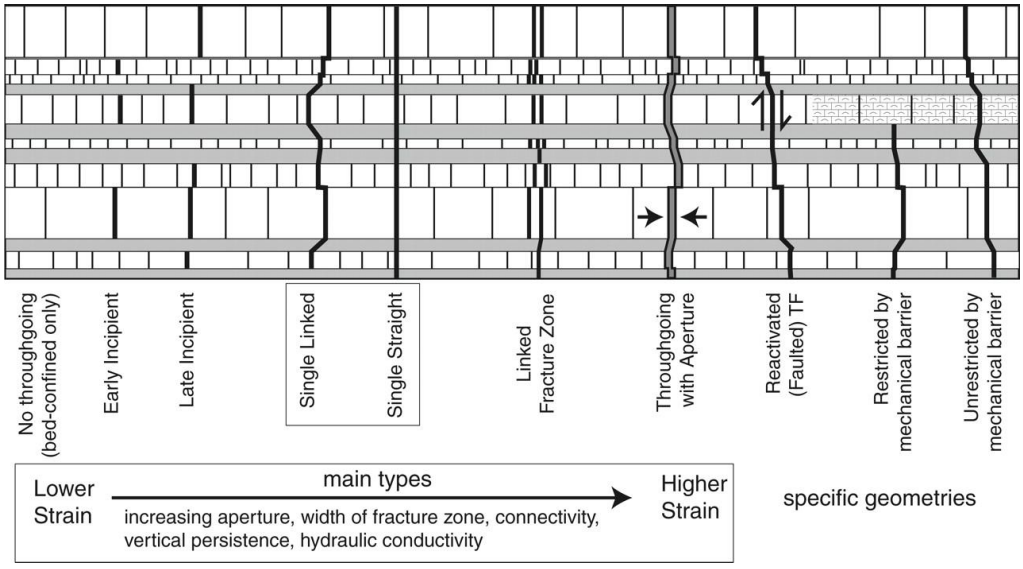


*Figure 1. Generalized classification of fractures in layered rocks. The strain is increasing to the right and responsible for the occurrence of throughgoing fracture (Gross and Eyal, 2007).*

Results from Gross and Eyal (2007) indicate that propagating fractures only occur when the strain in the layered rocks exceed the critical point, which relates to the rock mechanical properties and fracture saturation. Also, based on the field observation, the distribution of propagating fractures depends on the structural position, with the highest frequency located at the fold crest, which is also the position with the highest estimated strain intensity.

Additionally, the strain is also corresponding to the mechanical properties of the rock. Different lithologies of brittle layered rocks will have different responses to the stress and will generate a different type of fractures, such as mode I opening/tensile fracture or mode II sliding/shear fracture. Three of the mechanical properties that strongly related to the amount of strain within a rock body are rock strength, Poisson's ratio and Young's modulus.

When the reservoir consists of several lithological layers, the mechanical properties change beyond the layer interface (Becker and Gross, 1996). The contrast of rock strength, Young's modulus and Poisson's ratio between adjacent layers are responsible for changes in fracture behavior, such as fracture propagation or arrest, fracture aperture and aperture variation (Philipp and Reyer, 2010). Therefore, the term of mechanical contrast is introduced in this study for analysis purposes; it represents the strength ratio between adjacent rock layers.

As the mechanical properties and surrounding stress act as the major roles in fracture behavior, including fracture growth (propagation or termination), aperture (average and distribution) and orientation. Therefore, this study will try to examine and improve the understanding about the impact of (1) mechanical contrast and (2) confining pressure on the fracture behavior of layered rocks.

## 1.2. Research Overview

The first phase of the study was done by Regelink (2018) and Douma *et al.* (2017). Three layers of rocks with an equal length consisting of two different lithologies were attached to generate a mechanical contrast, which represents the ratio of rock strength between adjacent layers. The samples include various sandstones, siltstone and granite. Even though the layered sandstone-granite is not existing in nature, this sample will give more insight about the fracture behavior at an extremely high mechanical contrast.

Different combinations of layered rocks provide several numbers of different mechanical contrast of the samples and the fractures resulted in each sample will be evaluated by the information of their mechanical contrast. The samples were fractured in a pressure bench to find their ultimate strength in both confined and unconfined conditions. The confining pressures applied to the samples also varied (0, 15, 30 and 40 MPa) for the sample with the same compositions to analyze the impact of confining pressure on the fracture behavior. The fracture pattern of the deformed samples was visualized by the micro-CT scanner.

The results from Regelink (2018) and Douma *et al.* (2017) on the fractured layered rocks need to be analyzed further. Therefore, some detailed measurements on fracture aperture, orientation and aperture variation need to be done. In addition, numerical modeling was also performed in this study to understand the insitu stress distribution that responsible for the fractures in the layered samples. Both of the results will be combined to complete the investigation of the impact of mechanical contrast and applied confining pressure on the fractures in a layered rocks sample.

This study consists of five main parts. First, the micro-CT scan images from several samples were examined using Avizo software to highlight the fracture pattern within the samples. Second, Matlab was used to obtain the fracture aperture, length, and orientation from Avizo images. Third, the analysis of the measurement results divided into two categories, which are increasing confining pressure and increasing mechanical contrast. The fracture propagation and measurements in the

strong and weak layer are compared among samples to conclude the impact of increasing confining pressure or mechanical contrast on the fracture behavior in layered rocks. Fourth, modeling the sample in Abaqus to understand the stress field generated within the sample at various conditions. Finally, this research also includes parameters sensitivity study, including confining pressure, Poisson's ratio and Young's modulus and their impact on the stress distribution resulted within the model.

## 1.3. Research Questions and Objectives

This thesis aims to gain more information regarding the fracture behavior in layered media. The objectives are as follows:

1. Find the impact of confining pressure and mechanical contrast on the fracture behavior, including fracture propagation, aperture and orientation.
2. Modeling the stress distribution in the layered sample based on the applied stress and mechanical properties of the layered samples obtained through the laboratory experiments.
3. Analyzing the sensitivity of confining pressure and mechanical properties such as Young's modulus and Poisson's ratio on the stress distribution.

Those objectives are determined in order to answer these **research questions**:

1. **How do the confining pressure and mechanical contrast affecting the behavior of the fractures in layered rocks?**
2. **How is the stress distribution on the layered rocks at the time of failure?**
3. **How much influence do the confining pressure, Poisson's ratio and Young's modulus have on the resulted stress distribution?**

# 2. Methods and Material

## 2.1. Samples

This research focuses on fracture characterization in mechanically-layered rocks. All of the samples are consist of three-layered rocks with two different lithologies, illustrated in Figure 2. The lithologies that are used as the members in the layered rock samples include Red Felser sandstone, Bentheim sandstone, Ainsa sandstone, and Benin Granite. Each of these lithologies has their own characteristics that differ from others, such as color, constituent minerals, strength, elastic properties and porosity, which briefly described in Table 1.

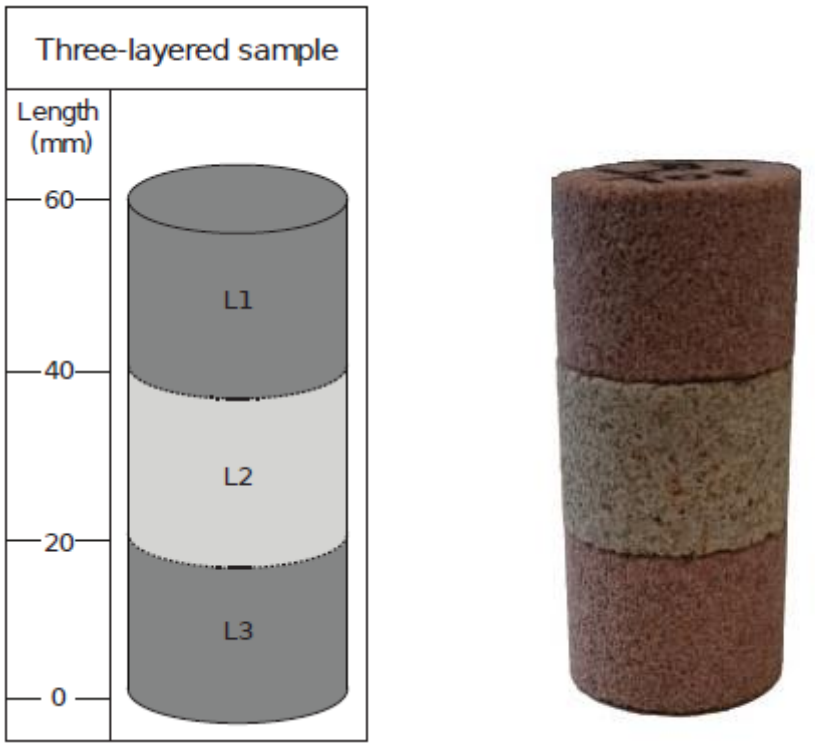


(a) (b)

*Figure 2. (a) Illustration and the dimensions of the samples, with L1 is layer 1, L2 is layer 2, and L3 is layer 3. (b) the actual image of the sample, consists of Red Felser sandstone as the weak outer layer and Bentheim sandstone as the strong middle layer* (Regelink, 2018).

*Table 1. Description and properties of lithologies of the samples (Regelink, 2018). RF is Red Felser sandstone, BNT is Bentheim sandstone, AIN is Ainsa sandstone and GRA is Benin granite.*

| Rock Sample | Unconfined Compressive Strength (Mpa) | Young's Modulus (Gpa) | Poisson's Ratio | Description |
|---|---|---|---|---|
| **RF** | 31.4±3.9 | 7.15±3.05 | 0.125±0.037 | Sandstone, red/pink color, friable, very porous, quartz-rich. |
| **BNT** | 42.7±0.9 | 9.09±2.42 | 0.206±0.038 | Sandstone, yellow/white color, friable, very porous. |
| **AIN** | 203.5±10.8 | 29.49±7.64 | 0.154±0.012 | Sandstone, dark grey color, calcite-cemented, turbidite, tight, fine-grained. |
| **GRA** | 222.1±21.2 | 30.82±3.16 | 0.181±0.018 | Granite, granular texture, predominantly white, white/grey orthoclase. |

The analyses of the samples that are used in this research are divided into two categories. A category in which we compare the fracture pattern for different mechanical contrast of the layers and a category where we compare fracture patterns formed under different confining pressure. Those categories will be useful to better understand the effect of those parameters on the fracture behavior in layered media. In Table 2, all the samples are classified into those categories and briefly explained.

*Table 2. Lithologies of each sample, the confining pressure (CP) experienced by each sample when fractured and the unconfined compressive strength (UCS) ratio between strong and weak layers.*

| *Group* | Sample | Lithologies | CP (MPa) | UCS (Ratio) |
|---|---|---|---|---|
| ***Different Mechanical Contrast*** | L13 | Ainsa sandstone – Benin granite – Ainsa sandstone | 15 | 1.1 |
| | L15 | Ainsa sandstone – Bentheim sandstone – Ainsa sandstone | 15 | 4.8 |
| | L12 | Bentheim sandstone – Benin granite – Bentheim sandstone | 15 | 5.2 |
| | L32 | Red Felser sandstone – Benin granite – Red Felser sandstone | 15 | 7.1 |
| ***Different Confining Pressure*** | L16 | Ainsa sandstone – Bentheim sandstone – Ainsa sandstone | 0 | 4.8 |
| | L15 | Ainsa sandstone – Bentheim sandstone – Ainsa sandstone | 15 | 4.8 |
| | L29 | Ainsa sandstone – Bentheim sandstone – Ainsa sandstone | 30 | 4.8 |
| | L19 | Ainsa sandstone – Bentheim sandstone – Ainsa sandstone | 40 | 4.8 |

### 2.1.1. Different Mechanical Contrast

Samples in this section have a different combination of lithologies among each other. The mechanical contrast is the unconfined compressive strength ratio between the strong and weak layers. The sample with the lowest ratio is L13, with a ratio of 1.1 between the strength of Ainsa sandstone and Benin granite, with Benin granite acts as the strong layer. Next, sample L15 consists of Ainsa sandstone and Bentheim sandstone with a mechanical contrast of 4.8. Followed by sample L12 with 5.2 mechanical contrast, made up by Benin granite as the strong layer and Bentheim sandstone as the weak layer . The last sample in this category is L32 with a mechanical contrast of 7.1, consists of Red Felser sandstone as the weak layer and Granite as the strong layer.

### 2.1.2. Different Confining Pressure

Samples in this category are differentiated by the confining pressure applied to the sample when they were deformed until failure was reached. All of the samples have the same lithologies, which are Bentheim sandstone in between Ainsa sandstone, resulting in a ratio of 4.8 for the mechanical contrast. The first sample in Table 2, L16 did not experience any confining pressure. The second sample, L15 sustained a 15 MPa of confining pressure. The third sample, L29 with 30 MPa and the last sample, L19 with the highest confining pressure of 40 MPa applied around the sample body when it fractured.

# 3. Fracture Analysis and Modelling

## 3.1. Fracture analysis with Avizo

The first computation work in this research was done by using Avizo 9.4 at TU Delft. This commercial software was used to perform image analysis with many useful functions to enhance the image quality and detecting specific parts of the images, for example fractures in rock. Some of the functions including filtering tools which are used to modify the input data and thresholding tools to select and separate the desirable part of the data. In this research, the fracture analysis was done in 2D, so three vertical slices were chosen from the whole sample. Those three slices were taken from the sides and middle part of the sample, so they can represent the whole sample, capturing different parts of fractures and also make the sample analysis more efficient. The slices are either in the XZ or YZ direction, the one which is perpendicular to the strike of the largest fracture.

In general, the workflow consists of image editing to enhance the quality of the original image (increasing the sharpness and contrast and also reducing the noise), followed by thresholding and then editing the threshold. Different samples require a different approach to enhance the image quality and to threshold the fractures. It all depends on the image quality and the amount of noise (parts of the sample with similar color frequency to the fractures).

The enhancing part including smoothing and denoising (median filter or despeckle) and sharpening the image (unsharp masking, deblur and delineate), so the fracture will be more distinctive and easier to threshold. Figure 3 (a) displays the original slice of the sample and (b) is the slice after performing smoothing and image sharpening. The process makes the fracture more stand out and easier to threshold in the next step.

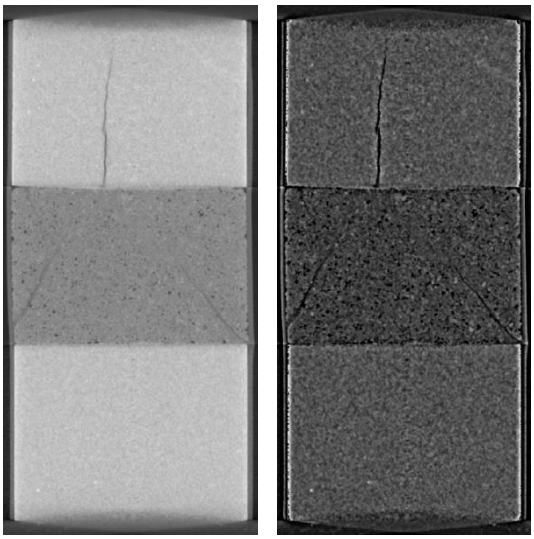

(a) (b)

*Figure 3. Enhancing the sample image by using smoothing and sharpening. (a) original slice image and (b) slice image after smoothing and sharpening.*

The thresholding part also has different options to choose, including interactive thresholding and interactive top-hat. In detail, the interactive threshold is a simple thresholding technique which allows interactive selection of a specific range of color frequency that can be adjusted by sliding the cursor on intensity range window. Meanwhile, interactive top-hat will extract small elements and details from the image, which must be chosen first between white top-hat or black top-hat before adjusting the intensity range window.

After the thresholding, the morphological operations (erosion, opening and closing) were used to reduce the noise and connect the object. Another function that is really helpful and commonly used is remove small spots in the image segmentation folder, which is effective in removing the small object with a size smaller than a specific size that the user has been defined. If they are still not enough for removing the necessary amount of noise, then edit new label field can be used to manually remove or add some objects by using lasso and brush in the segmentation window. Finally, the results from each slice are captured by using the camera icon located above the sample slice as a TIF file and ready to be analyzed in Matlab. Figure 4 represents the whole procedure which was performed to produce the final slice image of sample L15.

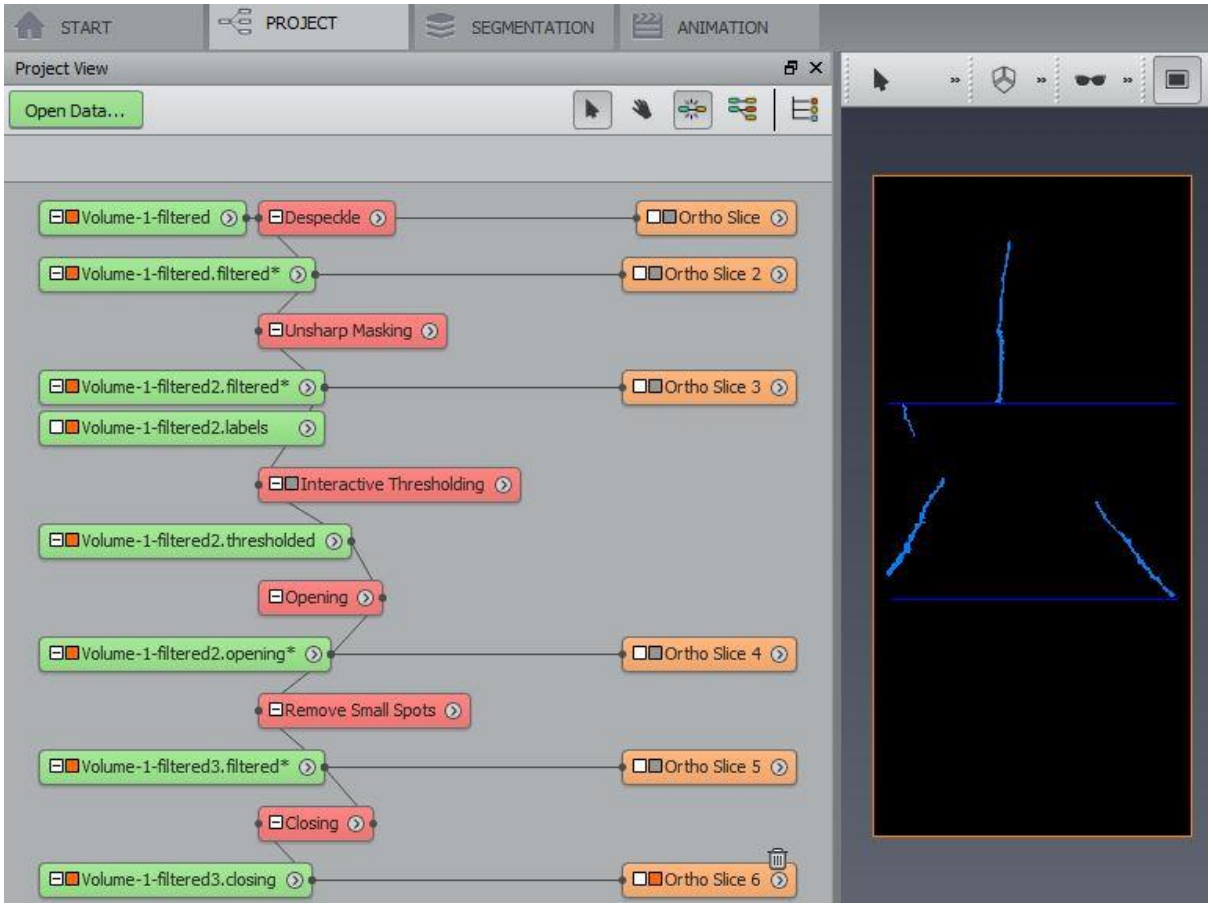


*Figure 4. Workflow and the results from processing a slice image from sample L15 using Avizo 9.4.*

The middle slice of the samples that were used for fracture analysis in Avizo and Matlab are shown in Figure 5 and Figure 6. Figure 5 shows three-layered samples consisting of Ainsa sandstone on the outer layers and Bentheim sandstone in the middle, with increasing confining pressure from left to right. The lithologies are the same between samples, generating a 4.8 mechanical contrast with Ainsa sandstone as the strong layer and Bentheim sandstone as the weak layer. In Figure 5 (a), the layered sample was loaded with an axial pressure without any confining pressure applied around it, resulted in a fracture that propagates through all the layers. There are at least five shear fractures in the weakest layer and propagating into the stronger layers as vertical tensile fractures.

Figure 5 (b) with 15 MPa confining pressure applied, resulting in shear fractures in the weak layer and tensile fracture in the strong layer. The fracture initiates in the weak layer and propagates to the strong layer. Fractures in Bentheim sandstone are diagonal and become finer towards the interface of top Ainsa sandstone, while the fracture in top Ainsa is an almost vertical open fracture. Figure 5 (c) shows the same sample which experienced a 30 MPa confining pressure. The combined axial and

confining pressure created a failure in the form of shear fracture which was arrested in the weak layer. The fracture in Figure 5 (c) is quite clear near the layer interface and become vague in the middle of the layer. Lastly, Figure 5 (d) was experiencing the highest confining pressure, equal to 40 MPa. The high number of confining pressure resisted the fracture propagation to the strong layer and made it contained in the weak layer.

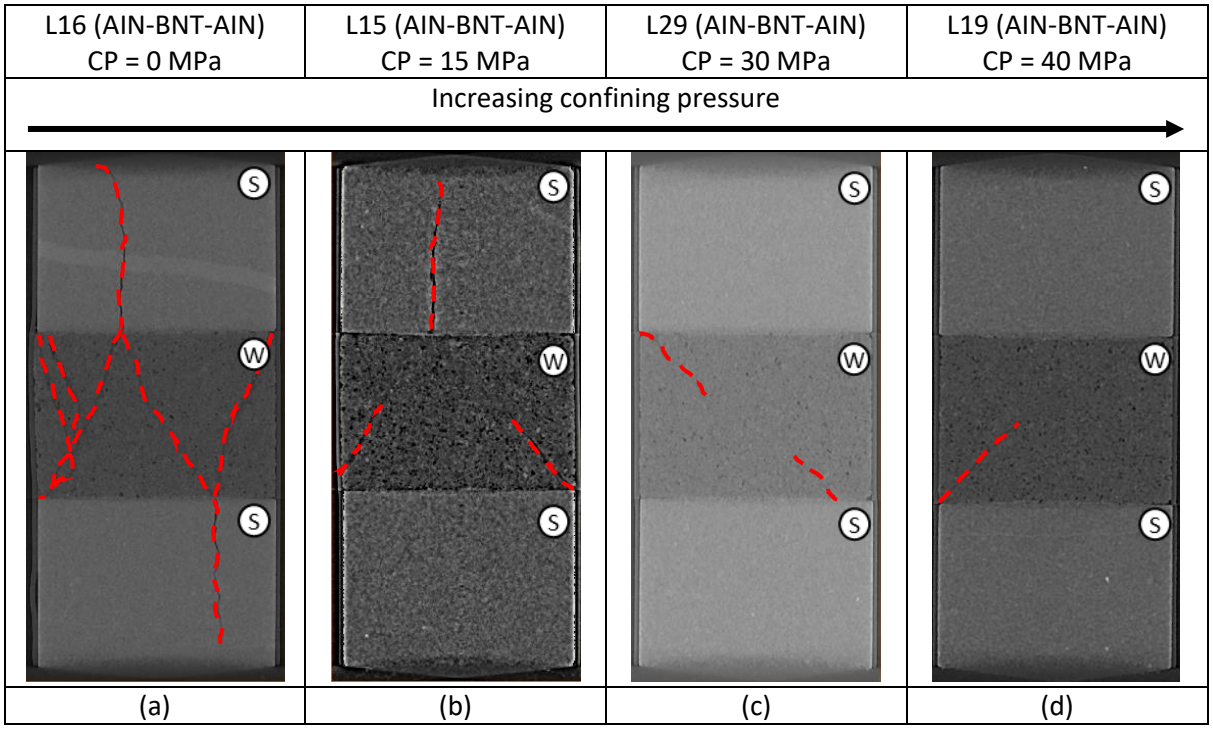


*Figure 5. Fractures (identified by the red dashed lines) occurred in the samples from increasing confining pressure group. The samples consist of Ainsa sandstone (AIN) and Bentheim sandstone (BNT), resulting in a 4.8 mechanical contrast. CP is confining pressure, S symbol is the strong layer and W is the weak layer.*

Figure 6 consists of 4 micro-CT scan results from the middle slice of samples with different composition of layered rocks, resulting in different mechanical contrast among samples. Figure 6 (a) is a layered rocks consisting of Benin granite in between Ainsa sandstone. Benin granite is slightly stronger than Ainsa sandstone with mechanical contrast equal to 1.1 and some of the fractures are propagating through all layers. The fracture is more vertical in the stronger layer (Benin granite) compared to the weaker layer (Ainsa sandstone). Next, Figure 6 (b) is the same with Figure 5 (b) and already described in the previous paragraph.

The third image, Figure 6 (c) is a layered sample consisting of two Bentheim sandstone disks on the top and bottom with a Benin granite in the middle. The mechanical contrast is 5.2, with Benin granite acts as the strong layer. Pretty similar to Figure 6 (b), the shear fractures occur in weak layer (Bentheim sandstone) which are diagonal fractures that becoming finer towards the interface of Benin granite. Then, the fracture propagates through the interface and Benin granite layer as a vertical open fracture.

Finally, Figure 6 (d) is the sample with the highest mechanical contrast, reaching 7.1 in mechanical contrast. This sample consists of Red Felser sandstone on top, followed by Benin granite in the middle and lastly a Red Felser sandstone again as the bottom layer. In this case, the fractures only appear in the top Red Felser sandstone, which is the weak layer.

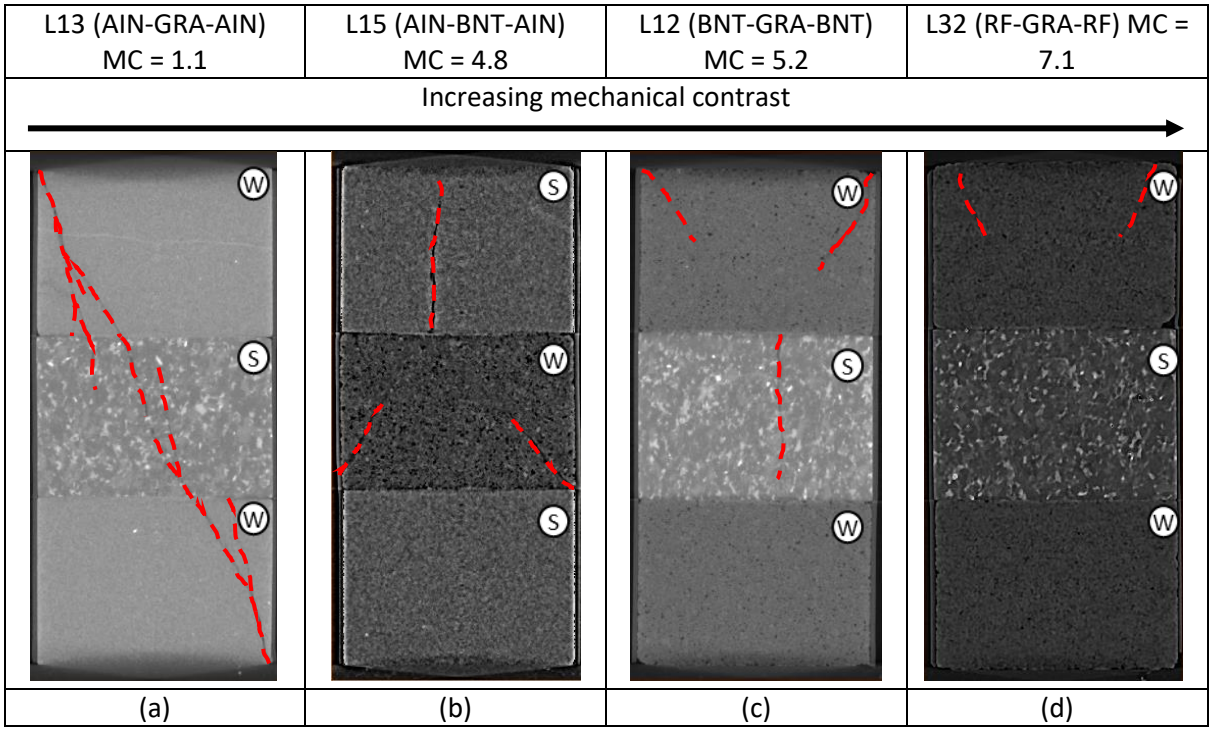


*Figure 6. Fractures (identified by the red dashed lines) of the samples in increasing mechanical contrast. All of the samples experienced a 15 MPa confining pressure. AIN is Ainsa sandstone, GRA is Benin granite, BNT in Bentheim sandstone and RF is Red Felser sandstone. MC is mechanical contrast, the S symbol regarding to the strong layer and W to the weak layer.*

Then, the images were analyzed in more detail using Avizo 9.4. The detected fractures from each sample are presented in Figure 7 for the case of increasing confining pressure, while Figure 8 shows the results from the increasing mechanical contrast.

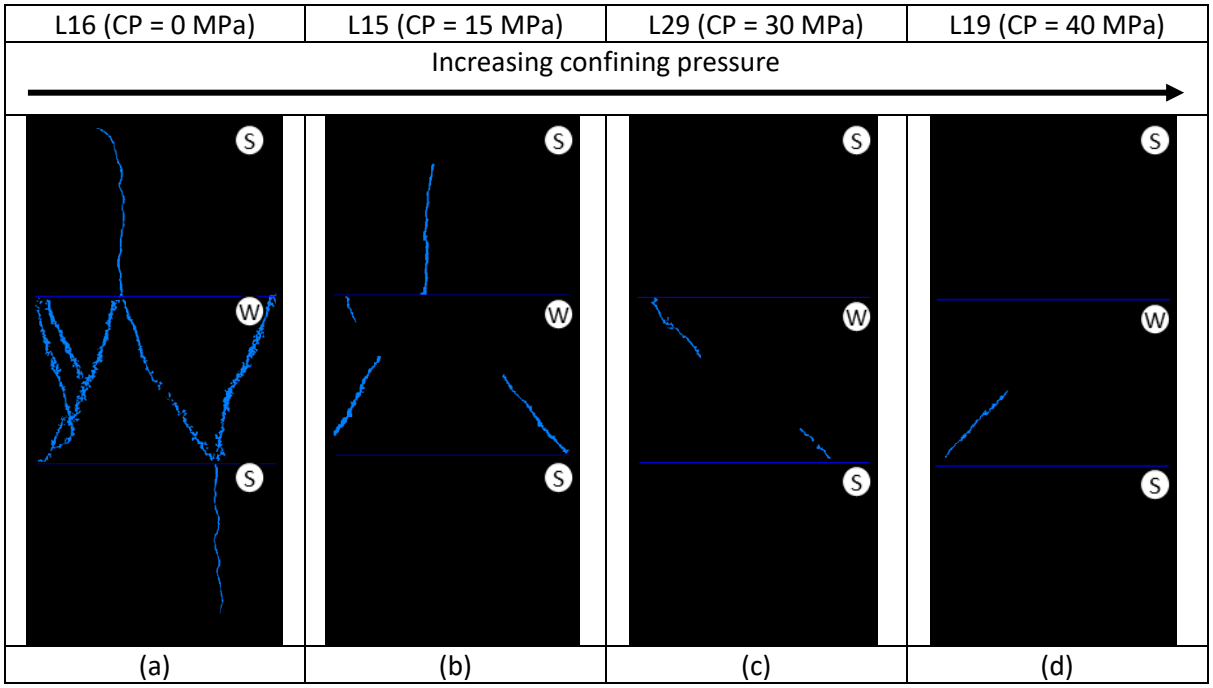


*Figure 7. Thresholding results from increasing confining pressure. The samples consist of Ainsa sandstone (AIN) and Bentheim sandstone (BNT), resulting in a 4.8 mechanical contrast. CP is confining pressure, S symbol is the strong layer and W is the weak layer.*

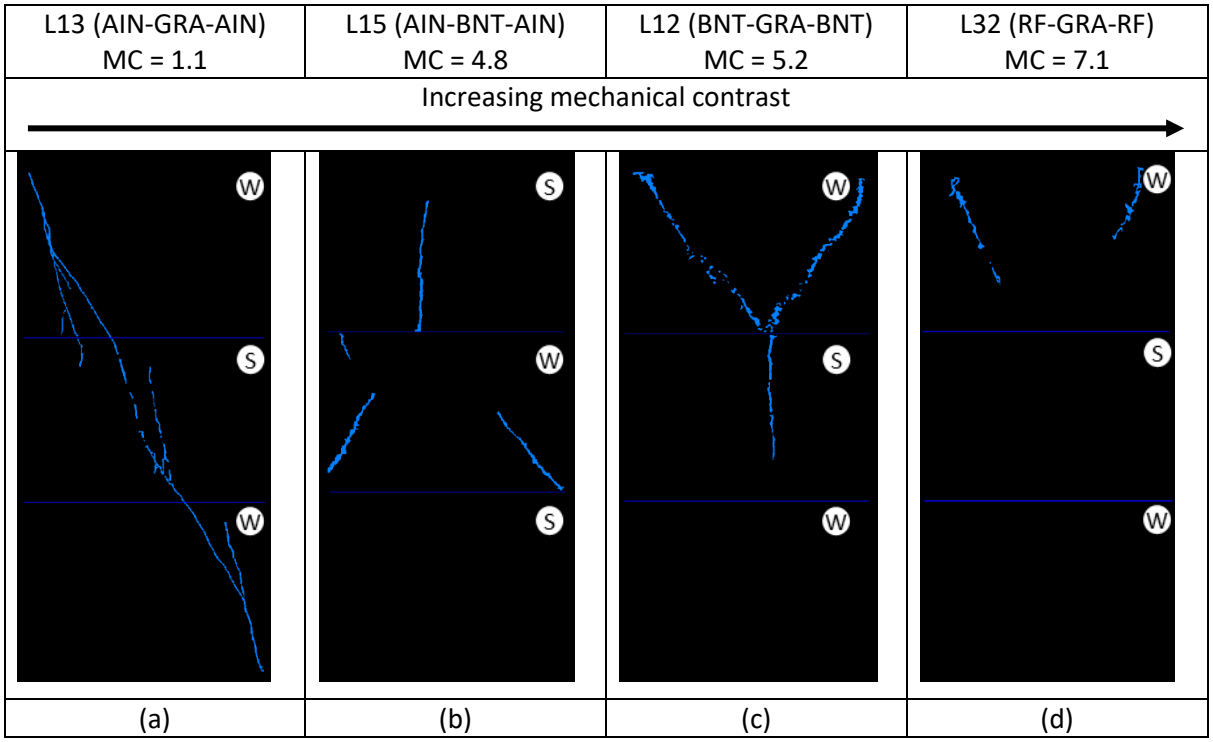


*Figure 8. Thresholding results for all the samples from increasing mechanical contrast. All of the samples experienced a 15 MPa confining pressure. AIN is Ainsa sandstone, GRA is Benin granite, BNT in Bentheim sandstone and RF is Red Felser sandstone. MC is mechanical contrast, the S symbol regarding to the strong layer and W to the weak layer.*

Figure 7 and Figure 8 indicate that fractures tend to arrest in the weak layer at high confining pressure (30 MPa and higher) or high mechanical contrast (7.1). In the increasing confining pressure group, the propagating fractures in strong layer always in the form of tensile fracture. While in the increasing mechanical contrast group, the propagating fracture in low mechanical contrast of 1.1 is shear fracture and becomes tensile fracture as the mechanical contrast increases.

The images in Figure 7 and Figure 8 will become the input for image analysis in Matlab. The analysis includes the measurement of fracture length, orientation, aperture and aperture variation. However, there is a limitation in detecting the fracture within the sample. Sometimes, the fracture becomes really fine and dominated by the zone of cataclastic flow, make it difficult to highlight and resulted in a truncated or incomplete thresholded fracture. For examples, the thresholded fracture in the weak layer in Figure 7 (b), (c), (d) and Figure 8 (b) and (d) supposed to continue towards the layer interface but can not detected by Avizo. Therefore, the fracture part with the zone of cataclastic flow is neglegted from the analysis.

## 3.2. Fracture analysis with Matlab

The thresholded images from Avizo in TIF format were examined using Matlab to get the aperture and orientation of the fractures. Before executing the process in Matlab, the images were edited by separating the fractures when it changes direction or considerable aperture, so a more detailed orientation and aperture measurement can be performed. The comparison of the original and edited image is shown in Figure 9.

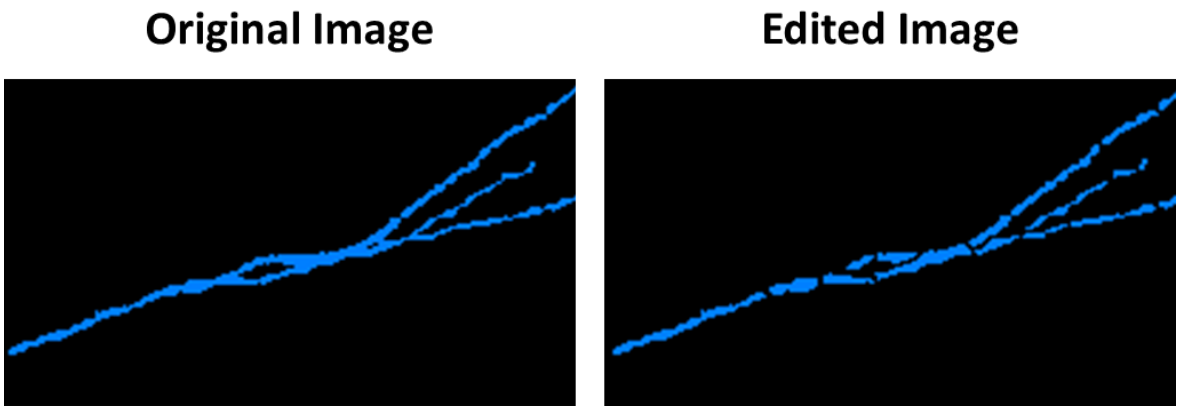


*Figure 9. Comparison between the original thresholded fractures and edited fractures for the matlab input.*

The Matlab coding used in the analysis is based on "farthest_points.m" created by "Image Analyst". The idea of the script is to find the outer pixels or boundary of the objects and the farthest points from the center of the object, which later will be used to find the length and area of the object. The distance between two farthest points is visualized by a straight red line and the outer pixels are in yellow, finely illustrated in Figure 10 and Figure 11.

In addition, some of the small parts of the fractures with an area less than 20 pixels are removed by using "bwareopen" command. Because the scanning process in Matlab is from left to right, the original image needs to be rotated 90° counterclockwise, so the object (blob index) in the result will be in order from the top layer to bottom layer.

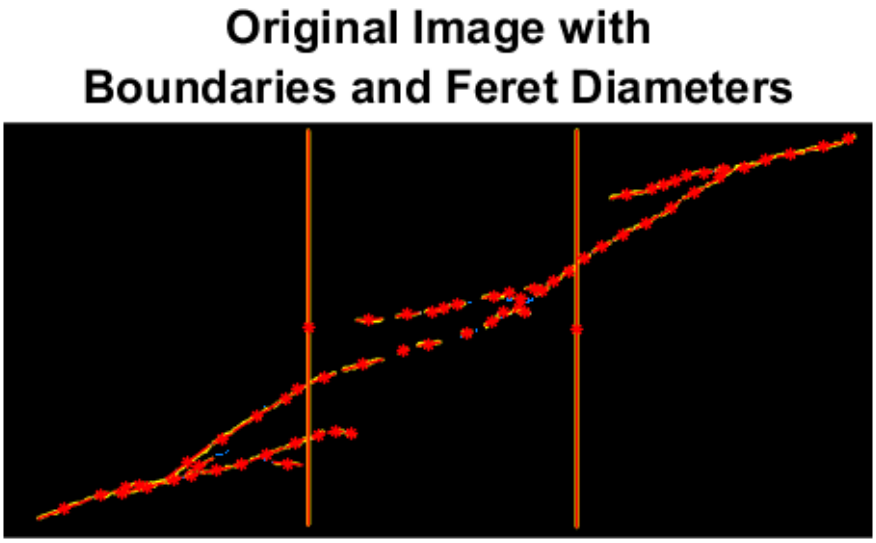


*Figure 10. Tracing result from the slice image of the sample. Two of the points from the boundary which are the farthest from the centroid connected by a red straight line which represents the fracture length.*

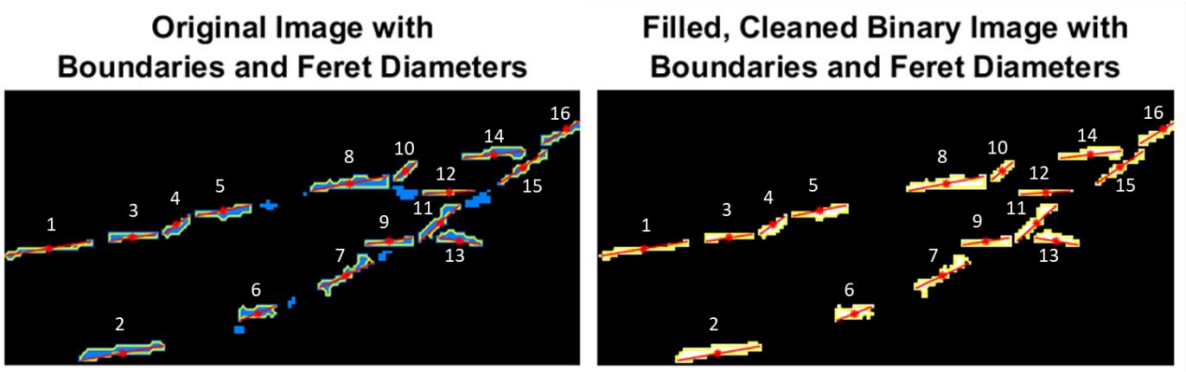


(a) (b)

*Figure 11. Details in tracing fractures, including length, area and orientation measurements. The numbers represent the order of the fracture parts (blob index) which scanned first, the red dot is the centroid, the red line is the length and the yellow color is the outer pixel of each fracture blob. The orientation was measured based on the angle of the red line. The small parts of fractures were eliminated because they do not have a reliable orientation*

After getting the area and the length, the average width of each object can be approximately calculated by simply dividing the area by the length. Besides the average width or aperture, the orientation of the object can be measured by using the "regionprops" command in Matlab. The angle of the orientations is varied from -90° to 90°. It measured the angle based on the x-axis, a horizontal object will be 0°, one with the slope toward the right direction will have a negative sign and vice versa. Since the image is rotated for 90° counterclockwise, the measurement of the angle needs to be adjusted as well. The numbers in Figure 11 are the blob index, which represents the order of the scanned fractures.

In addition, there are several cases in which some of the fracture parts are vague and dominated by the zone of cataclastic flow. In this case, the detected fractures are not connected and separated in many small parts. These small parts would not have any clear orientation, so to overcome this issue, "imclose" command was introduced to fill in all the vague zone and create one continues fracture with clear orientation. This orientation will be used for analysis, while the aperture is from the unfilled fracture. The result from filling the vague zone in sample L16 is illustrated in Figure 12.

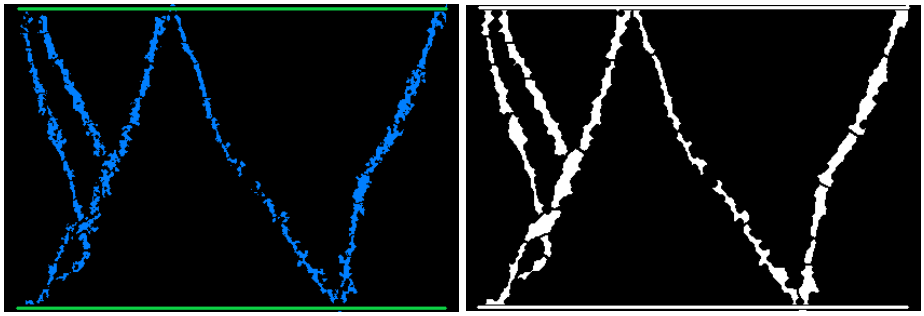

(a) (b)

*Figure 12. Comparison between (a) before and (b) after the filling of the vague zone in the middle slice of sample L16.*

## 3.3. Fracture modeling in Abaqus

In order to understand the nature behind the fractured samples, numerical modeling of the samples were done by using Abaqus software. All of the input in Abaqus need to be the same with the conditions when the samples were fractured in the laboratory. So, the result from the model can mimic the real stress field of the samples when they were fractured by Regelink, 2018 and Douma *et*

*al.*, 2017. The result from Abaqus is the deformed samples with Sigma 1 and Sigma 3 stress distributions that can be analyzed and compared to the fractured samples from the unconfined compressive strength (UCS) or confined compressive strength (CCS) test.

Each layer in the sample is assumed to be homogeneous and isotropic, with 29 mm in width and 20 mm in length. Several other parameters also needed as the input to complete the modeling of the actual samples, including Rock's Young modulus, Poisson's ratio, confining and axial loading pressure. In order to accurately mimic the actual experiment, the boundary condition also needs to be the same. The displacement of the bottom side will need to be fixed, while the top side can move in the vertical direction since the mechanical fracturing will push the top side downward.

The results show the stress distribution within the sample, which can be divided into two categories, namely minimum in-plane principle (Sigma 1) and maximum in-plane principle (Sigma 3); presented in Figure 13. In addition, Abaqus is an engineering software, so the compressive stress is presented in negative value while tensile stress in positive value. Furhtermore, because of the distinguishing feature that differs the sample from each other is the presence of tensile fracture in the strong layer, then studying the tensile stress distribution in Sigma 3 is more important.

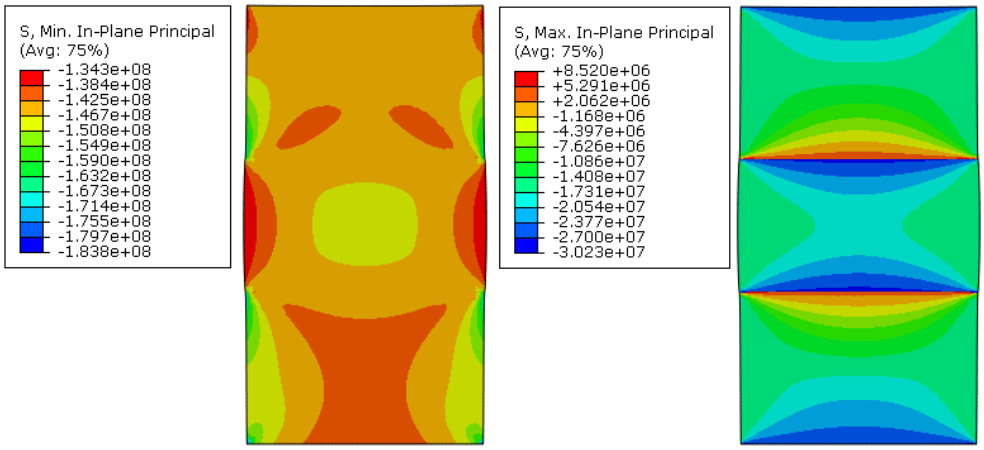


*Figure 13. The modeling results from Abaqus, (a) the distribution of minimum in-plane principal (Sigma 1) and (b) the distribution of maximum in-plane principal (Sigma 3). Negative values represent the compressive stress and positive values denote the tensile stress.*

## 3.4. Limitations of Research Methods

There are several limitations in the methods used for this study, including image analysis in Avizo and sample modeling with Abaqus. The limitations are (1) Avizo cannot detect all the fracture plane, fine part of the fracture which categorized as a zone of cataclastic flow in this study is difficult to highlight and therefore neglected in the fracture measurements. (2) In Abaqus modeling, the interface friction is not included and assumed as a strong bonded interface. (3) Poisson's ratio and Young's modulus of each lithology remain the same for every simulation and the effect of confining pressure on these properties is not accounted for.

# 4. Results

## 4.1. Fractures Measurements

Thresholding results from Avizo 9.4 were measured using Matlab for its length, aperture and orientation. The results are divided into two categories, increasing mechanical contrast and increasing confining pressure. Figure 14 shows the four results from different layered samples with increasing confining pressure. The x-axis is the width of the fractures (aperture) and y-axis is the number of edited fractures (blob). The result also includes an average aperture for all the fractures in one layer and the averaging is weighted with each blob length.

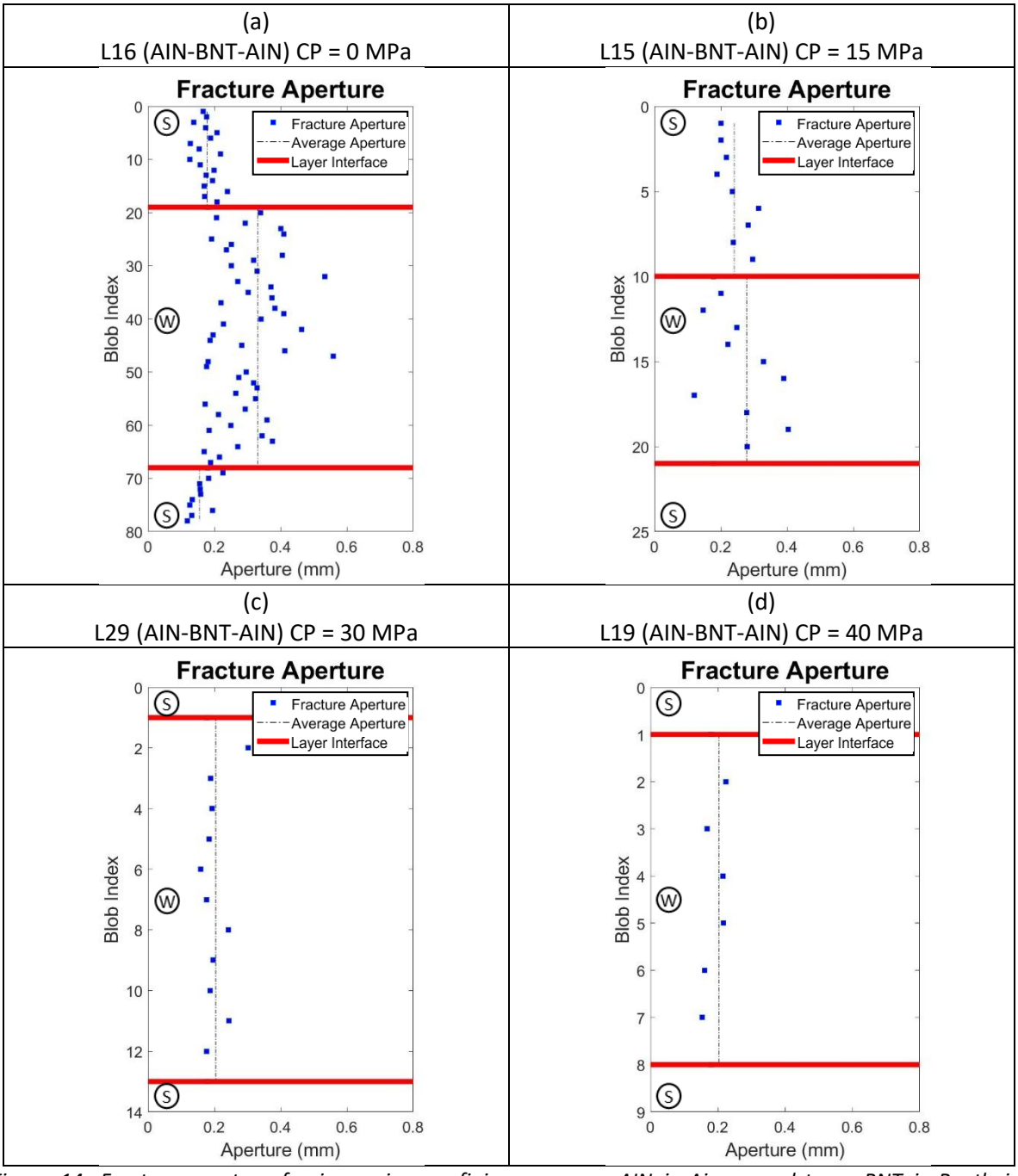


*Figure 14. Fracture aperture for increasing confining pressure. AIN is Ainsa sandstone, BNT is Bentheim sandstone, CP is confining pressure, blob index is the separated fracture part, S symbol is the strong layer and W is the weak layer.*

Figure 14 shows that there is a decrease in average aperture difference between strong and weak layer from 0 to 15 MPa. Moreover, the deviances of aperture readings from its average value in the strong layer are less than the ones in the weak layer. Also, the deviance of apertures in the weak layer is decreasing with the increasing of confining pressure.

Next, Figure 15 indicates that with increasing mechanical contrast, the average aperture difference between strong and weak layer is also increasing. The weak layer seems to have a bigger aperture compared to the strong layer and the apertures variation in strong layer seems narrower compared to the weak layer.

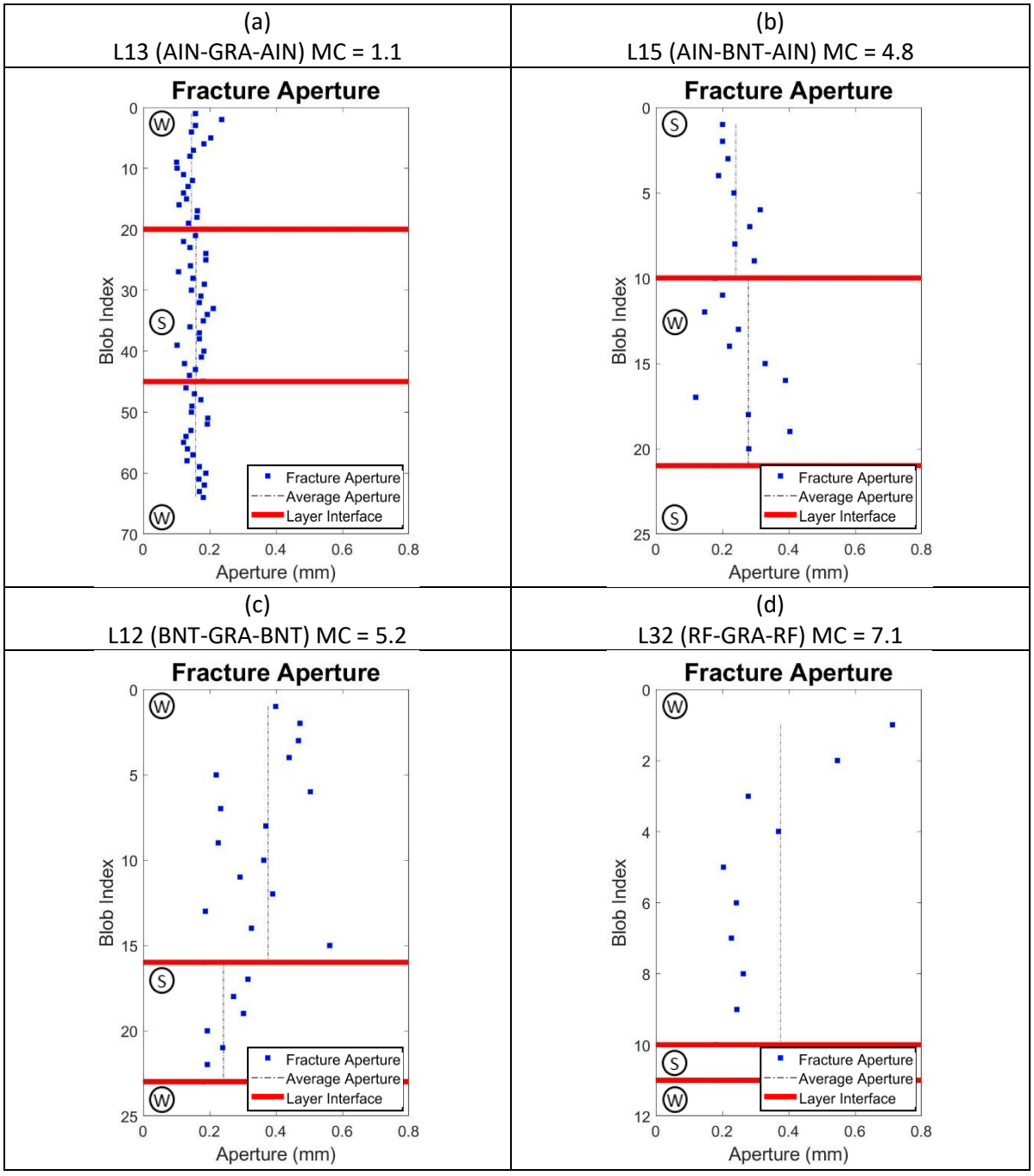


*Figure 15. Fracture aperture for increasing mechanical contrast. AIN is Ainsa sandstone, BNT is Bentheim sandstone, GRA is Benin granite, RF is Red Felser sandstone, MC is mechanical contrast, blob index is the separated fracture part, S symbol is the strong layer and W is the weak layer.*

Figure 16 represents the main points that can be concluded from the aperture measurements. The average aperture of the weak layer in Figure 16 (a) seems constantly declining with the increasing of confining pressure. While there are not enough data in the strong layer for drawing a conclusion. Figure 16 (b) shows the results from increasing mechanical contrast, the difference between the average aperture in the weak and strong layer is getting higher with increasing mechanical contrast.

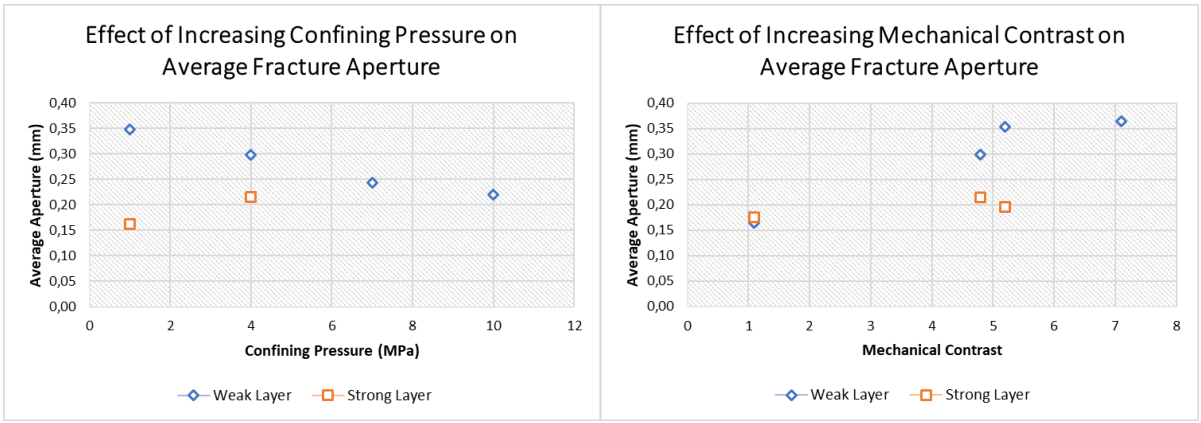


(a) (b)

*Figure 16. Average fracture aperture in (a) increasing confining pressure group and (b) increasing mechanical contrast group.*

Furthermore, it also can be seen from Figure 14 and Figure 15 that there is a difference in aperture variations from its average value with either increasing confining pressure or increasing mechanical contrast. In order to quantify the aperture variations, the standard deviation is used as a representative parameter and presented as a scatter diagram in Figure 17.

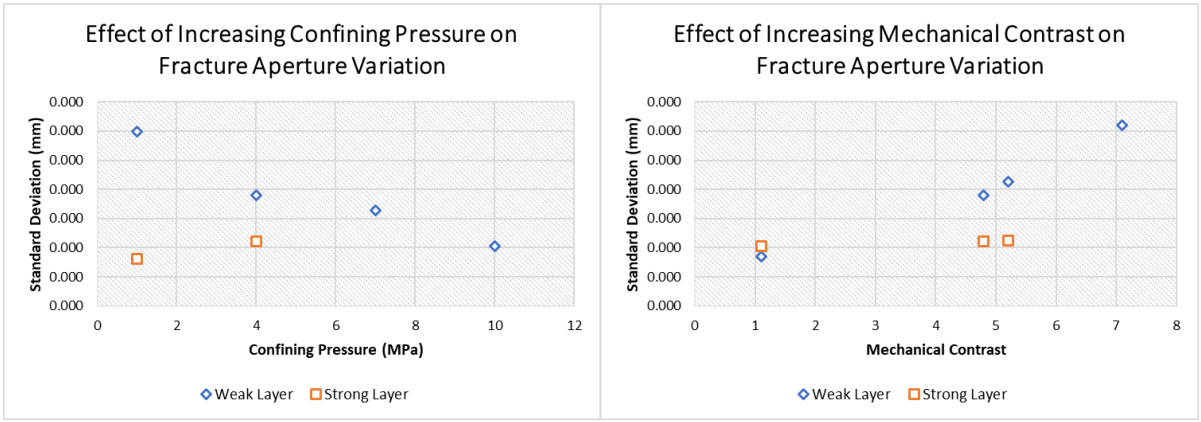


(a) (b)

*Figure 17. Standard variation of fracture aperture as (a) the confining pressure increases or (b) rising in mechanical contrast.*

Figure 17 indicates that there is a decrease in standard variation of fracture aperture in the weak layer as the confining pressure increases, which means that the aperture is becoming more homogenous with higher confining pressure in the weak layer. In contrast, as the mechanical contrast between adjacent layers increases, the range of apertures from its average value is also rising in the weak layer. Likewise, from the three available data of standard deviation in the strong layer, the distribution of fracture aperture is also getting wider from its average value.

Fracture analysis in Matlab also includes orientation measurement. The presentation of orientation results is similar to the aperture measurement, with the numbers of edited fractures are presented as blob index in y-axis and the orientation in degree in x-axis. The angle is measured regarding to x-axis,

which means 0° is horizontal and 90° or -90° is vertical. The range of the orientation is from -90° until 90°, with minus sign means that the slope is towards right while the positive number represents the slope with the left direction. The orientation results for increasing confining pressure group are shown in Figure 18 and increasing mechanical contrast group are in Figure 19.

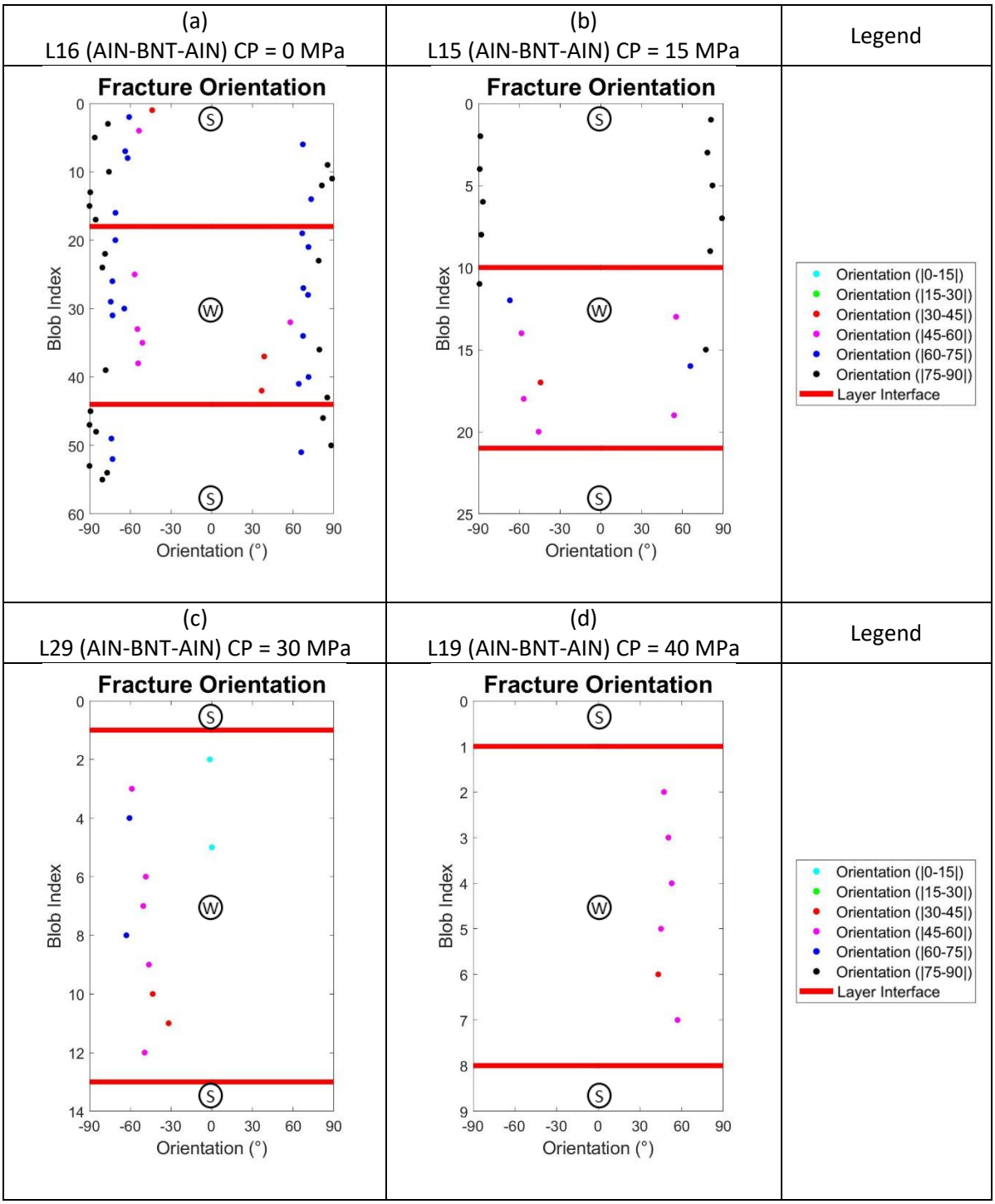


*Figure 18. Fracture orientation for increasing confining pressure. AIN is Ainsa sandstone, BNT is Bentheim sandstone, CP is confining pressure, blob index is the separated fracture part, S symbol is the strong layer and W is the weak layer.*

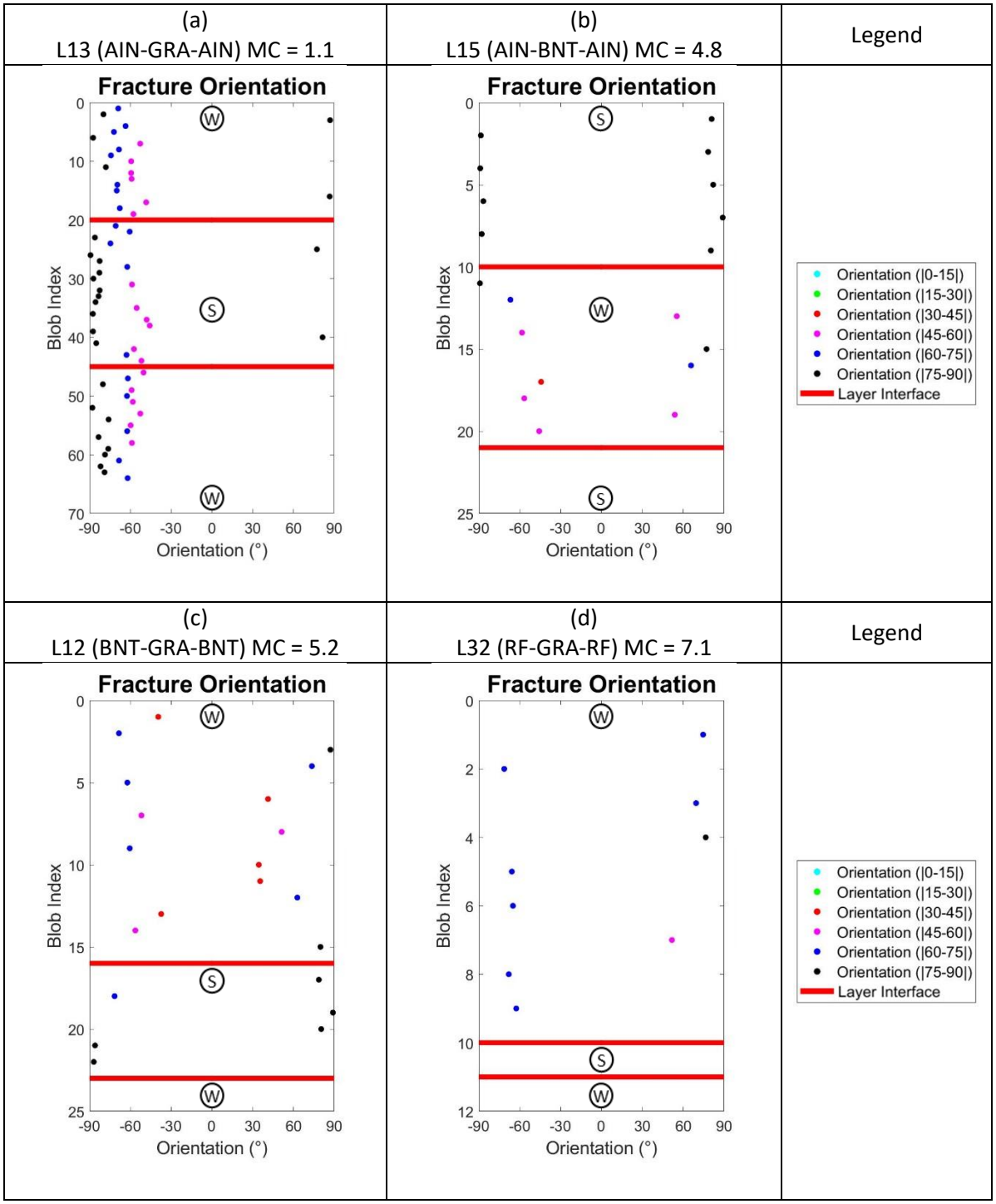


*Figure 19. Fracture orientation for increasing mechanical contrast. AIN is Ainsa sandstone, BNT is Bentheim sandstone, GRA is Benin granite, RF is Red Felser sandstone, MC is mechanical contrast, blob index is the separated fracture part, S symbol is the strong layer and W is the weak layer.*

In general, Figure 18 and Figure 19 show that the strong layer tends to have a vertical fracture. However, it also depends on the mechanical contrast, in the case of Figure 19 (a) with only 1.1 mechanical contrast, the fracture in the weak and strong layer has a similar angle. However, at 4.8 and 5.2 mechanical contrast, the fracture in the strong layer is almost vertical. In a higher mechanical contrast, reaching 7.1, the fracture is arrested in the weak layer.

In addition, Figure 18 (a) which did not experience any confining pressure indicates that there is a change in fracture orientation in the top part of the strong layer. The fracture orientation in the strong

layer started at almost 90° from the interface and become lower, reaching almost -45° near to the top side of the sample. While in a higher confining pressure (15 MPa), the whole fracture orientation in the strong layer are remain the same at around 84°. In addition, the fracture in the strong layer in Figure 18 (b) is shorter than the one in Figure 18 (a).

Then, all of the orientations in one layer were converted to their absolute value for averaging calculation. Then, the average of the orientation in the weak and strong layer are presented in Figure 20. In Figure 20 (a), the results from increasing confining pressure group show that the average orientation in the weak layer is declining with the rise of confining pressure. The declined average orientation stopped at around 45° and stay around that value even with the increasing confining pressure.

It is also visible from both images in Figure 20 that the fractures in the strong layer are getting more vertical with increasing confining pressure or mechanical contrast. In general, the strong layer will always have more vertical fracture compared to the one in the weak layer.

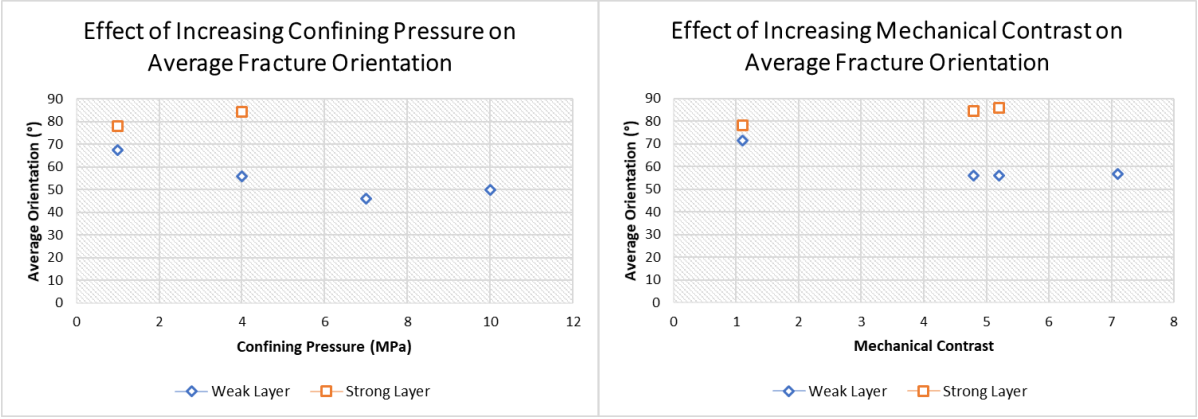


(a) (b)

*Figure 20. Average fracture orientation in (a) increasing confining pressure group and (b) increasing mechanical contrast group.*

## 4.2. Samples Modelling

The samples modeling with Abaqus resulted in the images of Sigma 1 and Sigma 3 distribution within the sample. The analysis of Sigma 3 distribution rather than Sigma 1 was chosen because Sigma 3 often shows both of compressive and tensile stresses. The Sigma 3 distribution results with input parameters from Table 3 and Table 4 are presented in Figure 21 and Figure 22 respectively. Figure 21 contains four models from increasing confining pressure. All of the samples consist of Bentheim sandstone in the middle of Ainsa sandstone.

*Table 3. Parameters used in Abaqus modeling for increasing confining pressure group. The lithologies compositions are the same between each samples, the outer layer is Ainsa sandstone and the middle layer is Bentheim sandstone.*

| ***Parameters*** | **L16** | **L15** | **L29** | **L19** |
|---|---|---|---|---|
| *Poisson's Ratio middle layer* | 0.206 | 0.206 | 0.206 | 0.206 |
| *Young's Modulus middle layer (GPa)* | 9.09 | 9.09 | 9.09 | 9.09 |
| *Poisson's Ratio outer layers* | 0.154 | 0.154 | 0.154 | 0.154 |
| *Young's Modulus outer layers (GPa)* | 29.49 | 29.49 | 29.49 | 29.49 |
| *Axial loading (MPa)* | 38.5 | 144.5 | 189.2 | 215.5 |
| *Confining Pressure (MPa)* | 0 | 15 | 30 | 40 |

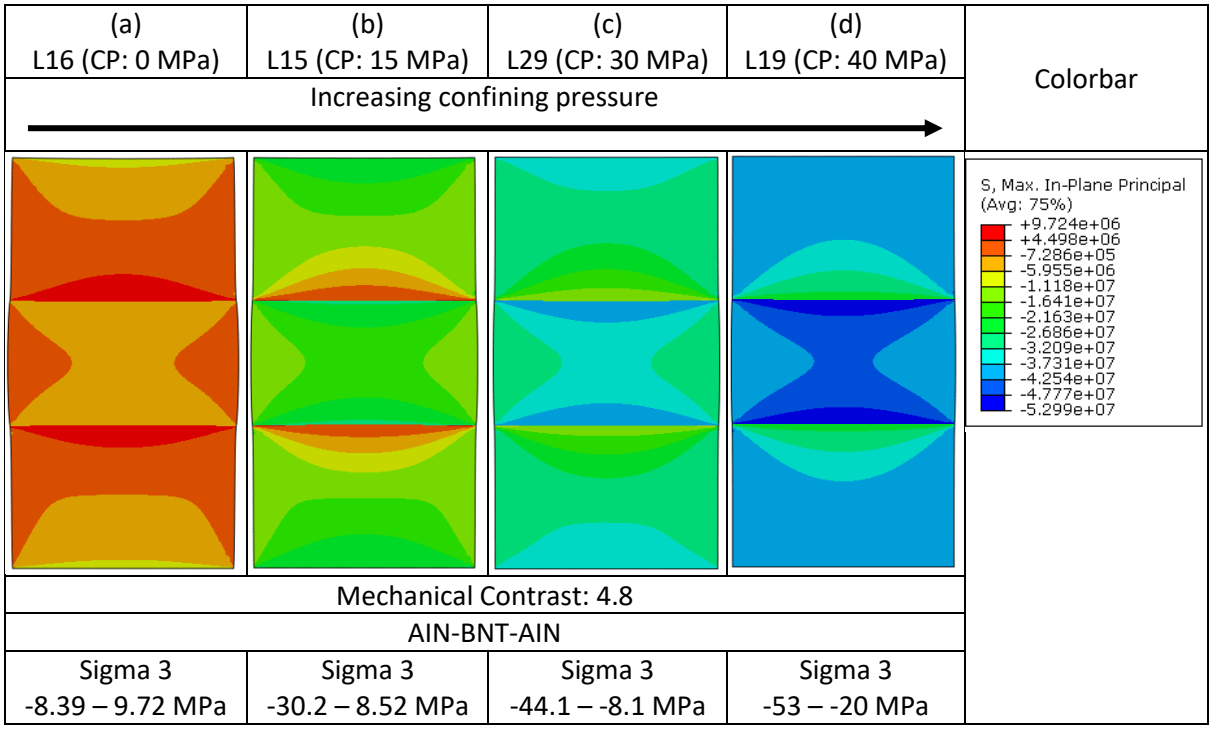


*Figure 21. Sigma 3 distribution model of the samples with increasing confining pressure. CP is confining pressure, AIN is Ainsa sandstone and BNT is Bentheim sandstone. The tensile stress only presence in figure (a) and (b), which shown in Sigma 3 range at the bottom part of the table.*

The results in Figure 21 are consistent with the laboratory experiment results. Sample L16 and L15 are showing some tensile stresses in the strong layer, with the maximum magnitude of 9.72 MPa in L16 and 8.52 MPa in L15. Figure 21 also shows that the tensile stresses are getting more restrained with increasing confining pressure, indicated by the decreasing of maximum Sigma 3 value and the thickness of tensile region (the reddish colored area).

*Table 4. Parameters used in Abaqus modeling for increasing mechanical contrast group. L13 (The outer layer is Ainsa sandstone and the middle layer is Benin granite), L15 (The outer layer is Ainsa sandstone and the middle layer is Bentheim sandstone), L12 (The outer layer is Bentheim sandstone and the middle layer is Benin granite) and L32 (The outer layer is Red Felser sandstone and the middle layer is Benin granite).*

| ***Parameters*** | **L13** | **L15** | **L12** | **L32** |
|---|---|---|---|---|
| *Poisson's Ratio middle layer* | 0.181 | 0.206 | 0.181 | 0.181 |
| *Young's Modulus middle layer (GPa)* | 30.82 | 9.09 | 30.82 | 30.82 |
| *Poisson's Ratio outer layers* | 0.154 | 0.154 | 0.206 | 0.125 |
| *Young's Modulus outer layers (GPa)* | 29.49 | 29.49 | 9.09 | 7.15 |
| *Axial loading (MPa)* | 285 | 144.5 | 127 | 149 |
| *Confining Pressure (MPa)* | 15 | 15 | 15 | 15 |

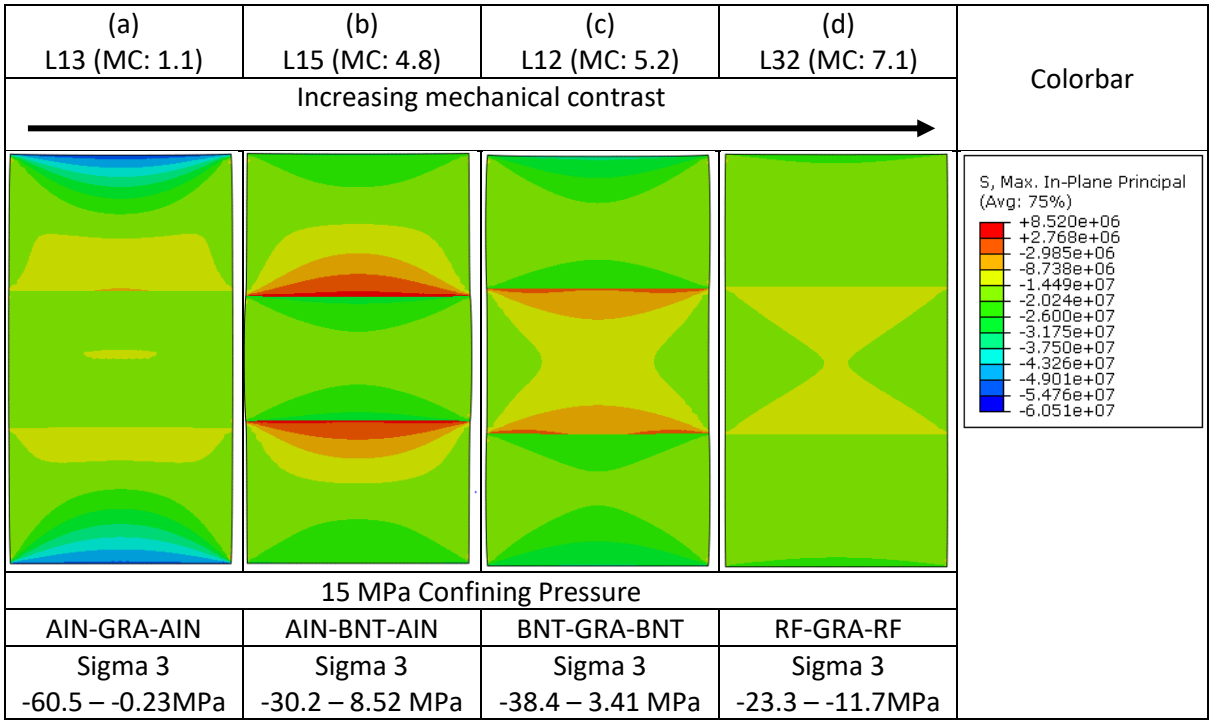


*Figure 22. Sigma 3 distribution model of samples with increasing mechanical contrast. MC is mechanical contrast, AIN is Ainsa sandstone, GRA is Benin granite, BNT is Bentheim sandstone and RF is Red Felser sandstone. The tensile stress only presence in figure (b) and (c), which shown in Sigma 3 range at the bottom part of the table.*

The results in Figure 22 (a) and (d) show that sample L13 and L32 do not have any tensile stress, while sample L15 and L12 show some tensile stresses in the strong layers. Therefore, the tensile failure may only happen in sample L15 and L12, which are proven by the actual sample in Figure 6 (b) and (c). Moreover, increasing mechanical contrast does not show any relation to the tensile stress distribution. Figure 22 indicates that the lowest and highest mechanical contrast resulting in all compressive stress distribution for the whole sample body.

However, for the mechanical contrast of 4.8 (sample L15) and 5.2 (sample L12), there are some tensile stresses distributions in the strong layer near to the layer interface. Changing the rock order, for example from weak-strong-weak into strong-weak-strong will not bring up or eliminate the tensile stress. Then, it might be possible that Poisson's ratio is the main control (beside confining pressure) for tensile stresses to occur rather than the rock strength, in this case represented by Young's modulus.

The results of the modeling will depend on the input parameters in Table 3 and Table 4, so it is also necessary to asses how those parameters impact the modeling outcome individually. A sensitivity study was performed for several parameters such as Young's Modulus, Poisson's Ratio and confining pressure to observe their impact to the stess distributions and the resulting fractures.

## 4.3. Parameters Sensitivity

Further study about the modeling part is regarding to the sensitivity of input parameters. In Abaqus the input parameters, such as Young's modulus, Poisson's ratio and confining pressure are the main factor that influence the stress distributions. The first experiment is variating the confining pressure and its impact on the maximum value and the thickness of tensile stress region. In Figure 23, the results from changing confining pressure were displayed. When varying the confining pressure, the required axial stress for fracturing the layered sample is also increasing. The number of axial stress applied in this experiment was obtained from Regelink (2018) experiment. The tensile stresses

distribution is the most visible difference that can be compared among all results. Also, the maximum tensile stress of each result appears to be different as well.

Figure 23 shows the comparison among all results with increasing confining pressure. The real thickness of tensile region is calculated by dividing the thickness of tensile region in Figure 23 with the layer thickness and finally multiplied by the real layer thickness. The results of this measurement are presented in Table 5. Based on the images alone, the decreasing of the tensile region is visible for unconfined model until around 6 MPa. As the confining pressure continue to increase, the tensile regions are decreasing in thickness, but not as much as before 6 MPa and finally disappear around 20 MPa confining pressure.

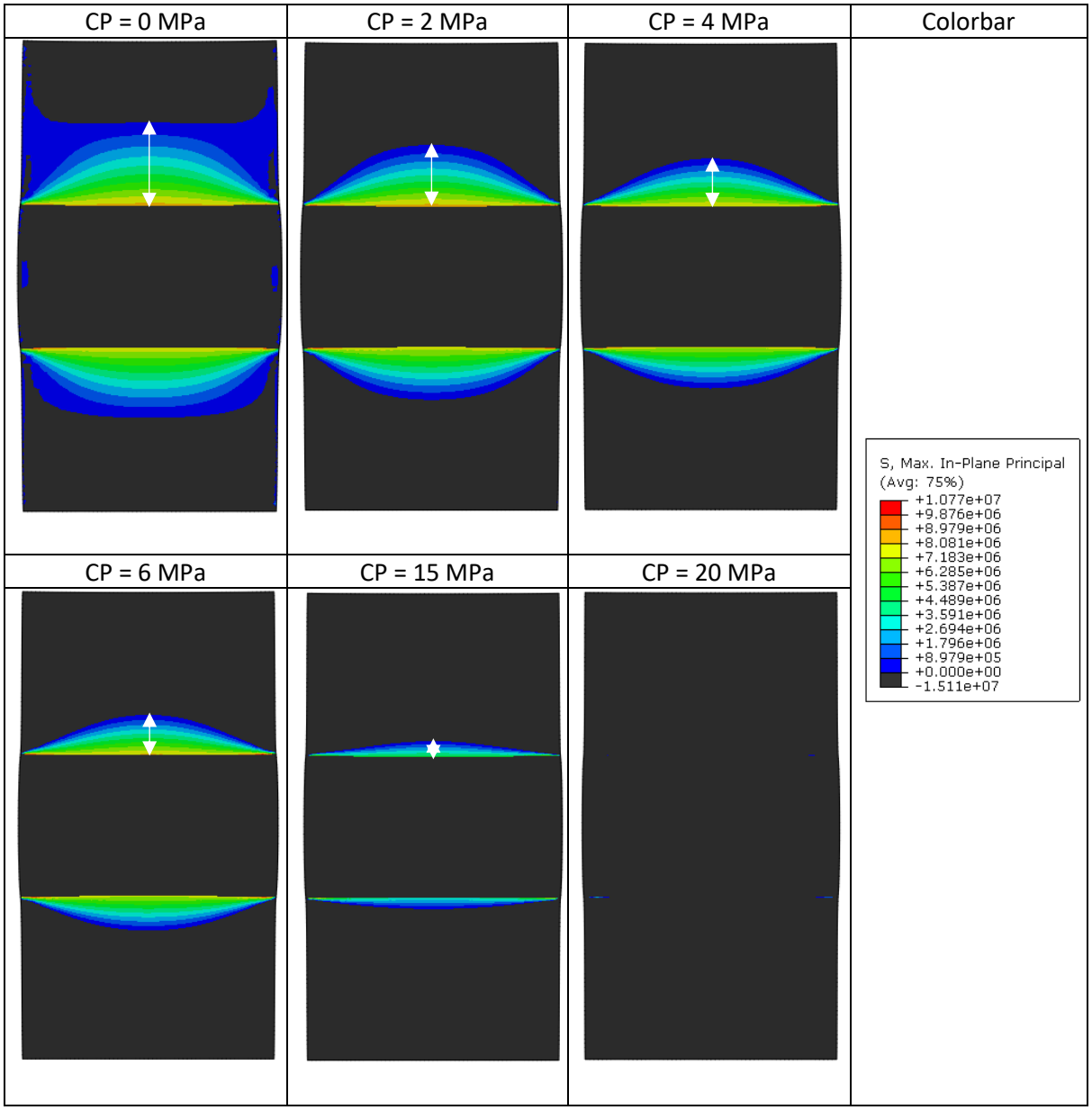


*Figure 23. Effect of increasing confining pressure on the thickness of tensile region. The sample model consist of Ainsa sandstone (strong) as the outer layer and Bentheim sandstone (weak) as the middle layer. CP is confining pressure.*

Further study regarding the reduced thickness of tensile region displayed in a scatter plot in Figure 24. It seems that there are two different regression lines which intersect around 4 MPa confining pressure.

The first regression line from 1-4 MPa has a steeper slope compared to the second line, with a decline rate of -0.1015 cm/MPa compared to the second line with -0.0373/MPa.

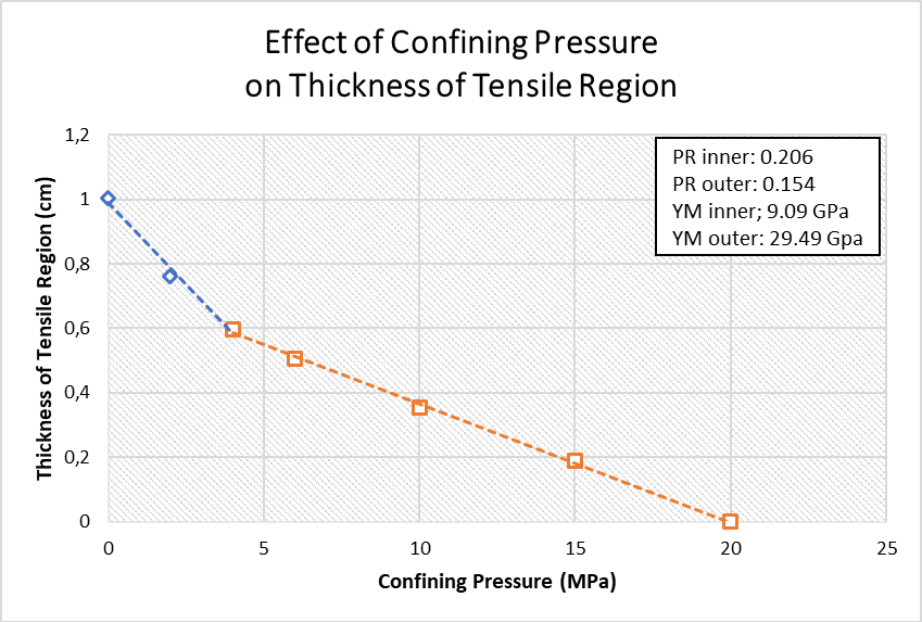


*Figure 24. Effect of increasing confining pressure on the thickness of tensile region. The sample consist of Ainsa sandstone (strong) as the outer layer and Bentheim sandstone (weak) as the middle layer. PR is Poisson's ratio and YM is Young's modulus.*

*Table 5. Parameters and results from confining pressure sensitivity simulation.*

| Confining Pressure (MPa) | 0 | 2 | 4 | 6 | 15 | 20 |
|---|---|---|---|---|---|---|
| Axial Pressure (MPa) | 38.5 | 55 | 70 | 87 | 144.5 | 158 |
| Tensile Thickness (cm) | 1.003 | 0.763 | 0.597 | 0.505 | 0.188 | 0 |
| Maximum Sigma 3 (Mpa) | 9.724E+06 | 1.016E+07 | 1.021E+07 | 1.077E+07 | 8.520E+06 | 2.627E+06 |

The maximum Sigma 3 of each experiment were also compared and written in Table 5. Maximum Sigma 3 for the first four experiments are slightly increasing. When the confining pressure was increased to 15 MPa, the maximum Sigma 3 dropped significantly to 8.52 MPa and continue to decrease until 2.62 MPa for 20 MPa confining pressure. This event might be the result of the significant increase of the confining pressure, which started to resist the tensile stresses generated from the strain of adjacent rock layers.

The next studies of sensitivity are Poisson's ratio and Young's modulus. In this case, the Poisson's ratio and Young's modulus of sample L16 will be varied based on its original value. Specifically, the values of the outer layers always remain the same, while the middle layer changes. There will be four simulations by increasing and decreasing the base value of 30% and 50%. The model results are presented in Figure 25 and Figure 26, the thickness of tensile region and maximum Sigma 3 will be compared among all results in Table 6 and Table 7.

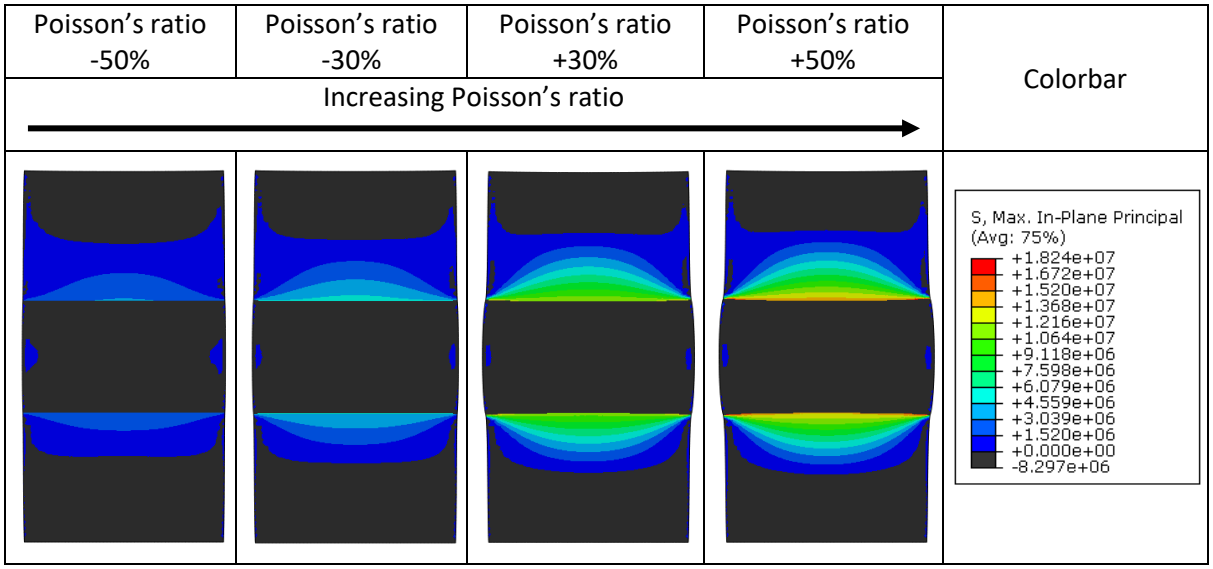


*Figure 25. The effect of changing Poisson's ratio on Sigma 3 distribution.*

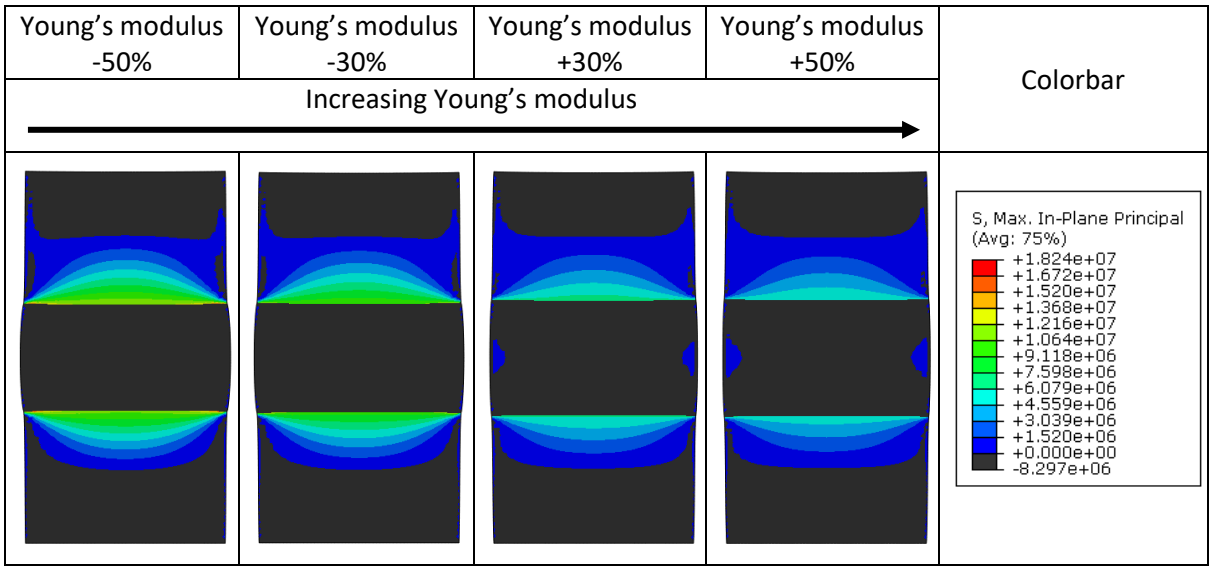


*Figure 26. The effect of changing Young's modulus on Sigma 3 distribution*

Figure 25 indicates that by increasing the Poisson's ratio of the middle layer, the maximum Sigma 3 and the thickness of tensile region are also increasing. On the other hand, Figure 26 shows that increasing Young's modulus will reduce both maximum Sigma 3 and thickness of tensile region. The exact numbers of the parameters and its results are presented in Table 6 and Table 7. The comparison of the effect on varying Poisson's ratio or Young's modulus are visualized in Figure 27 and Figure 28.

*Table 6. Parameters and results from Poisson's ratio sensitivity simulation.*

| Parameters | -50% | -30% | Original | 30% | 50% |
|---|---|---|---|---|---|
| BNT Poisson ratio | 0.103 | 0.144 | 0.206 | 0.268 | 0.309 |
| AIN Poisson ratio | 0.154 | 0.154 | 0.154 | 0.154 | 0.154 |
| PR Weak (BNT)/PR Strong (AIN) | 0.67 | 0.94 | 1.34 | 1.74 | 2.01 |
| Maximum Sigma 3 (Mpa) | 3.223 | 5.394 | 9.724 | 14.64 | 18.24 |
| Thickness of Tensile Region (cm) | 0.875 | 0.939 | 1.003 | 1.062 | 1.095 |

*Table 7. Parameters and results from Young's modulus sensitivity simulation.*

| Parameters | -50% | -30% | Original | 30% | 50% |
|---|---|---|---|---|---|
| BNT Young's Modulus (Gpa) | 4.545 | 6.363 | 9.09 | 11.817 | 13.635 |
| AIN Young's Modulus (Gpa) | 29.49 | 29.49 | 29.49 | 29.49 | 29.49 |
| YM Weak (BNT)/YM Strong (AIN) | 0.15 | 0.22 | 0.31 | 0.40 | 0.46 |
| Maximum Sigma 3 (Mpa) | 16.21 | 13.02 | 9.724 | 7.479 | 6.345 |
| Thickness of Tensile Region (cm) | 1.041 | 1.010 | 1.003 | 0.984 | 0.980 |

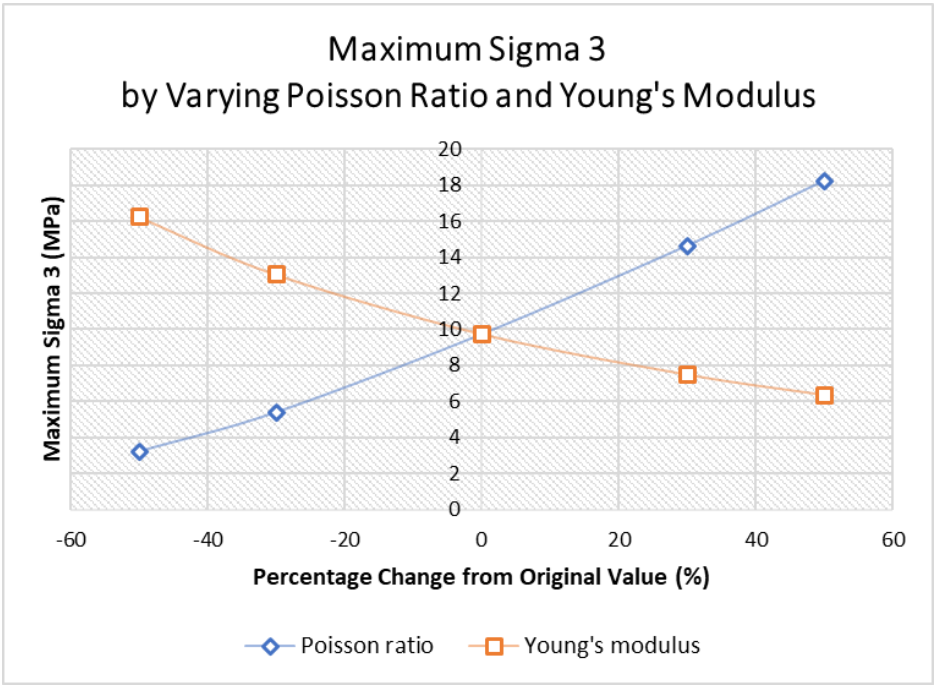


*Figure 27. Comparison between Poisson's ratio and Young's modulus sensitivity on maximum Sigma 3.*

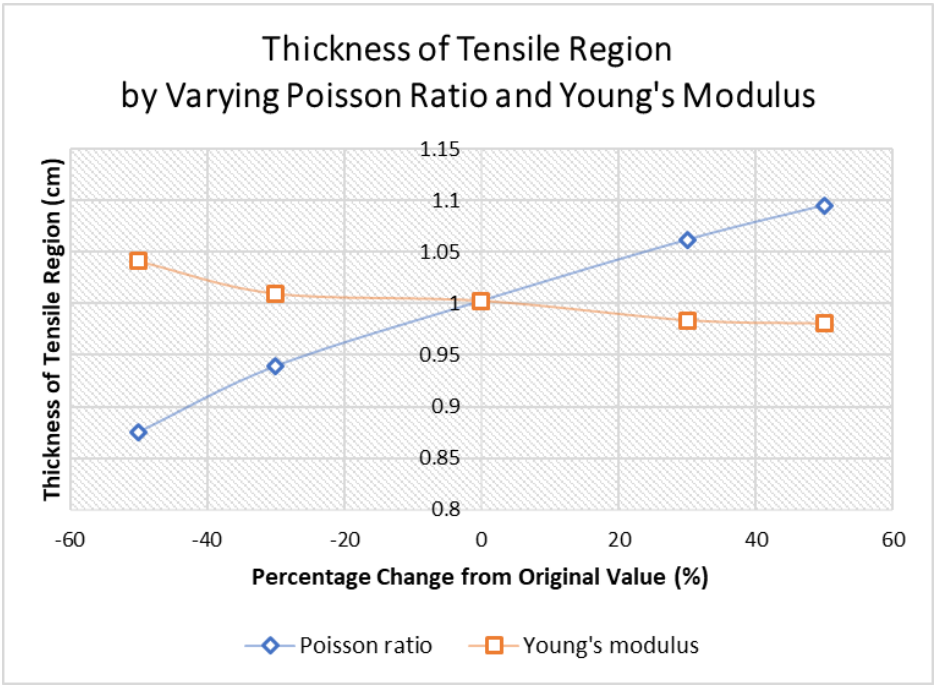


*Figure 28. Comparison between Poisson's ratio and Young's modulus sensitivity on the thickness of tensile region.*

Based on Figure 27 and Figure 28, both results show that Poisson's ratio line has a steeper slopes compared to Young's modulus. It means that changing Poisson's ratio has a more significant impact than changing Young's modulus on both maximum Sigma 3 and thickness of tensile region. Furthermore, the effect of those parameters contrast between the middle and outer layer will also be studied in this chapter, so a clear conclusion can be extracted from these simulations.

Further analysis regarding to the ratio of Poisson's ratio and Young's modulus between the middle and outer layer also performed in this study. The maximum Sigma 3 resulted from the modeling then plotted in a chart with the number of Poisson's ratio/Young's modulus of the middle layer on the x-axis and the outer layer on the y-axis. Then, linear interpolation between points is performed in Phyton 2.7 and the colormap in Figure 29 and Figure 30 are the results.

The range of Poisson's ratio used in these simulations is 0.1 - 0.4 for both outer and middle layer, as it is the reasonable range of Poisson's ratio for most of the rocks. There are 16 experiments performed in total and presented as the black dots. The Young's modulus of the layers are the same for all of the simulations, with the middle layer having a lower Young's modulus, 9.09 GPa compared to 29.9 GPa for the outer layers.

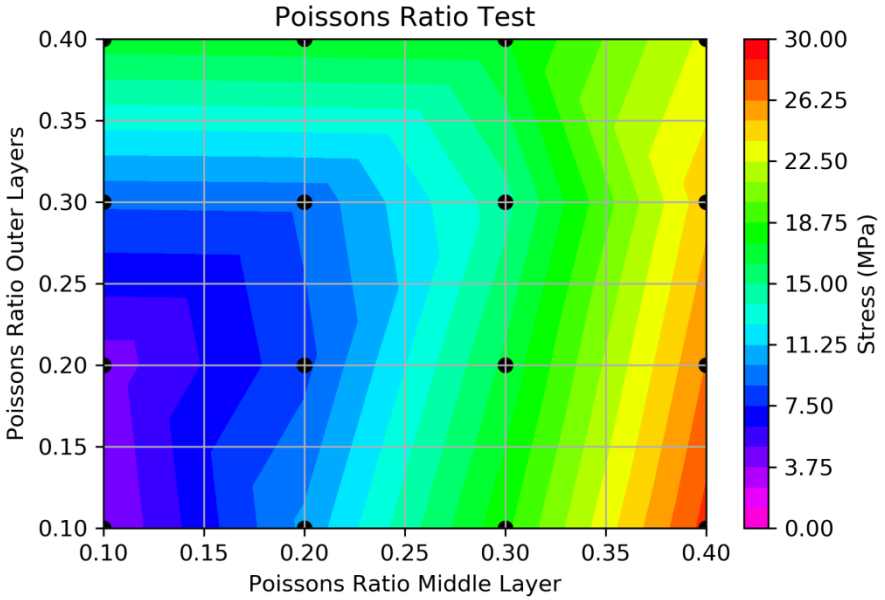


*Figure 29. Colormap of the maximum Sigma 3 for a variation of Poisson's ratio in both outer and middle layer, with constant Young's modulus, middle layer = 9.09 GPa, outer layers = 29.49 GPa, axial loading = 38.5 MPa and confining pressure = 0 MPa.*

Figure 29 indicates that the rise in maximum Sigma 3 is more significant by increasing the Poisson's ratio of the middle layer rather than the outer layer. By increasing the proportion of the Poisson's ratio of the middle layer to the outer layers, the generated maximum Sigma 3 will also increase. Nevertheless, even the proportion stays the same, but the number of Poisson's ratio keeps growing, then the resulted maximum Sigma 3 will always rise.

Next, similar simulations were performed to find out the effect of Young's modulus ratio between the middle and outer layers. In these experiments, the range of Young's modulus is 5-35 GPa for both middle and outer layers, while the Poisson's ratio remained the same, 0.206 for the middle layer and 0.154 for outer layers. The result in Figure 30 shows that no matter how high the number of Youngs' modulus, as long as it has the ratio of 1 between the outer and middle layer, then the resulted maximum Sigma 3 will always be the same. Also, same with the Poisson's ratio effect, the higher the

contrast of Young's modulus between the outer and middle layer, the greater the maximum Sigma 3 resulted.

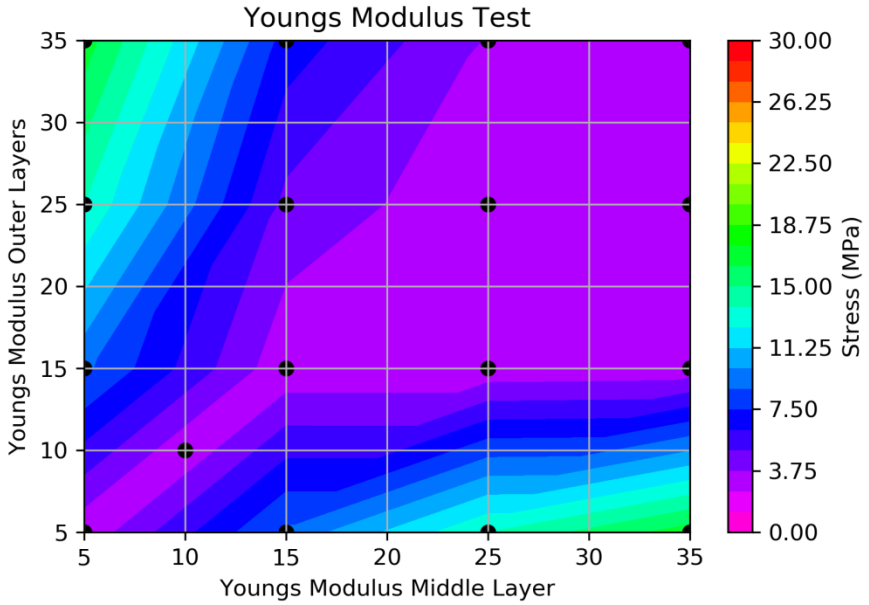


*Figure 30. Colormap of the maximum Sigma 3 for a variation of Young's modulus in both outer and middle layer, with constant Poisson's ratio, middle layer = 0.206, outer layers = 0.154, axial loading = 38.5 MPa and confining pressure = 0 MPa.*

From Figure 29 and Figure 30, it also can be concluded that the tensile stresses will always occur in this unconfined sample, regardless the number of Poisson's ratio or Young's modulus in the outer or middle layer.

The same study with a confining pressure of 15 MPa is also included and shown in Figure 31 and Figure 32. The results indicate the same pattern with the unconfined one, but with a more extreme value of maximum tensile stress produced. The white zone represents the value of which the tensile stress is not existing in the layered sample and the tensile fracture will not be generated as well.

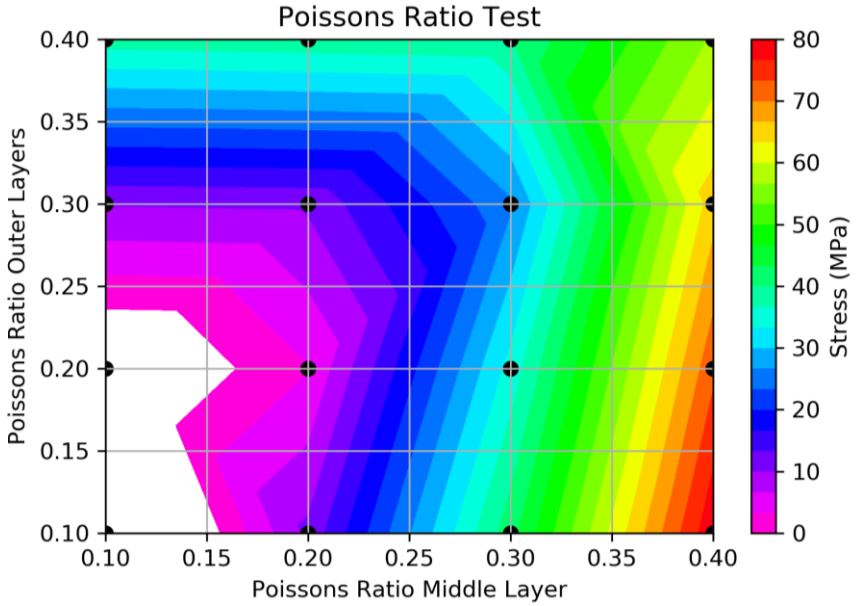


*Figure 31. Colormap of the maximum Sigma 3 for a variation of Poisson's ratio in both outer and middle layer, with constant Young's modulus, middle layer = 9.09 GPa, outer layers = 29.49 GPa, axial loading = 38.5 MPa and confining pressure = 15 MPa. The white zone is representing the compressive stress and no tensile stress occurs in the sample.*

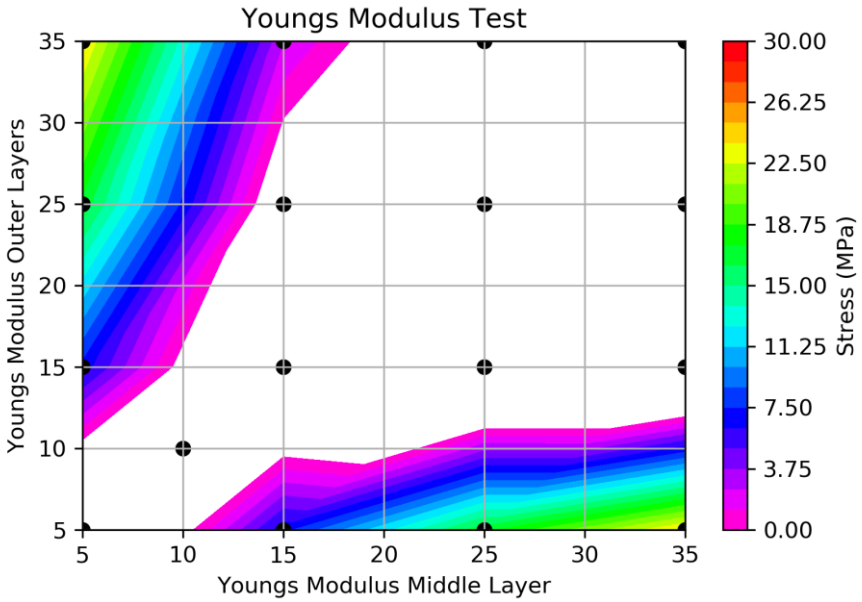


*Figure 32. Colormap of the maximum Sigma 3 for a variation of Young's modulus in both outer and middle layer, with constant Poisson's ratio, middle layer = 0.206, outer layers = 0.154, axial loading = 38.5 MPa and confining pressure = 15 MPa. The white zone is representing the compressive stress and no tensile stress occurs in the sample.*

The results from the simulations of 15 MPa confining pressure indicates that the magnitude of Poison's ratio is more important for the generation of tensile stresses. While in the Young's modulus the ratio of the outer and inner layer is more crucial than the magnitude for generating the tensile stresses.

## 4.4. Fracture Introduction and Its Impact on The Stress Distribution

The presence of tensile stresses are important for the generation of the tensile fracture but sometimes the magnitude is rather to low and need to be boosted to trigger the tensile failure. The propagation of a fracture from the weak layer seems to be the factor that might responsible for the tensile fracture generation in a low tensile stresses case.

Therefore, a fracture is introduced in the weak layer which extend to the interface. The combination of the stress field generated around the crack-tip and the existed tensile stresses in the strong layer will be examined. In order to determine the location of fracture initiation, the stress field of the sample was extracted from Abaqus model and then sorted in an excel file. The parameters needed for this analysis including node, minimum in-plane principle stress (Sigma 1), maximum in-plane principle stress (Sigma 3) and also X and Y coordinates.

The next process is to input the excel file into Matlab and write some codes to finally extract the location with the compressive stress (Sigma 1) higher than the sample ultimate strength. The X and Y coordinates will determine in which layer the node is located and will be the point of fracture initiation.

For sample L16, the fracture initiation is located on the bottom corner of the weak layer. Thus, one set of fracture is introduced starting from the bottom corner of the weak layer and extend to the layer interface. The fracture model orientation are based on the actual fracture of sample L16 in Figure 5 (a). So, the stress distribution around the crack-tip resulted from this model will hopefully represent the actual L16 sample. Figure 33 visualized the stress distribution of Sigma 1 and Sigma 3 of the fractured model.

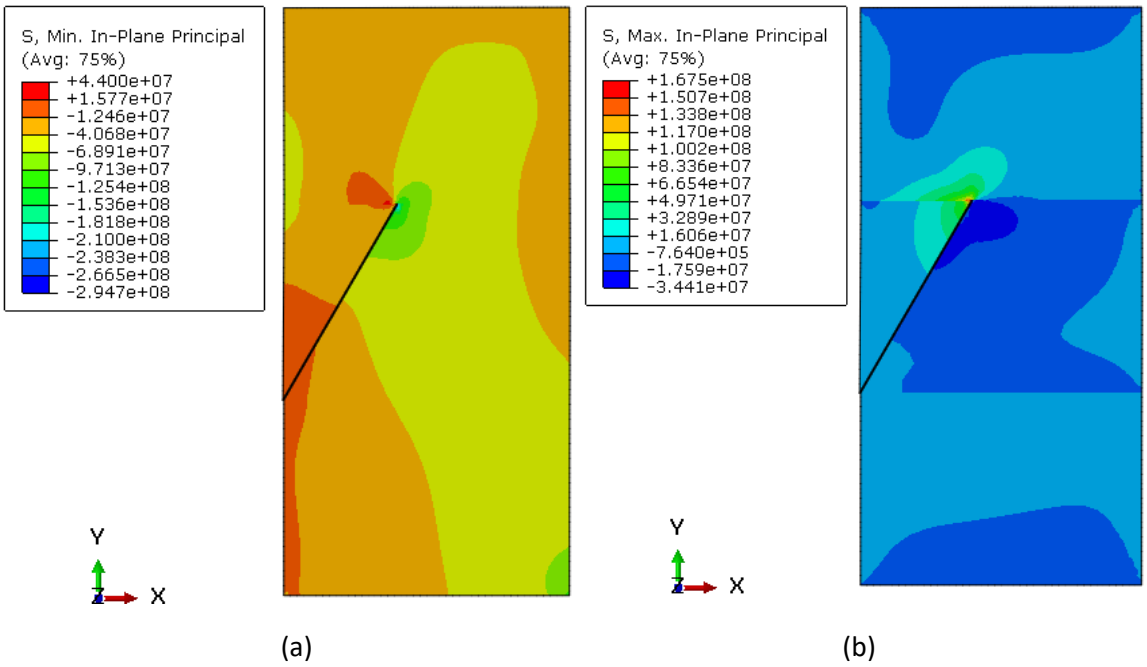


*Figure 33. Introducing a fracture to the weak layer (Bentheim sandstone) in sample L16 (Outer layer is Ainsa sandstone and middle layer is Bentheim sandstone) and its effect on (a) the Sigma 1 and (b) Sigma 3 distribution.*

Figure 33 shows that with the introduction of a fracture, the stress distribution is concentrated around the crack-tip. Figure 33 (a) indicates that the high compressive stresses of Sigma 1 around the crack-tip is concentrated in the weak layer, while Figure 33 (b) shows the concentration of high tensile stresses of Sigma 3 around the crack-tip is located in the strong layer.

The crack-tip stresses of Sigma 1 far exceed the ultimate strength of Bentheim sandstone in the middle, so a reflected shear fracture will be generated and propagate downward. At the same time, the tensile stresses of Sigma 3 around the crack-tip which concentrate in the top Ainsa sandstone also have an enormous value, and will trigger the initiation of a mode I opening/tensile fracture which will propagate upward. By comparing the results from fracture modeling with the real fractured sample of L16 in Figure 5, it can be concluded that the layered sample model is sufficient enough to represent the stress distribution of the real sample.

# 5. Discussion

## 5.1. Factors Affecting the Vertical Connectivity of Fractures in Layered Rocks

Differences in mechanical properties between adjacent layers affect the fracture behavior. In this study, the fracture propagation, aperture and orientation within mechanically layered rocks are observed. Besides, the contrast in mechanical properties is not the only factor that affects the fracture behavior. Confining pressure and layer interface properties such as interface strength and friction also have their own respective role, which will discuss further in this chapter.

### 5.1.1. Confining Pressure

A fracture initiating in the weak layer continues to propagate as long as the stress at the crack-tip is high enough to exceed the ultimate strength of the rock. Rock strength enhances with the increase of confining pressure (Fossen, 2010) and may prevent the neighboring fracture to develop in the stronger layer. Confining pressure is related to the burial depth, and many studies indicate that fractures are typically arrested at several kilometers burial depth (Valkó and Economides, 1995; Nolte and Economides, 2000; Yew and Weng, 2015). On the other hand, propagating fractures are more common at shallower depths (Odling *et al.*, 1999).

The results from this study show that the fractures tend to arrest in the weak layer when the confining pressure is considerably high. It is because at low or no confining pressure (in this experiment until 15 MPa), tensile stress can develop in the strong layer as the response from the rock strain contrast between strong and weak layer. This strain represented by the number of Poisson's ratio. The high contrast of Poisson's ratio between adjacent layers will result in a higher tensile stresses concentration in the strong layer and the greater the chance of tensile failure to occurs.

Even if the initial tensile stresses is not sufficient, the introduction of the shear fracture from the weak layer will disturb the stress distribution and generated an even higher tensile stresses around the tip of the fracture.

In contrast, sample L29 and L19 which experienced a 30 MPa and 40 MPa confining pressure respectively, only develop fracture in the weak layer. As the confining pressure increases, the sample will be under compression from every direction. The impact of strain contrast will be insignificant and tensile stresses will be overwhelmed by the compressive stresses.

Moreover, the strong layers experienced the compressive stresses but not high enough to overcome the rock strength. Then, it may act as stress barriers and tend to arrest propagating fracture in the weak layer (Gudmundsson and Brenner, 2001). The terms stress barriers mean the layers with high fracture-normal compressive stresses (Gudmundsson and Brenner, 2001). Also, the concentration of compressive stresses at the crack-tip is not sufficient for the fracture to develop in the strong layer.

### 5.1.2. Mechanical Contrast

The layered rocks samples consist of different lithologies generates the mechanical contrast between adjacent layers. Changes in mechanical properties, such as rock strength, Young's modulus and Poisson's ratio between adjacent layers influence the fracture propagation, aperture and orientation (Gross and Eyal, 2007, Ferrill *et al*., 2017).

The increasing mechanical contrast in a 15 MPa confining pressure comparison shows that the fractures in samples with mechanical contrast range from 1.1-5.2 propagate through the interface towards the strong layer. On the other hand, sample L32 with 7.1 mechanical contrast arrested the fractures in the weak layer. Brenner and Gudmundsson (2004) findings also in agreement with these results, they state that the fracture can be arrested at any depth if there is a high mechanical contrast between adjacent layers.

The effect of crack-tip stress also can be insignificant if the adjacent strong layer acts as the stress barriers, which may arise due to the elastic contrast (Gudmundsson and Brenner, 2001). Eventhough Gudmundsson and Brenner (2001) findings refer to the Young's modulus rather than rock strength, this information is still useful to this research, as Young's modulus is positively correlated with the rock strength.

### 5.1.3. Interface Strength

Interface strength can be divided into three categories, weak, moderate and strong contacts. Most sedimentary contacts are categorized into weak and strong contacts (Cooke and Underwood, 2001). The weak interface will have resulted in termination, moderate strength can produce step-over or termination, while strong contacts will allow fracture propagation across layers, illustrated in Figure 34.

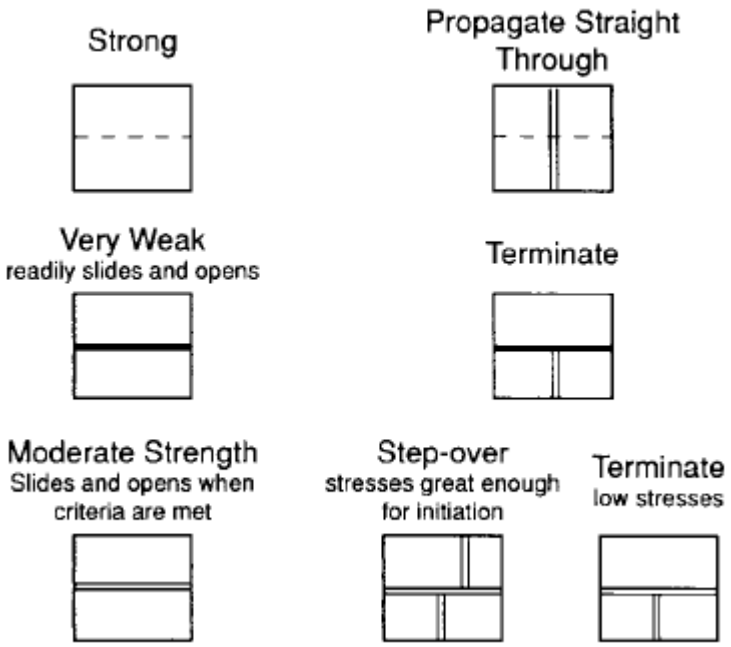


*Figure 34. Type of contact in layered rocks in term of its bonding strength and the impact on fracture continuity (Cooke and Underwood, 2001)*.

For moderate contacts, the local opening can have resulted in step over fractures, and if the stresses are not high enough to produce new fractures, then the parent fracture will terminate at the moderate-strength contact. Also, the study from Teufel and Clark (1984) shows that a decrease in friction along the interface will require more interface-normal compressive stress so that the fracture can continue to propagate across the interface.

In nature, fracture propagation has been observed through bedding contacts that silicified during diagenesis and appear well cemented (Cooke and Underwood, 2001). On the other hand, fracture termination has been observed at weak contacts such as unmineralized pre-existing joints (Dyer, 1988; Gross, 1993), thin organic layers (Cooke and Underwood, 2001), and uncemented bedding contacts (Narr and Suppe, 1991; Becker and Gross, 1996).

In the deeper subsurface, contact slip and opening are both inhibited. Increasing pressure in greater depth could suppress the small and localized contact opening that acts to terminate fractures. Thus, step-over fractures or fracture propagation may occur through the weak and moderate-strength interfaces. However, as the depth increase, the confining pressure also increases. This study and

Regelink (2018) show that high confining pressure (≥30 MPa) will inhibit the fracture propagation to the strong layer and contained it in the weak layer.

### 5.1.4. Effect of Friction on Layer Interface

Understanding the distribution of stress in different mechanical layers is essential to the interpretation of fracture networks. The response from the rocks to stress have a significant impact on fracture propagation. The modeling results in Figure 21 and Figure 22 show that the presence of tensile stresses will always result in fracture propagation.

Friction at crack or layer interface will alter the stress distribution within the rock body. In the extreme cases of friction at the interface, there will be bonded and unbonded interface. Under remote compressive stresses, contrasts of elastic properties between adjacent bonded rock layers may trigger the fractures propagation to occur within the layered rocks in the subsurface (Bourne, 2003).

Typically in the subsurface, stresses are coming from all direction forming a compressive force to the rock bodies, but the contrast of elastic properties between layers can provide a mechanism for the tensile stress to occur (Figure 35). The tensile stresses may arise without the requirement for an additional body force such as internal fluid pressure (Bourne, 2003).

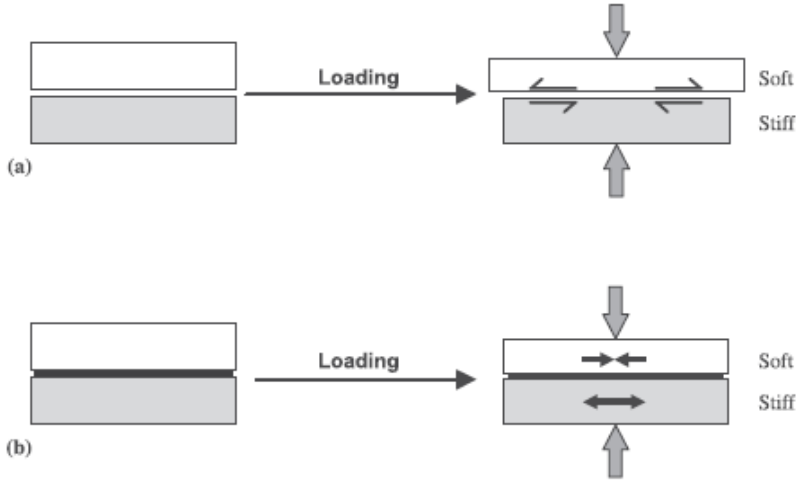


*Figure 35. The effect of bonding in layered rocks. (a) Free-slip occurs along the interface for the unbonded case and the stress within each layer is identical to the remote load. (b) The bonded one will have no slip and tensile stress will occur in the stiff layer (Bourne, 2003).*

Figure 35 demonstrates the effect of bonding in layered rocks. The unbonded interface will result in free-slip along the interface and no stress transfer will occur between the adjacent layers. On the other hand, the bonded interface will cause the horizontal components of stress to be discontinuous and differ between adjacent layers, with the stiff layer concentrate on the tensile stress.

Abaqus model in this study designed with the bonded interface, thus the tensile stresses concentration is expected in the strong layer. This mechanism is responsible for the fracture refraction across layers and tensile failure to occur in the strong layer.

### 5.1.5. Change in aperture across different layers

Mechanical properties of the rocks contribute to the changes in fracture aperture across layers. The strong layer with high Young's modulus produced fractures with less aperture compared to the weak layer. It happens because rock with high Young's modulus resists more to fracture opening than the one with low Young's modulus (Gudmundsson, 2011).

The results from image analysis in Matlab shows that the average fracture aperture in the weak layer is decreasing with increasing confining pressure. It also seems in Figure 16 (a) that the decline is quite

linear from 0 – 40 MPa. As the fracture aperture decrease with increasing confining pressure, the fracture porosity and permeability also declining as well (Watanabe *et al.*, 2011; Li, Huo and Benson, 2014).

As mentioned before, the remote loading has an impact on the fracture aperture. Under compression, the stiff layer built up more compressive stress and inhibit the opening of the fracture (Brenner and Gudmundsson, 2004). It is also the case in increasing mechanical contrast experiment, when the contrast is getting higher, the average aperture difference between the strong and weak layer also becomes greater due to the increase of compressive stresses concentration in the strong layer. This average aperture plays an important role in fluid flow, Li, Huo and Benson (2014) state that the average aperture and aperture variance directly influence the capillary pressure, with the former has the larger impact.

### 5.1.6. Change in orientation across different layers

There are several factors that can cause fracture refraction in layered rocks, one of them is the switching from shear to tensile fracture due to the difference in mechanical properties of the adjacent rock layers (Ferrill *et al*., 2017). Mandl (1988) proposed that fracture angle is subjected to rock mechanical properties and effective stress at the time of failure.

Álso, fracture orientation is generally related to the fracturing mode, with mode I opening fracture characterized by a highly steep orientation (≈90°), while shear fractures developed with a moderate dip (≈50°) (A. Ferrill and Morris, 2003; Roche, Homberg and Rocher, 2012). The steep angled tensile fracture occurs in the strong layer and more gently angle shear fracture in the weak layer (Ferrill *et al.*, 2017).

Figure 8 shows that the orientation of fractures change when it passes through the layer interface of different mechanical layers for sample with 4.8 and 5.2 mechanical contrast. In the same figure, sample L13 with 1.1 mechanical contrast in a 15 MPa confining pressure have a rather similar orientation in all layers. When the adjacent layers have similar mechanical properties, the tensile stress did not occur, all layers concentrate on compressive stresses and generated shear fractures when it reaches the failure point.

However, the experiment by Regelink (2018) found that when the confining pressure is not introduced in the experiment, the low mechanical contrast (1.1) can generate a tensile fracture in the strong layer as well. So, it can be concluded that the combination of confining pressure and mechanical contrast has a significant role in the occurrence of the tensile fracture and therefore the changes in orientation across layer interface.

## 5.2. The implication of Fracture Behavior for The Layered Reservoir and Fluid Flow

The study of mechanical contrast and confining pressure effect on the fracture propagation will give some insight about the quality of the reservoir and the seal rock. The presence of propagating fractures within the layered reservoir will increase its permeability and may provide vertical connectivity with other separated reservoir targets (Gross and Eyal, 2007). On the other hand, if the propagating fractures occur in the seal rock, the integrity of the seal rock will be threatened and will cause leakage of the reservoir fluid (Lavrov, 2016).

Furthermore, the permeability of a fracture is approximately proportional to the cube of its aperture (Oron and Berkowitz, 1998). However, in order to get a more reliable fracture permeability calculation, more aspects of the fracture need to be included in the assessment. Those aspects include internal compositions, geometries, and diagenetic history (e.g., block size, tortuosity, mineralization, fracture and segment orientation, density, and aperture) (Odling, 2001; Laubach *et al.*, 2004). Also, Gross and

Eyal (2007) suggest that a propagating fracture can become the main flow conduits if its length and aperture are at least one order of magnitude greater than the arrested fracture.

Moreover, accurately interpret 3D natural fracture distribution can help the estimation of the resource and recoverable potential early in field life. It will also contribute to optimizing the well placement and completion design for efficient production planning (Pietraszsek-Mattner *et al.*, 2017).

### 5.2.1. Effect of Fracture Type for The Reservoir Quality

This study shows that there are two types of fracture generated from the fracturing of layered rocks sample, namely mode I opening/tensile fracture and mode II sliding/shear fracture. The micro-CT scan images show that Mode I opening fracture provide a clear space for fluid storage and flow. However, Zoback (2007) proposes that mode I opening fractures are less likely to affect fluid flow in the reservoir because their aperture is insignificant at depth.

If preserved, mode I opening fractures is more favorable for fluid flow as it always has less aperture variation compare with the shear fracture, as shown in Figure 17. Thus, less channeled fluid flow is expected to occur because small aperture variations mean less irregular aperture geometry (Brown, Caprihan and Hardy, 1998). Mode I opening fracture is more likely to preserves its open space at a few hundred meters deep of the solid crust. They are related to deformation under low or no confining pressure and formed at low differential stress. However, mode I opening fracture can also occur when the high fluid pressure present in the deeper subsurface and reduces the effective stress (Loosveld and Franssen, 1992).

On the other hand, even if the shear fracture in this study is not showing clear aperture like the one in the tensile fracture, but there are some parts of the shear fracture network which provide open space for fluid storage and flow. Shear fractures often have irregular geometry and its slip movement may results in dilation of steep fracture segment, generating releasing overlaps zones (jogs) which can be preserved as open space along the fracture plane even at depths of kilometers (Ferrill *et al.*, 2014). Jogs and irregularities on the fracture surfaces are responsible for the openings along the shear fracture, which illustrated in Figure 36 (Wennberg *et al.*, 2016). However, the fluid flow in the shear fracture tends to be channeled in the releasing overlap zones and resulting in a strong flow anisotropy (Peacock and Anderson, 2012).

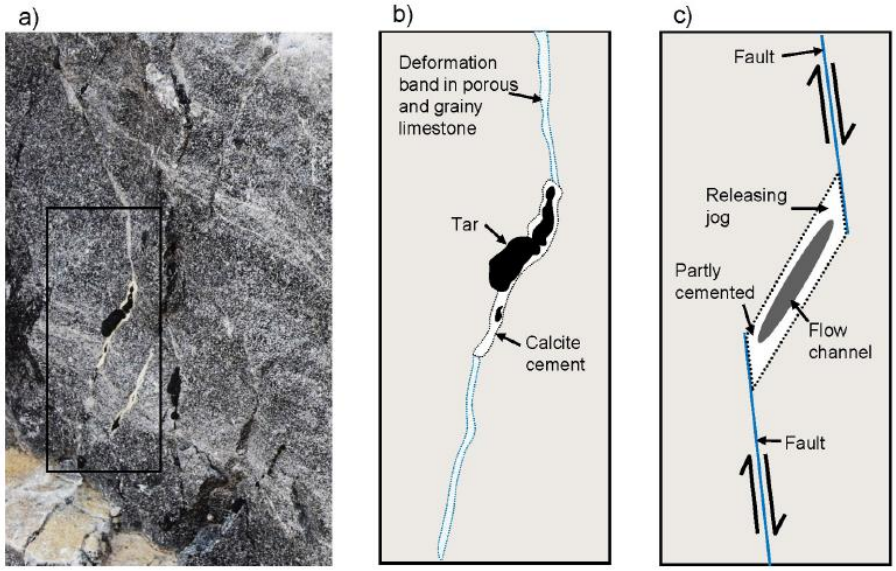


*Figure 36. Opening in a shear fracture in the form of releasing overlap (jog). (a) Photograph with a tar-filled jog, (b) simplified drawing of the section in black rectangle in (a) and (c) schematic interpretation of the jog* (Wennberg *et al.*, 2016).

Therefore, in the deep-layered reservoir with high confining pressure, a low mechanical contrast between adjacent layers is preferred so that the propagating shear fracture can be generated and provided open spaces for fluid flow. On the other hand, higher mechanical contrast is desirable for the shallow layered reservoir, because it can generate tensile fractures in the strong layer and the aperture might be preserved in the lower confining pressure condition.

### 5.2.2. Effect of Fracture Aperture Distribution on Fluid Flow

The distribution of fracture apertures in the reservoir have quite some impact on the flow of the reservoir fluid. Wang, Wu and Zhou (2017) experiment shows that the value of both average and standard deviation of fracture aperture will affect the capillary pressure-saturation relation. The average aperture has a bigger impact on capillary pressure compare to aperture distribution (Li, Huo and Benson, 2014).

Figure 37 (a) illustrates that when the average aperture increases, the capillary pressure-saturation curve will be steeper. It means that only a small boost of pressure needed to produce the fluid when the average aperture is high (0.5 mm). In the case of standard deviation, which shown in Figure 37 (b), more qualitative assessment is needed. At saturation range from 0.8 - 0.2, it is clear that with increasing standard deviation, the pressure required for the water to flow is also rising.

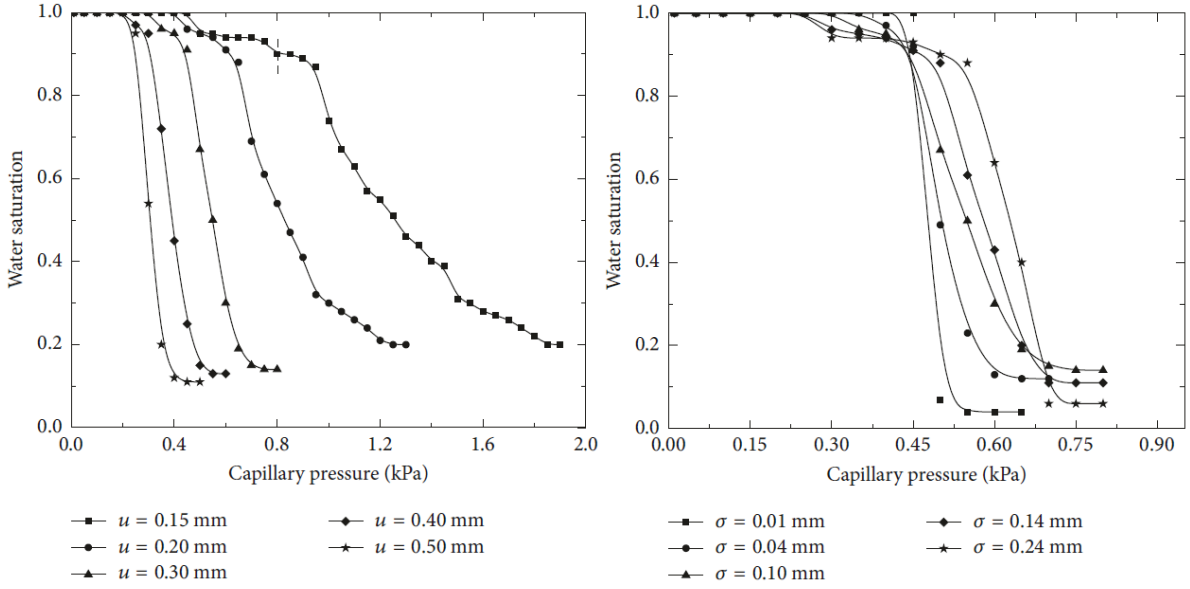


(a) (b)

*Figure 37. Capillary pressure-saturation curve response with increasing average aperture (a) and increasing standard deviation (b) (Wang, Wu and Zhou, 2017).*

In addition, Figure 37 shows that at some point, increasing the pressure will not reduce water saturation anymore. The saturation point at which the capillary pressure end is the fraction of trapped water in the fracture. Figure 37 (a) shows that as the average aperture decreases, the amount of trapped water increase. At the same time, there is no exact conclusion can be taken from increasing standard variation in the case of the amount of trapped water.

Results from image analysis in Matlab in Figure 17 shows that with increasing confining pressure, the standard deviation of the aperture will decrease. However, the experiment from Li, Huo and Benson (2014) indicates the opposite. By applying higher confining pressure, the fracture aperture will decrease. Consequently, the average aperture is smaller, more heterogeneous and makes the standard variation raise. The possible explanation might come from the setup difference between Li, Huo and Benson (2014) and Regelink (2018) experiment. Li, Huo and Benson (2014) introduce the fluid

flow within the sample and considering the effect of pore pressure, while Regelink (2018) use dried samples and refer to confining pressure rather than effective stress.

Figure 17 also indicates that fracture aperture distributions spread more from its average value as the mechanical contrast increases. It happens for both weak and strong layer, but with a different pace, as the weak layer has a steeper increase compared to the strong layer. Understanding the effect of confining pressure and mechanical contrast on aperture standard variation is useful for realizations of friction factor, as it is included in the calculation along with fracture surface contact area and shapes of the obstructions (Walsh, 1981; Zimmerman, Chen and Cook, 1992; Renshaw, 1995). Within a fracture, friction factor will multiply the stresses on crack-tip (Ballarini and Plesha, 1987) and for layer interface, it determined the fracture containment (Eshiet and Sheng, 2017) and the amount of stress transfer between adjacent layers (Bourne, 2003).

## 5.3. The effect from Micro-CT scan Resolution

The results from Regelink (2018) and Douma *et al.* (2017) experiments consist of two different resolution of Micro-CT scan images, half and full resolution. All of the samples in this study have half resolution because not all of the samples have the full one. So, comparing these two types of Micro-CT scan image will be useful for the next similar study.

The sample used for this study is L37, consists of Bentheim sandstone in the middle of Beringen sandstone. Figure 38 shows the comparison of Micro-CT scan image with half resolution on the left (a) and full resolution on the right (b).

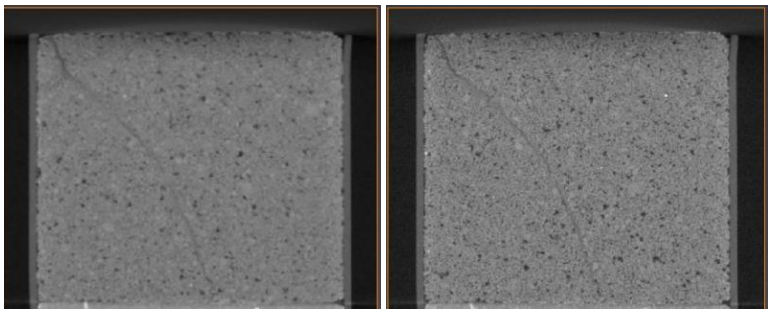

(a) (b)

*Figure 38. Comparison between half resolution (a) and full resolution (b) Micro-CT scan image of sample L37.*

The image looks sharper in the full resolution, especially for the fracture part. Then, those images were thresholded and the results in Figure 39 will be the input for image analysis in Matlab. The thresholding results also indicate some differences, the fracture in Figure 39 (b) which is from the full resolution one is more continuous compared to Figure 39 (a). In other words, more part of the fracture was discovered in full resolution Micro-CT scan image.

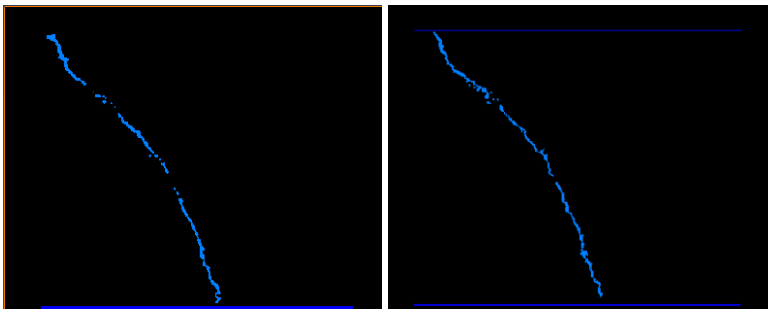

(a) (b)

*Figure 39. Comparison between thresholding results from half resolution (a) and full resolution (b) Micro-CT scan image of sample L37.*

However, the thresholding process for those to images is not necessarily the same. The full resolution requires more and rather complex step to remove the noise and bring up the fracture. It is only natural as the full resolution catch more details of the rock component, which might have the same color frequency with the fracture itself.

Next, images in Figure 39 were analyzed in Matlab and resulted in fracture aperture and orientation for each image. The analysis for both figures is exactly the same, using the identical coding from scanning the image until calculating the average value. Figure 40 compares the result from the fracture aperture between (a) half resolution and (b) full resolution.

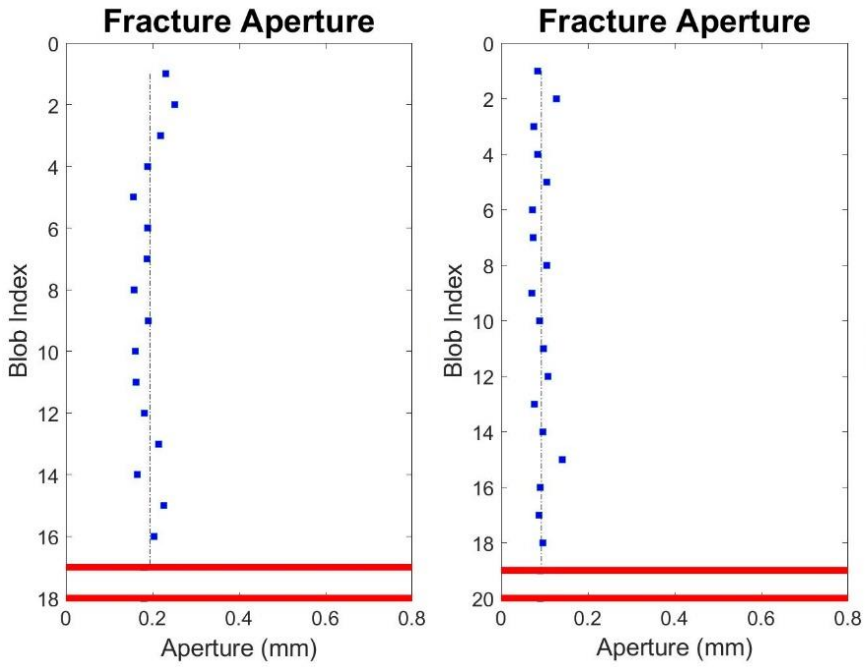


(a) (b)

*Figure 40. Aperture measurement comparison between half resolution (a) and full resolution (b) Micro-CT scan image of sample L37.*

The difference between aperture from half and full resolution is quite substantial. The average aperture of half resolution is 0.1944, twice the average aperture of full resolution, 0.0972. The immense difference mostly comes from the multipliers from pixels to mm, in this case is voxel size from Avizo. The voxel size for half resolution is 0.06 while in full resolution is 0.03. However, it is not the only reason the full resolution having a smaller average aperture. Even if the voxel size is the same, the full resolution will have a slightly smaller average aperture equal to 0.1855, 4.6% less than the half resolution.

Figure 41 shows the orientations reading from (a) half resolution and (b) full resolution. The average aperture calculation is also different for the two of them, 60.88 for half resolution and 58.94 full resolution. The difference was expected because the thresholding results also quite dissimilar and might alter the calculation of the average orientation. However, from Figure 41, it is quite visible that the orientation pattern is similar and none of the blobs is too far off from each other.

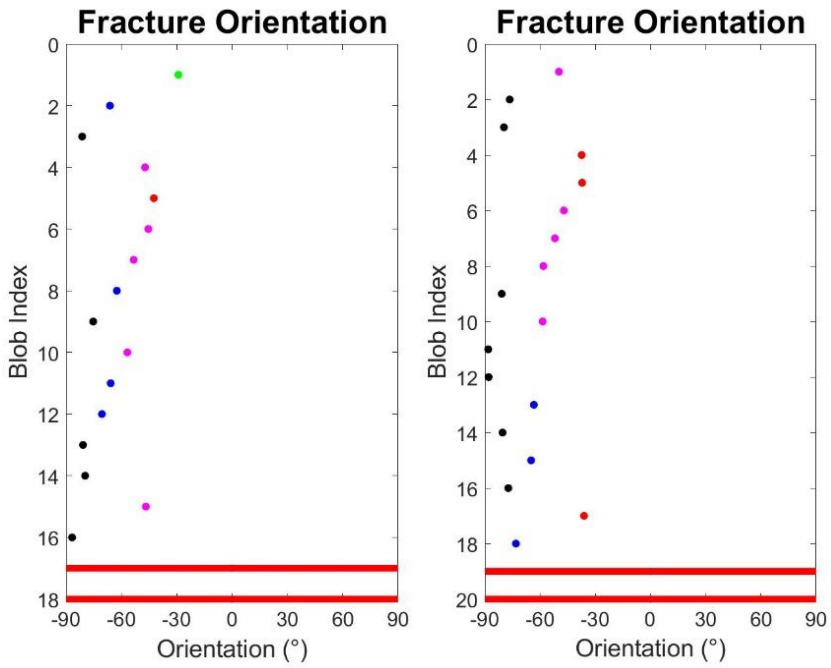


(a) (b)

*Figure 41. Orientation measurement comparison between half resolution (a) and full resolution (b) Micro-CT scan image of sample L37.*

The observation was also performed in two other slices from sample L37, the results always indicate that the full resolution Micro-CT scan image has a smaller aperture compared to the half one. The reason might come from the voxel size that used in thresholding the images, the full resolution using smaller voxel size which can detect the fracture more precisely than the voxel size used in half resolution.

# 6. Conclusions and recommendations

Various aspects on the impact of increasing confining pressure or mechanical contrast on mechanically-layered rocks are analyzed in this study. Main focuses of this study are as follows: (1) fracture growth in a layered rocks, (2) the characteristics of fractures in each layer, including aperture and orientation, and (3) stress distribution in layered samples. After careful investigation, several main ideas can be concluded from this study and some recommendations are provided for future research on this topic.

## 6.1. Conclusions

This study shows the impact of (1) mechanical contrast and (2) confining pressure on the fracture behavior in layered rocks. Fracture propagation and arrest highly depend on these two factors. Fracture tends to propagate through layer interface when the mechanical contrast between adjacent layers and the confining pressure are low. On the other hand, fracture arrest is expected in a high mechanical contrast, which in this study is found at 7.1 in a 15 MPa confining pressure.

In the increasing confining pressure group, the lithologies are the same between the samples and the strength ratio between Ainsa sandstone and Bentheim sandstone generates a 4.8 mechanical contrast. By comparing those samples with various confining pressure, this study shows that at 30 MPa and higher, the fractures are contained in the weak layer (Bentheim sandstone) and propagate at lower confining pressures.

The fracture characteristics such as aperture and orientation indicate some notable changes when it crosses adjacent layers with contrasting mechanical properties. The fracture in the weak layer developed at a gentler dip (around 50°) compared to the ones in the strong layer and can be categorized as a shear fracture. When the fracture propagates through the layer interface, it is refracted to almost vertical tensile fracture in the strong layer. However, at a very low mechanical contrast around 1.1 in a 15 MPa confining pressure, the fracture aperture and orientation did not change when a fracture propagates from one layer to another.

The orientation of the fractures is related to the fracture mode. Vertical fractures associated with mode I opening/tensile fracture and a gentler dip fractures categorized as mode II sliding/shear fracture. The fracture aperture is generally wider in the weak layer (shear fracture) compared to the ones in the strong layer (tensile fracture). However, the shear fracture in the weak layer usually accompanied by the zone of cataclastic flow while the tensile fracture has a more clear pathway for fluid flow.

Mode I opening/tensile fractures are less likely to affect fluid flow in the reservoir because their aperture is insignificant at depth. While in mode II sliding/shear fractures, only several parts along the fracture that can provide the open space, which depend on the presence of jogs and irregularities on the fracture surfaces.

Therefore, in the deep-layered reservoir with high confining pressure, a low mechanical contrast between adjacent layers is preferred so that the propagating shear fracture can be generated and provided open spaces for fluid flow. On the other hand, higher mechanical contrast is more desirable for the shallow layered reservoir. Thus, the tensile fractures can develop in the strong layer and the aperture might be preserved in the lower confining pressure condition.

Furthermore, average fracture aperture and distribution have a significant role in capillary pressure; the higher average aperture will reduce the amount of pressure needed to flow the fluid. On the other hand, a higher number of aperture standard deviation (aperture distribution) means that the fracture has a higher tortuosity and will require higher pressure to makes the fluid to flow.

The results from fracture measurement show that with increasing confining pressure, the average aperture and aperture distribution will reduce in the weak layer. On the other hand, increasing mechanical contrast have a positive impact on the average aperture and distribution in the weak layer. Even though the effect of those two results seems to cancel out, but the average aperture has a bigger impact on capillary pressure compare to aperture distribution. Thus, it can be concluded that by increasing the confining pressure or decreasing the mechanical contrast, the required pressure for fluid to flow is increasing.

The modeling results confirm that a region of tensile stresses presents around the interface in the strong layer, which is needed to create tensile fractures. The tensile stresses occur because of the stress transfer between adjacent stiff and soft layer with a bonded interface. Even if the tensile stresses is rather small, the introduction of fracture which propagates to the layer interface is essential, as the crack-tip can greatly enhance the tensile stresses. Also, Confining pressure has an important role in the presence of tensile stresses in the strong layer; as the confining pressure increases, the tensile stress distribution is reduced in thickness and vanished at some point (Figure 23).

The sensitivity study shows that Poisson's ratio has a more significant impact compared to Young's modulus on both maximum tensile stress and thickness of tensile region. Higher Poisson's ratio resulting in higher tensile stresses, while on Young's modulus it depends more to the contrast between adjacent layers rather than the magnitudes itself (see Figure 31 and Figure 32).

Understanding the fracture behavior in layered rocks is beneficial for reservoir characterization, as fractures can enhance the permeability and providing vertical connectivity between isolated reservoirs. Accurately interpret 3D natural fracture distribution can help the estimation of the resource and recoverable potential early in field life. It will also contribute to optimizing the well placement and completion design for efficient production planning.

## 6.2. Recommendations

There are several points that can improve the accuracy and quality of the study on fracture behavior within a layered rocks sample. First, the interface friction and accurate Poisson's ratio and Young's modulus for every confining pressure condition needs to be known and included as one of the parameters in the Abaqus model. The inclusion of these parameters will alter the stress distribution, which is important in this study because the presence of tensile stress depends on them and is crucial for the generation of tensile fracture in the strong layer.

In addition, the fracture friction will also alter the stress distribution, especially at the crack-tip. The stress distribution at the crack-tip is important as it is the main factor that will determine either the fracture will be propagated or arrested at the layer interface.

Lastly, based on the results comparison between the half and full resolution micro-CT scan image, it is recommended to use the images from full resolution. It is because full resolution image visualized the fracture in more detail and will affect the measurement of the fracture, especially the fracture aperture.

# Bibliography


A. Ferrill, D. and Morris, A. (2003) 'Dilational normal faults', *Journal of Structural Geology*. doi: 10.1016/S0191-8141(02)00029-9.

Ballarini, R. and Plesha, M. E. (1987) 'The effects of crack surface friction and roughness on crack tip stress fields', *International Journal of Fracture*, 34(3), pp. 195–207. doi: 10.1007/BF00019717.

Becker, A. and Gross, M. R. (1996) 'Mechanism for joint saturation in mechanically layered rocks: an example from southern Israel', *Tectonophysics*, 257(2–4), pp. 223–237. doi: 10.1016/0040-1951(95)00142-5.

Bonnell, B. and Hurich, C. (2008) 'Characterization of Reservoir Heterogeneity : An Investigation of the Role of Cross-Well Reflection Data', pp. 32–38.

Bourne, S. J. (2003) 'Contrast of elastic properties between rock layers as a mechanism for the initiation and orientation of tensile failure under uniform remote compression', *Journal of Geophysical Research*, 108(B8), p. 2395. doi: 10.1029/2001JB001725.

Brenner, S. L. and Gudmundsson, A. (2004) 'Arrest and aperture variation of hydrofractures in layered reservoirs', *Geological Society, London, Special Publications*, 231(1), pp. 117–128. doi: 10.1144/GSL.SP.2004.231.01.08.

Brown, S., Caprihan, A. and Hardy, R. (1998) 'Experimental observation of fluid flow channels in a single fracture', *Journal of Geophysical Research*, 103(B3), p. 5125. doi: 10.1029/97JB03542.

Cooke, M. L. and Underwood, C. A. (2001) 'Fracture termination and step-over at bedding interfaces due to frictional slip and interface opening', *Journal of Structural Geology*, 23(2–3), pp. 223–238. doi: 10.1016/S0191-8141(00)00092-4.

Douma, L. A. N. R. *et al.* (2017) 'The influence of rock-mechanical properties on fracture characteristics in finely-layered reservoirs', *51 st US Rock Mechanics/Geomechanics Symposium. American Rock Mechanics Association*.

Dyer, R. (1988) 'Using joint interactions to estimate paleostress ratios', *Journal of Structural Geology*, 10(7), pp. 685–699. doi: 10.1016/0191-8141(88)90076-4.

Eshiet, K. I. I. and Sheng, Y. (2017) 'The role of rock joint frictional strength in the containment of fracture propagation', *Acta Geotechnica*. Springer Berlin Heidelberg, 12(4), pp. 897–920. doi: 10.1007/s11440-016-0512-2.

Ferrill, D.A., McGinnis, R.N., Morris, A.P., Smart, K.J., Sickmann, Z.T., Bentz, M., Lehrmann, D., Evans, M.A. (2014) 'Control of mechanical stratigraphy on bedrestricted jointing and normal faulting: eagle Ford Formation, south-central Texas, U.S.A', *AAPG Bull,* 98, 2477-2506.

Ferrill, D. A., Morris, A. P., McGinnis, R. N., Smart, K. J., and Wigginton, S. S. (2017) 'Mechanical stratigraphy and normal faulting', *Journal of Structural Geology*, 94:275-302.

Fossen, H. (2010) *Structural Geology*, Cambridge: Cambridge University Press. doi: 10.1017/CBO9780511777806.

Grammer, G. M., Harris, P. M. "Mitch" and Eberli, G. P. (2004) 'Integration of Outcrop and Modern Analogs in Reservoir Modeling: Overview with Examples from the Bahamas', *Integration of Outcrop and Modern Analogs in Reservoir Modeling*. *American Association of Petroleum Geologists.*

Gross, M. R. (1993) 'The origin and spacing of cross joints: examples from the Monterey Formation, Santa Barbara Coastline, California', *Journal of Structural Geology*, 15(6), pp. 737–751. doi: 10.1016/0191-8141(93)90059-J.

Gross, M. R. and Eyal, Y. (2007) 'Throughgoing fractures in layered carbonate rocks', *Bulletin of the Geological Society of America*, 119(11–12), pp. 1387–1404. doi: 10.1130/0016-7606(2007)119[1387:TFILCR]2.0.CO;2.

Gudmundsson, A. (2011). *Rock Fractures in Geological Processes*. Cambridge University Press, Cambridge, United Kingdom.

Gudmundsson, A. and Brenner, S. L. (2001) 'How hydrofractures become arrested', *Terra Nova*, 13(6), pp. 456–462. doi: 10.1046/j.1365-3121.2001.00380.x.

Laubach, S. E. *et al.* (2004) 'Opening histories of fractures in sandstone', *Geological Society, London, Special Publications*, 231(1), pp. 1–9. doi: 10.1144/GSL.SP.2004.231.01.01.

Lavrov, A. (2016) 'Dynamics of stresses and fractures in reservoir and cap rock under production and injection', *Energy Procedia*. Elsevier B.V., 86(1876), pp. 381–390. doi: 10.1016/j.egypro.2016.01.039.

Li, B., Huo, D. and Benson, S. M. (2014) 'Investigating Aperture-Based Stress-Dependent Permeability and Capillary Pressure in Rock Fractures', *SPE Annual Technical Conference and Exhibition*, (September), pp. 2014–2015. doi: 10.2118/170819-MS.

Loosveld, R. J. H. and Franssen, R. C. M. W. (1992) 'Extensional vs. shear fractures; implications for reservoir characterisation', *Proceedings; European petroleum conference; Moving the frontiers, sharing solutions; Volume 2.*, pp. 23–30. doi: 10.2118/25017-MS.

Mandl, G., 1988. *Mechanics of Tectonic Faulting, Models and Basic Concepts*. Elsevier, 407 pp.

Narr, W. and Suppe, J. (1991) 'Joint spacing in sedimentary rocks', *Journal of Structural Geology*, 13(9), pp. 1037–1048. doi: 10.1016/0191-8141(91)90055-N.

Nolte, K. G. and Economides, M. J. (2000) *Reservoir stimulation*. Chichester, West Sussex: John Wiley & Sons.

Odling, N. E. *et al.* (1999) 'Variations in fracture system geometry and their implications for fluid flow in fractures hydrocarbon reservoirs', *Petroleum Geoscience*, 5(4), pp. 373–384. Available at: http://dx.doi.org/10.1144/petgeo.5.4.373.

Odling, N. E. (2001) 'The scaling of hydraulic conductivity in rock fracture zones', *Geophysical Research Letters*, 28(15), pp. 3019–3022. doi: 10.1029/2000GL011863.

Oron, A. P. and Berkowitz, B. (1998) 'Flow in rock fractures: The local cubic law assumption reexamined', *Water Resources Research*, 34(11), pp. 2811–2825. doi: 10.1029/98WR02285.

Peacock, D. and Anderson, M. (2012) 'The scaling of pull-aparts and implications for fluid flow in areas with strike-slip faults', *Journal of Petroleum Geology*. doi: 10.1111/j.1747-5457.2012.00537.x.

Philipp, S. L. and Reyer, D. (2010) 'Mechanical rock properties , fracture propagation and permeability development in deep geothermal reservoirs', 12, p. 11145.

Pietraszsek-Mattner, S. *et al.* (2017) 'Predicting the Impact of Natural Fractures on Reservoir Performance', *22nd World Petroleum Congress*. Istanbul, Turkey: World Petroleum Congress, p. 9.

Regelink, J. A. (2018) 'Influence of Mechanical Contrast and Confining Pressure on Fracture Behaviour in Layered Rocks'.

Renshaw, C. (1995) 'On the relationship between mechanical and hydraulic apertures in rough-walled fractures', *Journal of Geophysical Research*. doi: 10.1029/95JB02159.

Roche, V., Homberg, C. and Rocher, M. (2012) 'Architecture and growth of normal fault zones in multilayer systems: A 3D field analysis in the South-Eastern Basin, France', *Journal of Structural*

*Geology*. Elsevier Ltd, 37, pp. 19–35. doi: 10.1016/j.jsg.2012.02.005.

Sirat, M. *et al.* (2014) 'Mechanical Layering: Implications for Hydraulic Fracturing in an Unconventional Tight Carbonate Reservoir in Abu Dhabi, UAE', *SPE/EAGE European Unconventional Resources Conference and Exhibition*. Vienna, Austria: Society of Petroleum Engineers, p. 9. doi: 10.2118/167738-MS.

Teufel, L. W. and Clark, J. A. (1984) 'Hydraulic Fracture Propagation in Layered Rock: Experimental Studies of Fracture Containment', *Society of Petroleum Engineers Journal*. doi: 10.2118/9878-PA.

Valkó, P. and Economides, M. J. (1995) *Hydraulic fracture mechanics*. Chichester: Wiley.

Walsh, J. B. (1981) 'Effect of pore pressure and confining pressure on fracture permeability', *International Journal of Rock Mechanics and Mining Sciences & Geomechanics Abstracts*. doi: 10.1016/0148-9062(81)90006-1.

Wang, Y., Wu, C. and Zhou, Y. (2017) 'Effect Study of Aperture Distribution on the Capillary Pressure-Saturation Relation for the Single Fracture', *Geofluids*. doi: 10.1155/2017/9656393.

Watanabe, N. *et al.* (2011) 'X-ray CT based numerical analysis of fracture flow for core samples under various confining pressures', *Engineering Geology*. Elsevier B.V., 123(4), pp. 338–346. doi: 10.1016/j.enggeo.2011.09.010.

Wennberg, O. P. *et al.* (2016) 'The characteristics of open fractures in carbonate reservoirs and their impact on fluid flow: a discussion', *Petroleum Geoscience*.

Yew, C. H. and Weng, X. (2015) *Mechanics of hydraulic fracturing*. Gulf Professional Publishing.

Zimmerman, R. W., Chen, D. W. and Cook, N. G. W. (1992) 'The effect of contact area on the permeability of fractures', *Journal of Hydrology*, 139(1–4), pp. 79–96. doi: 10.1016/0022-1694(92)90196-3.

Zoback, M. D. (2007) *Reservoir Geomechanics*. Cambridge: Cambridge University Press. doi: DOI: 10.1017/CBO9780511586477.

# Appendix A: Flowchart

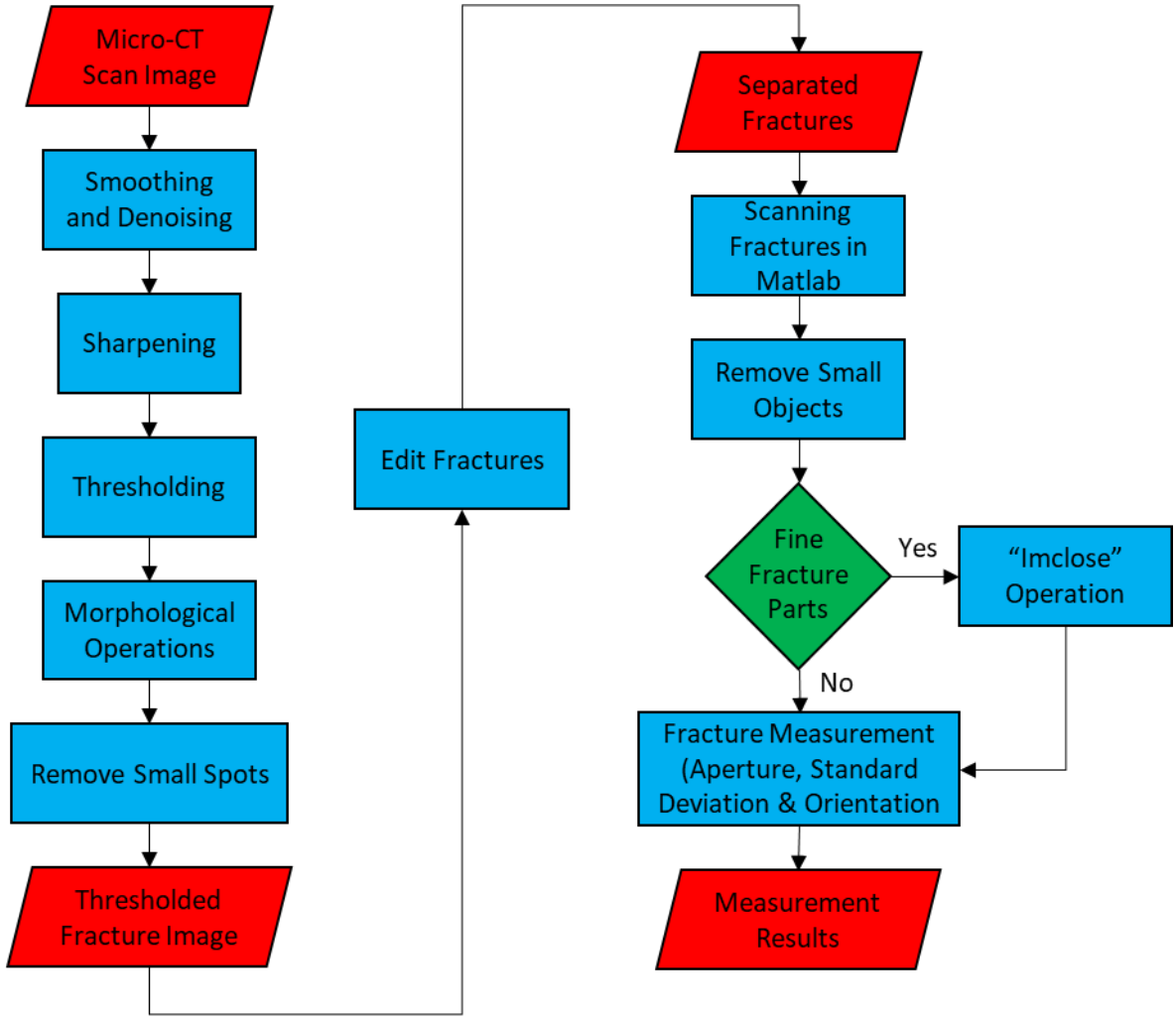


*Figure 42. Flowchart for image analysis of the samples using Avizo and Matlab.*

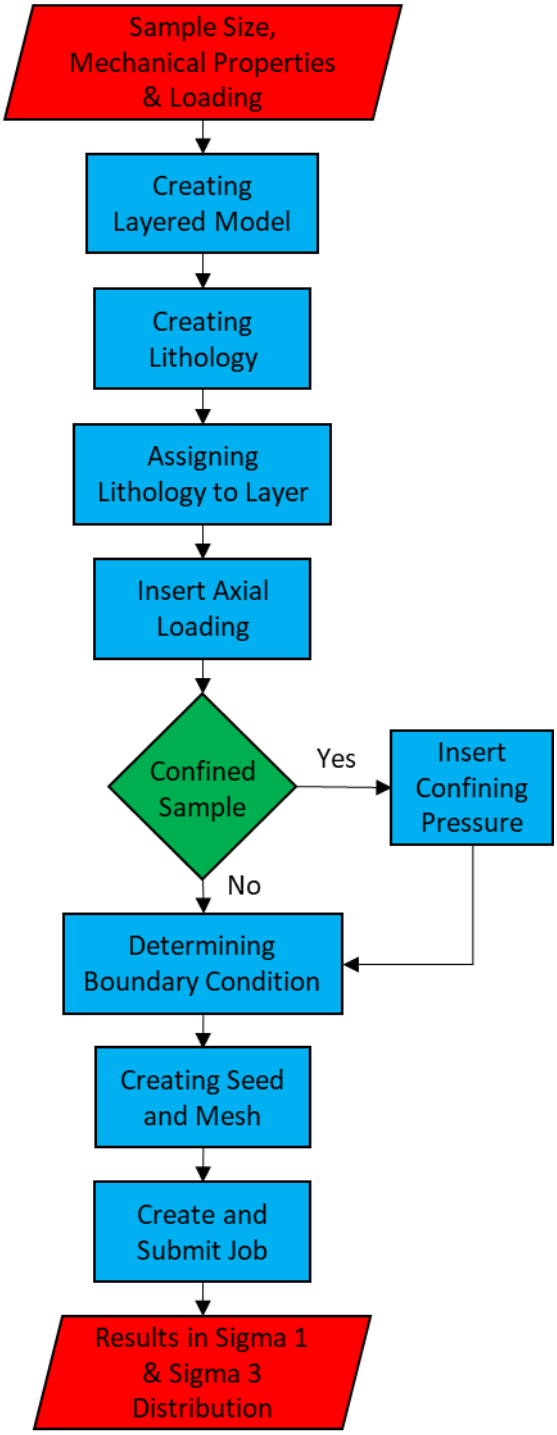


*Figure 43. Flowchart for Abaqus modeling of the samples.*

# Appendix B: Image Analysis

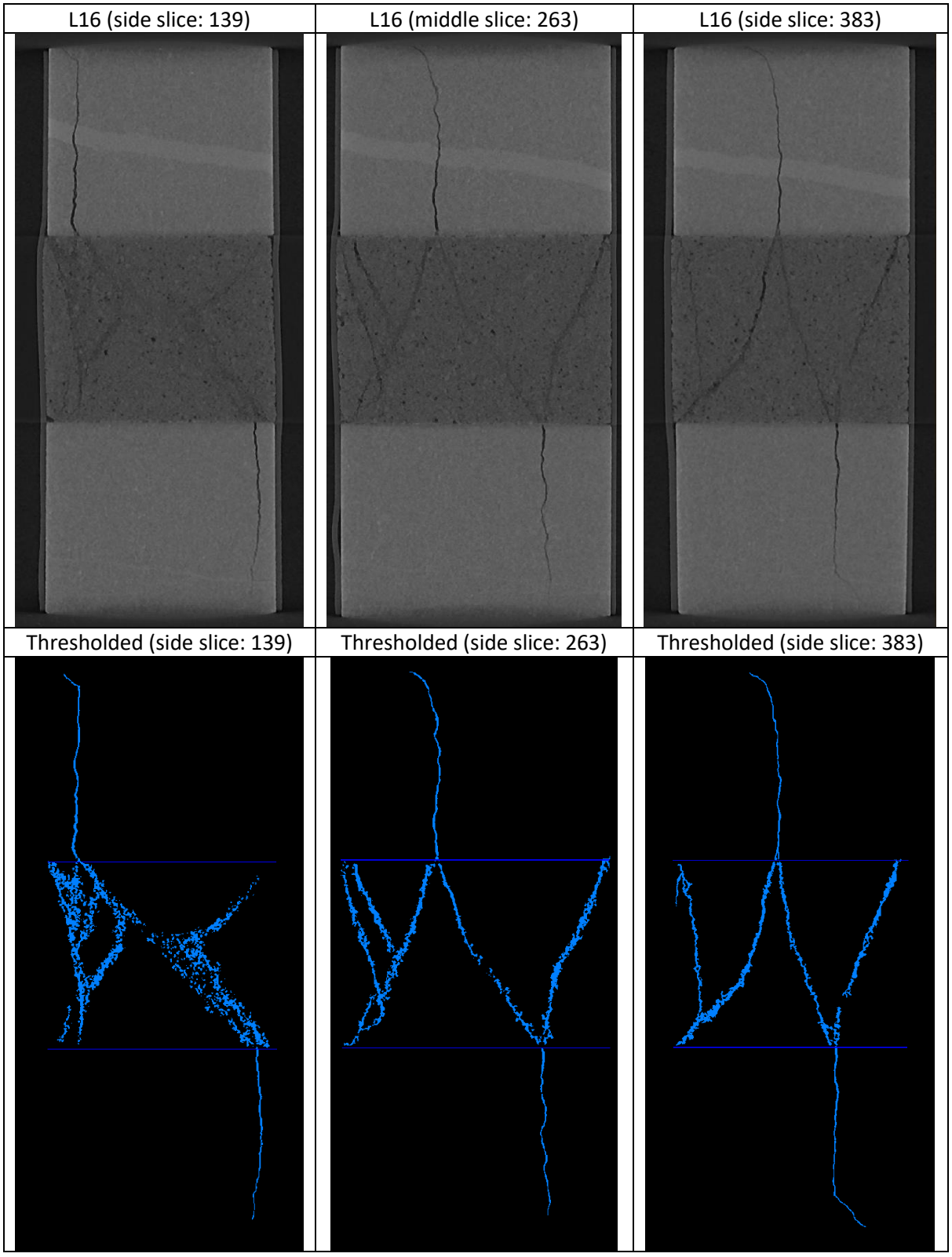


*Figure 44. Sample L16, consists of Ainsa sandstone (strong layer) – Bentheim sandstone (weak layer) – Ainsa sandstone (strong layer), generating 4.8 mechanical contrast in 0 MPa confining pressure.*

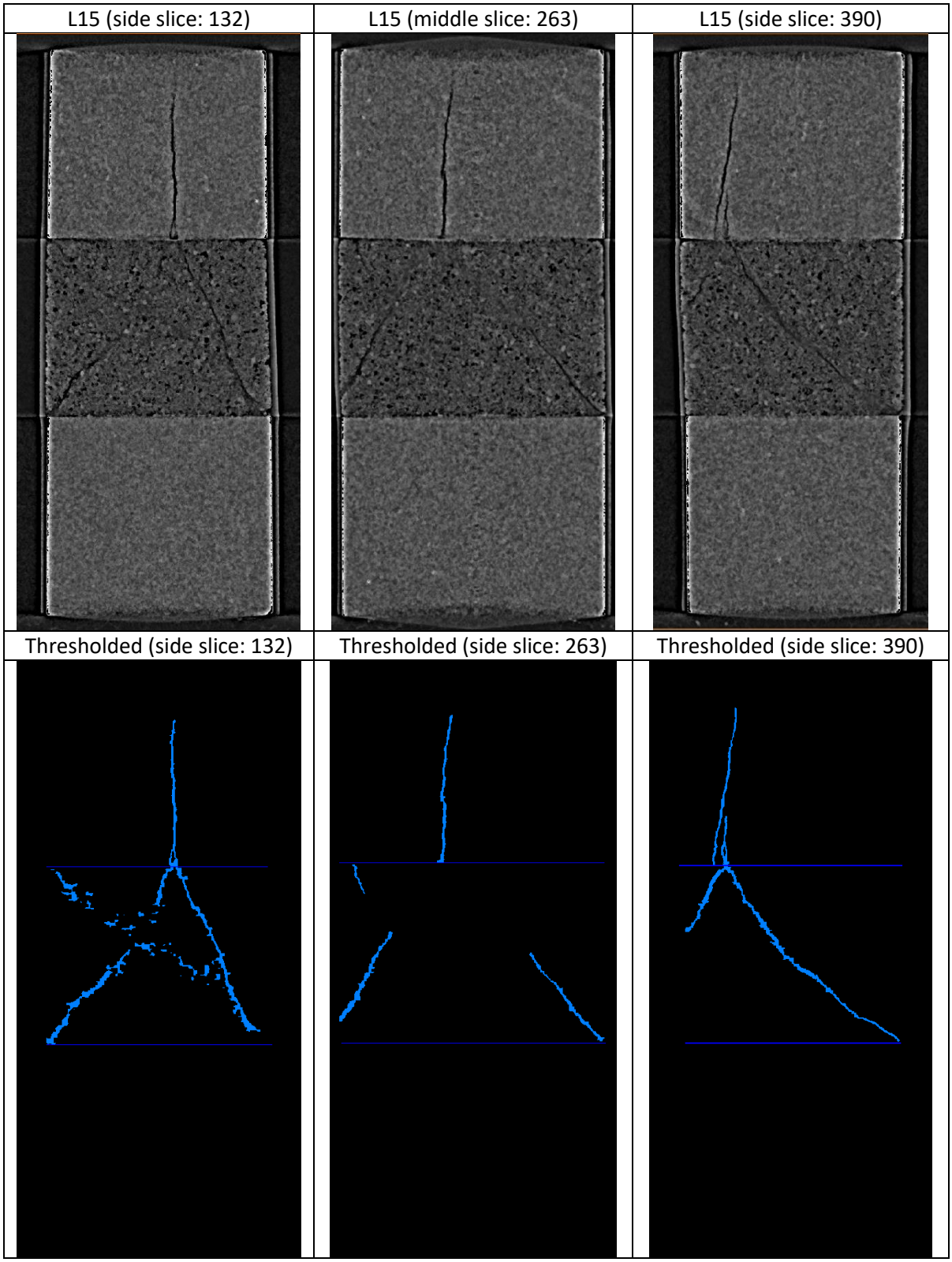


*Figure 45. Sample L15, consists of Ainsa sandstone (strong layer) – Bentheim sandstone (weak layer) – Ainsa sandstone (strong layer), generating 4.8 mechanical contrast in 15 MPa confining pressure.*

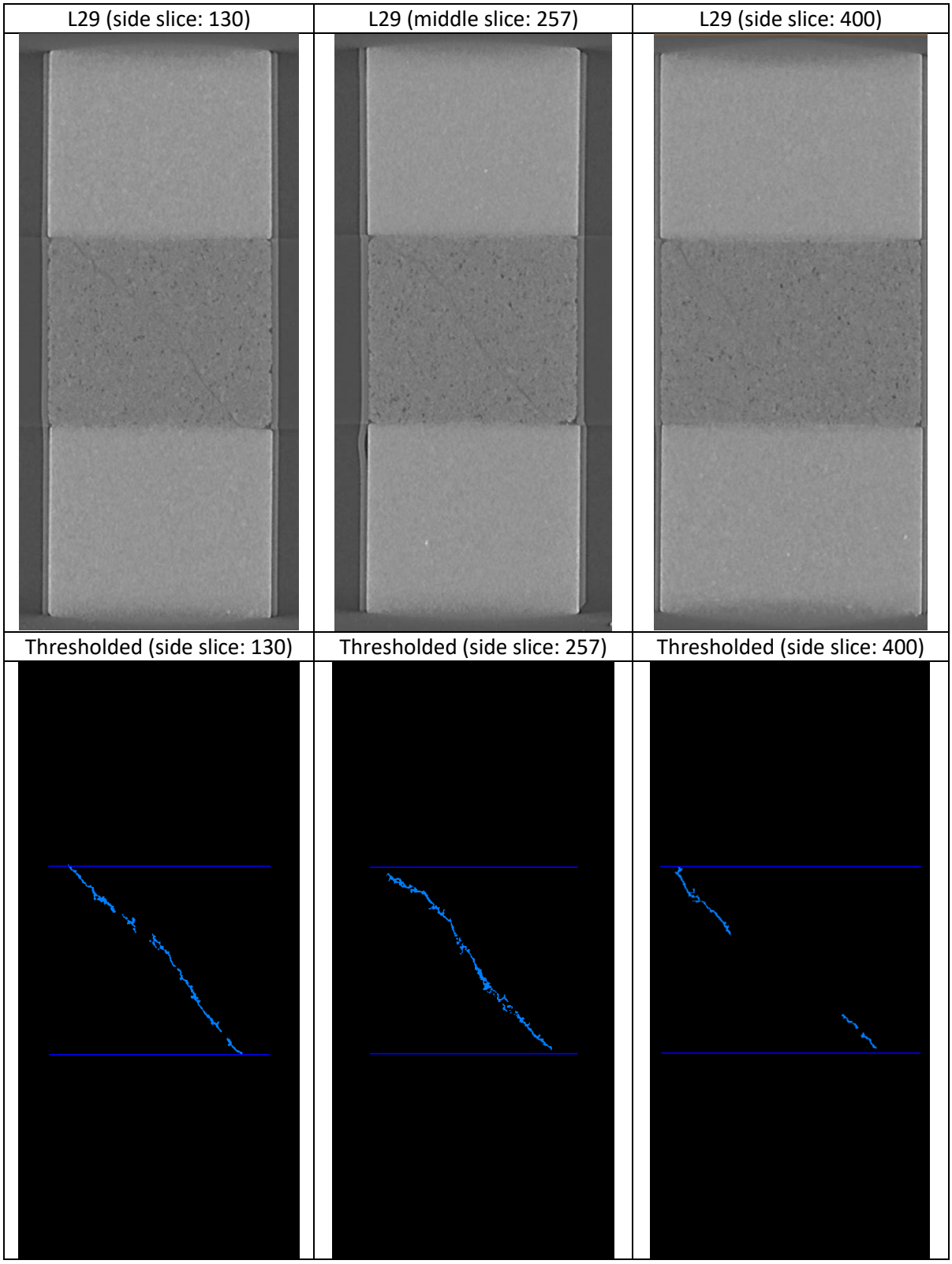


*Figure 46. Sample L29, consists of Ainsa sandstone (strong layer) – Bentheim sandstone (weak layer) – Ainsa sandstone (strong layer), generating 4.8 mechanical contrast in 30 MPa confining pressure.*

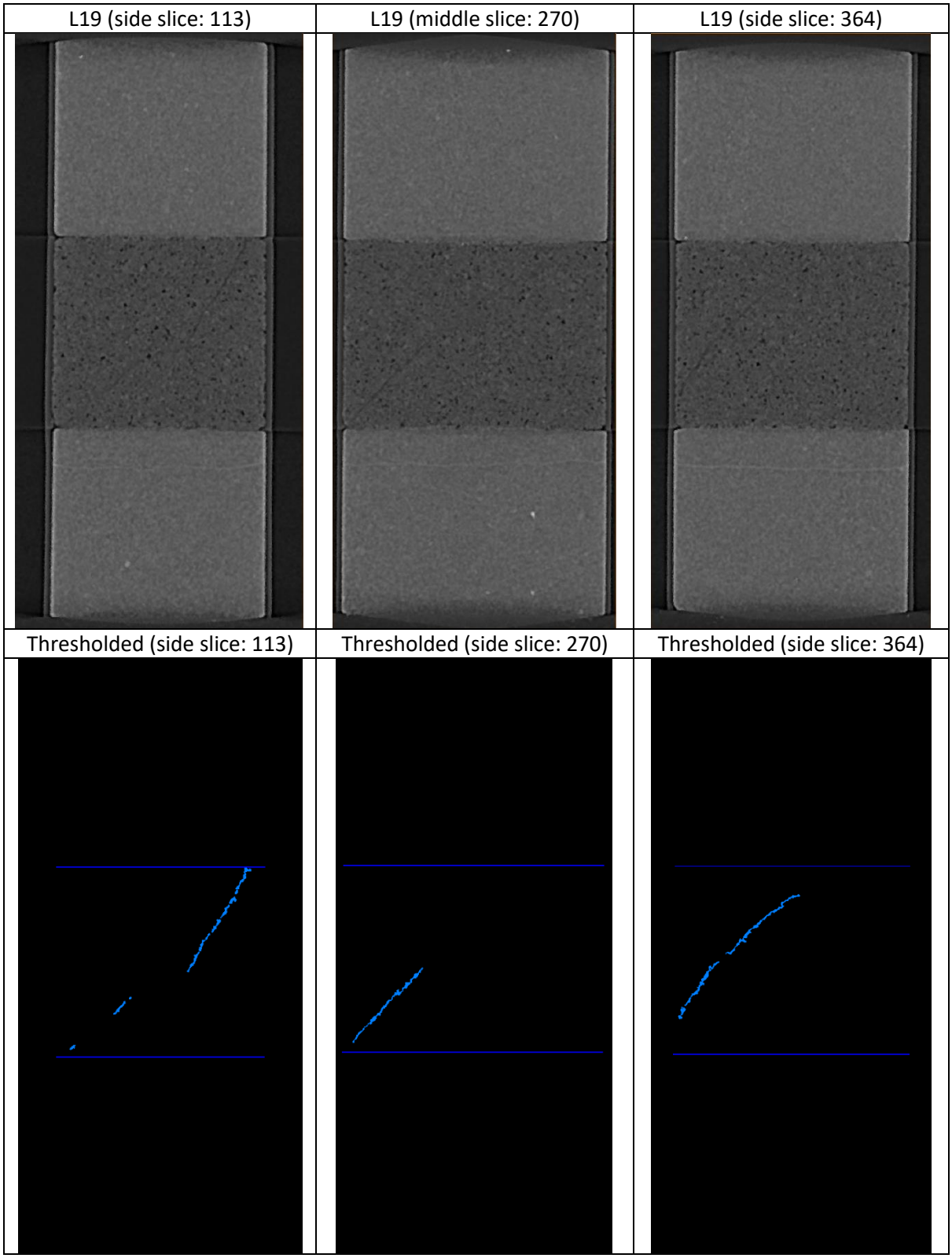


*Figure 47. Sample L19, consists of Ainsa sandstone (strong layer) – Bentheim sandstone (weak layer) – Ainsa sandstone (strong layer), generating 4.8 mechanical contrast in 40 MPa confining pressure.*

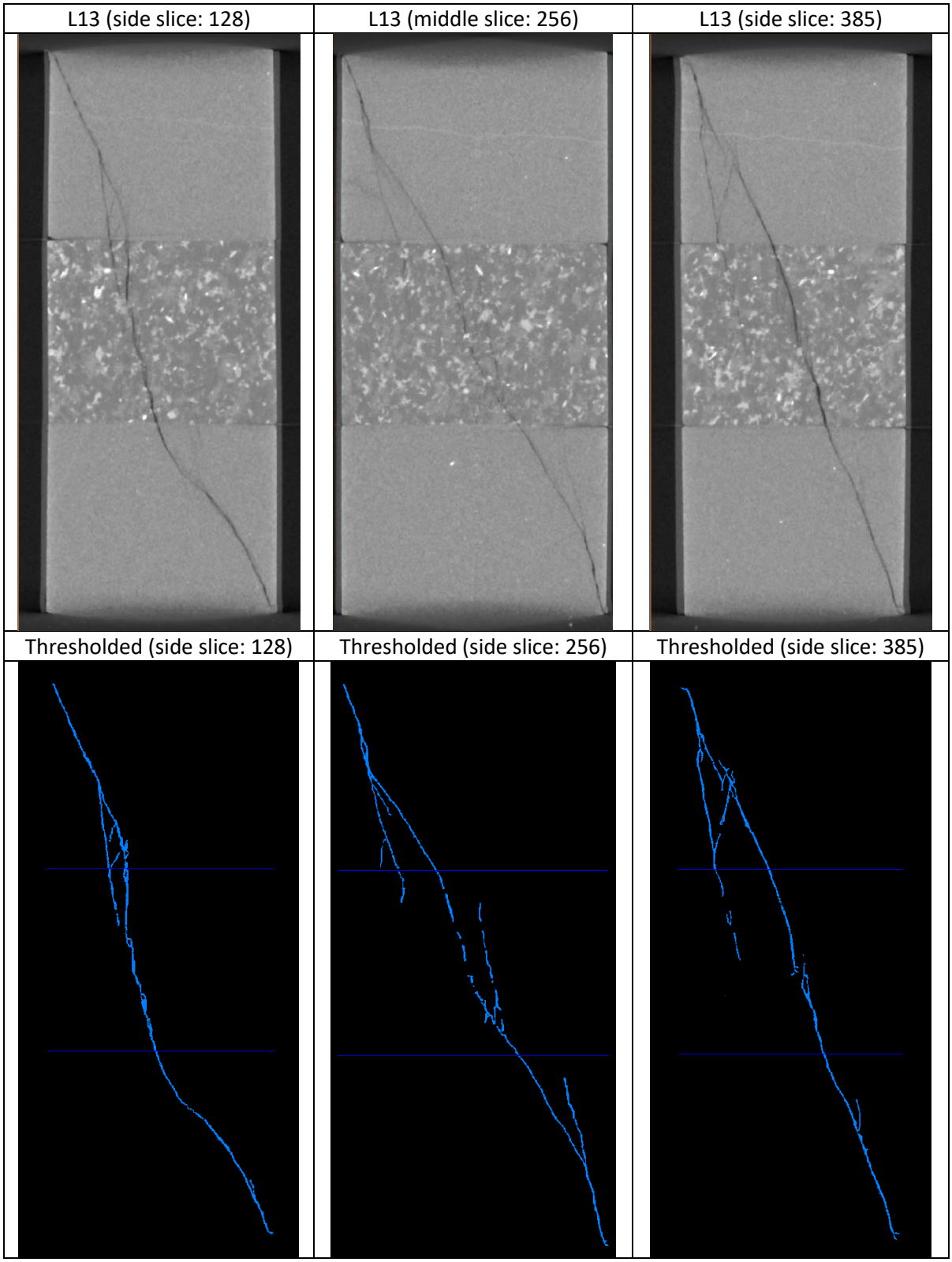


*Figure 48. Sample L13, consists of Ainsa sandstone (weak layer) – Benin granite (strong layer) – Ainsa sandstone (weak layer), generating 1.1 mechanical contrast in 15 MPa confining pressure.*

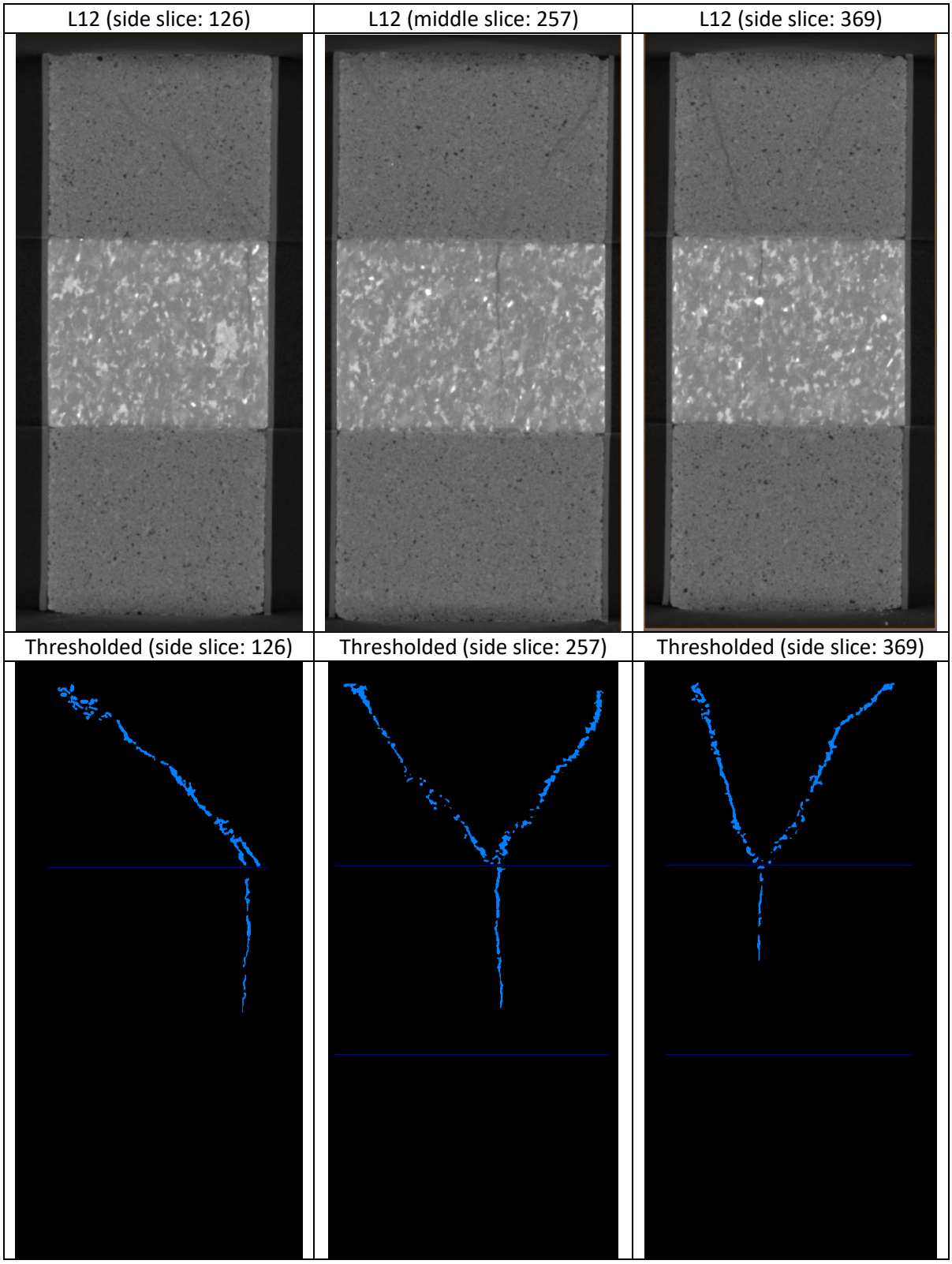


*Figure 49. Sample L12, consists of Bentheim sandstone (weak layer) – Benin granite (strong layer) – Bentheim sandstone (weak layer), generating 5.2 mechanical contrast in 15 MPa confining pressure.*

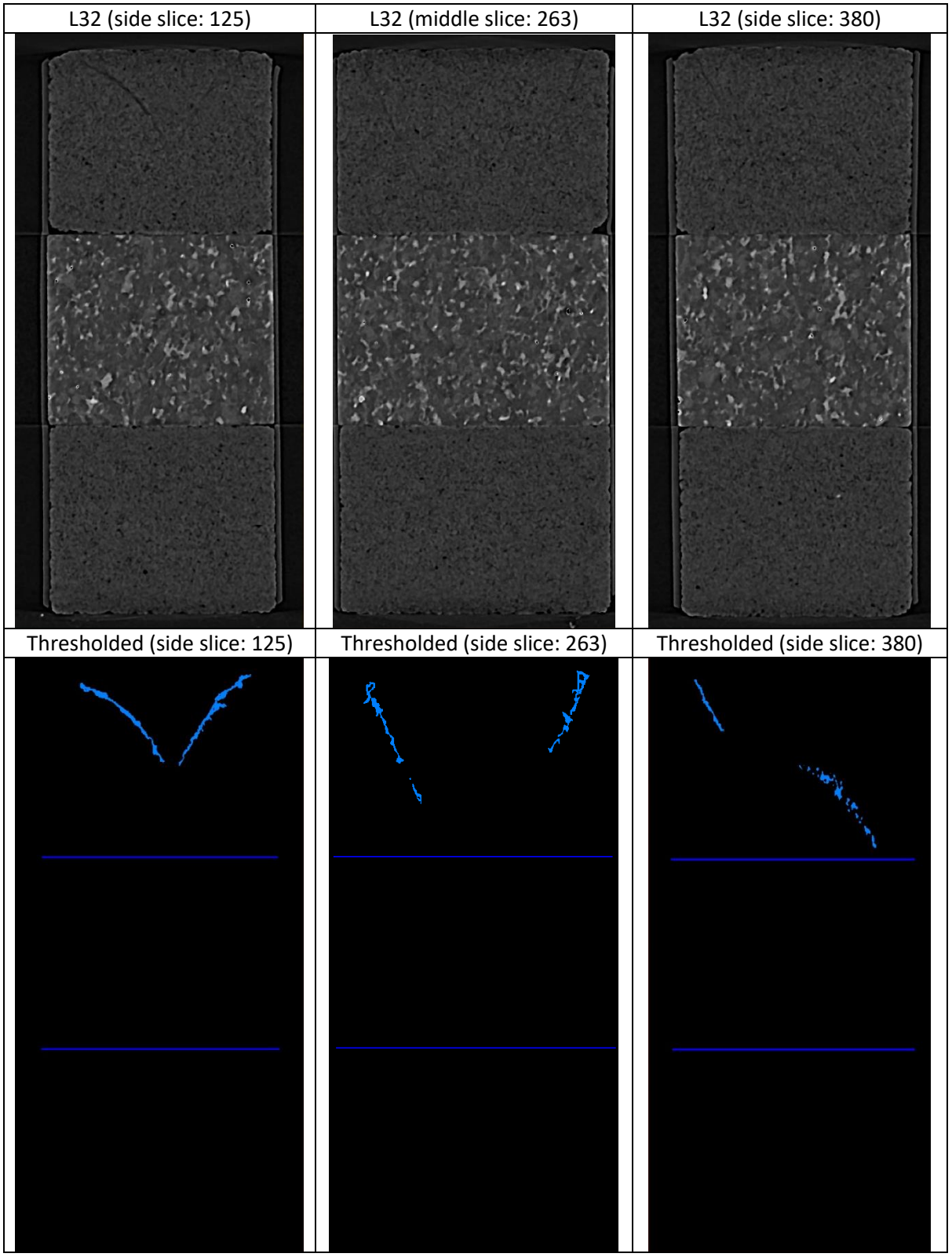


*Figure 50. Sample L32, consists of Red Felser sandstone (weak layer) – Benin granite (strong layer) – Red Felser sandstone (weak layer), generating 7.1 mechanical contrast in 15 MPa confining pressure.*

*Table 8. Aperture, standard variation and orientation measurement results and averaging from all three slices in each sample from increasing confining pressure group.*

| **Sample Name** | | **L16** | | | **L15** | | | **L29** | | | **L19** | | |
|---|---|---|---|---|---|---|---|---|---|---|---|---|---|
| **Confining Pressure** | | **0 MPa** | | | **15 MPa** | | | **30 MPa** | | | **40 MPa** | | |
| **Mechanical Contrast** | | **4.8** | | | | | | | | | | | |
| Aperture | Strong Layer 1 | 0.163 | 0.178 | 0.147 | 0.202 | 0.241 | 0.202 | | | | | | |
| | Average | 0.163 | | | 0.215 | | | | | | | | |
| | Weak Layer | 0.392 | 0.331 | 0.321 | 0.318 | 0.279 | 0.297 | 0.243 | 0.204 | 0.281 | 0.229 | 0.204 | 0.228 |
| | Average | 0.348 | | | 0.298 | | | 0.243 | | | 0.220 | | |
| | Strong Layer 2 | 0.131 | 0.155 | 0.154 | | | | | | | | | |
| | Average | 0.147 | | | | | | | | | | | |
| Standard Variation (Aperture) | Strong Layer 1 | 0.033 | 0.030 | 0.033 | 0.030 | 0.043 | 0.059 | | | | | | |
| | Average | 0.032 | | | 0.044 | | | | | | | | |
| | Weak Layer | 0.162 | 0.098 | 0.098 | 0.064 | 0.091 | 0.072 | 0.062 | 0.040 | 0.095 | 0.044 | 0.032 | 0.047 |
| | Average | 0.119 | | | 0.076 | | | 0.066 | | | 0.041 | | |
| | Strong Layer 2 | 0.040 | 0.033 | 0.044 | | | | | | | | | |
| | Average | 0.039 | | | | | | | | | | | |
| Orientation | Strong Layer 1 | 78.38 | 76.68 | 78.71 | 85.78 | 84.77 | 82.87 | | | | | | |
| | Average | 77.92 | | | 84.47 | | | | | | | | |
| | Weak Layer | 65.15 | 66.10 | 71.31 | 59.54 | 58.74 | 49.44 | 48.15 | 43.76 | 46.18 | 56.06 | 48.89 | 45.28 |
| | Average | 67.52 | | | 55.91 | | | 46.03 | | | 50.07 | | |
| | Strong Layer 2 | 87.17 | 80.39 | 77.70 | | | | | | | | | |
| | Average | 81.76 | | | | | | | | | | | |

*Table 9. Aperture, standard variation and orientation measurement results and averaging from all three slices in each sample from increasing mechanical contrast group.*

| **Sample Name** | | **L13 (AIN-GRA-AIN)** | | | **L15 (AIN-BNT-AIN)** | | | **L12 (BNT-GRA-BNT)** | | | **L32 (RF-GRA-RF)** | | |
|---|---|---|---|---|---|---|---|---|---|---|---|---|---|
| **Mechanical Contrast** | | **1.1** | | | **4.8** | | | **5.2** | | | **7.1** | | |
| **Confining Pressure** | | **15 MPa** | | | | | | | | | | | |
| Aperture | Weak Layer 1 | 0.175 | 0.145 | 0.174 | 0.318 | 0.279 | 0.297 | 0.329 | 0.377 | 0.355 | 0.363 | 0.376 | 0.355 |
| | Average | 0.165 | | | 0.298 | | | 0.354 | | | 0.365 | | |
| | Strong Layer | 0.203 | 0.159 | 0.165 | 0.202 | 0.241 | 0.202 | 0.196 | 0.204 | 0.188 | | | |
| | Average | 0.176 | | | 0.215 | | | 0.196 | | | | | |
| | Weak Layer 2 | 0.174 | 0.158 | 0.185 | | | | | | | | | |
| | Average | 0.172 | | | | | | | | | | | |
| Standard Variation (Aperture) | Weak Layer 1 | 0.030 | 0.033 | 0.040 | 0.064 | 0.091 | 0.072 | 0.075 | 0.111 | 0.070 | 0.115 | 0.167 | 0.090 |
| | Average | 0.034 | | | 0.076 | | | 0.086 | | | 0.124 | | |
| | Strong Layer | 0.052 | 0.028 | 0.043 | 0.030 | 0.043 | 0.059 | 0.058 | 0.049 | 0.028 | | | |
| | Average | 0.041 | | | 0.044 | | | 0.045 | | | | | |
| | Weak Layer 2 | 0.026 | 0.023 | 0.030 | | | | | | | | | |
| | Average | 0.026 | | | | | | | | | | | |
| Orientation | Weak Layer 1 | 73.16 | 67.62 | 73.75 | 59.54 | 58.74 | 49.44 | 48.44 | 58.38 | 60.95 | 44.17 | 68.26 | 58.02 |
| | Average | 71.51 | | | 55.91 | | | 55.92 | | | 56.81 | | |
| | Strong Layer | 82.81 | 74.35 | 77.66 | 85.78 | 84.77 | 82.87 | 86.33 | 84.29 | 86.53 | | | |
| | Average | 78.27 | | | 84.47 | | | 85.72 | | | | | |
| | Weak Layer 2 | 57.83 | 68.85 | 71.12 | | | | | | | | | |
| | Average | 65.94 | | | | | | | | | | | |

# Appendix C: Samples Modeling

| (a) L16 (CP: 0 MPa) | (b) L15 (CP: 15 MPa) | (c) L29 (CP: 30 MPa) | (d) L19 (CP: 40 MPa) | Colorbar |
|---|---|---|---|---|
| Increasing confining pressure | | | | |
| 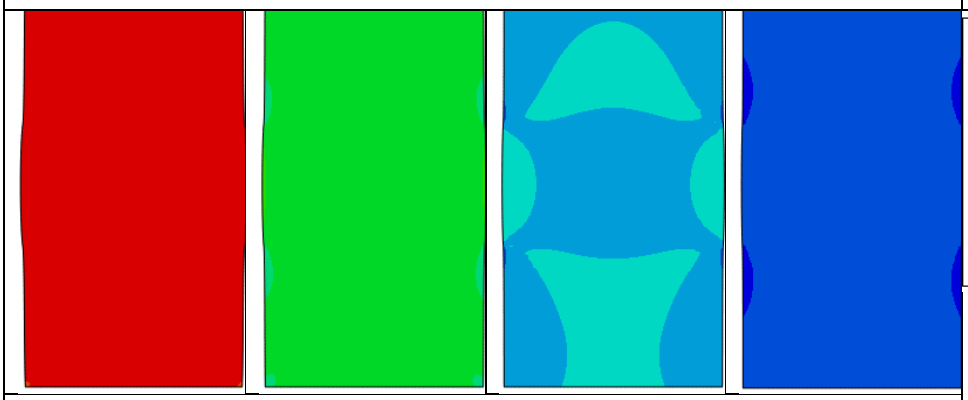 | | | | 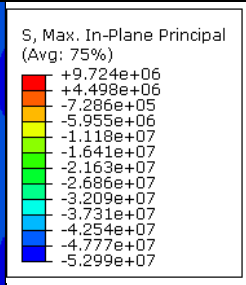 |
| Mechanical Contrast: 4.8 | | | | |
| AIN-BNT-AIN | | | | |
| Sigma 1 -63.1 – 31.9 MPa | Sigma 1 -183.8 – 134.3 MPa | Sigma 1 -215.7 – -180.3 MPa | Sigma 1 -240 – -207.4 MPa | |



*Figure 51. Sigma 1 distribution model of the samples with increasing confining pressure. CP is confining pressure, AIN is Ainsa sandstone and BNT is Bentheim sandstone. The tensile stress only presence in figure (a) and (b), which shown in Sigma 1 range at the bottom part of the table.*

| (a) L13 (MC: 1.1) | (b) L15 (MC: 4.8) | © L12 (MC: 5.2) | (d) L32 (MC: 7.1) | Colorbar |
|---|---|---|---|---|
| Increasing mechanical contrast | | | | |
| 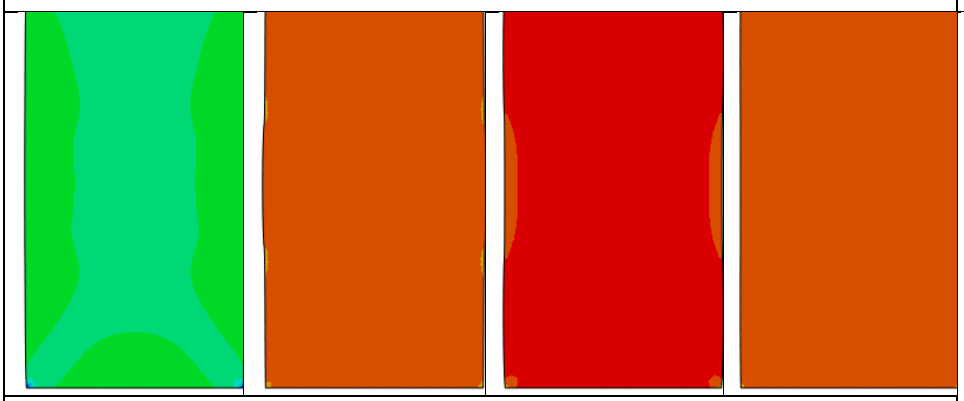 | | | | 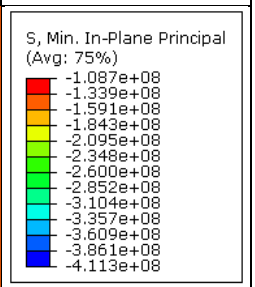 |
| 15 MPa Confining Pressure | | | | |
| AIN-GRA-AIN | AIN-BNT-AIN | BNT-GRA-BNT | RF-GRA-RF | |
| Sigma 1 -411.3 – -248.6MPa | Sigma 1 -183.8 – 134.3 MPa | Sigma 1 -185.8 – 108.7 MPa | Sigma 1 -170 – -142.7MPa | |



*Figure 52. Sigma 1 distribution model of samples with increasing mechanical contrast. MC is mechanical contrast, AIN is Ainsa sandstone, GRA is Benin granite, BNT is Bentheim sandstone and RF is Red Felser sandstone. The tensile stress only presence in figure (b) and (c), which shown in Sigma 1 range at the bottom part of the table.*

| (a) L16 (CP: 0 MPa) | (b) L15 (CP: 15 MPa) | (c) L29 (CP: 30 MPa) | (d) L19 (CP: 40 MPa) | Colorbar |
|---|---|---|---|---|
| Increasing confining pressure | | | | |
| 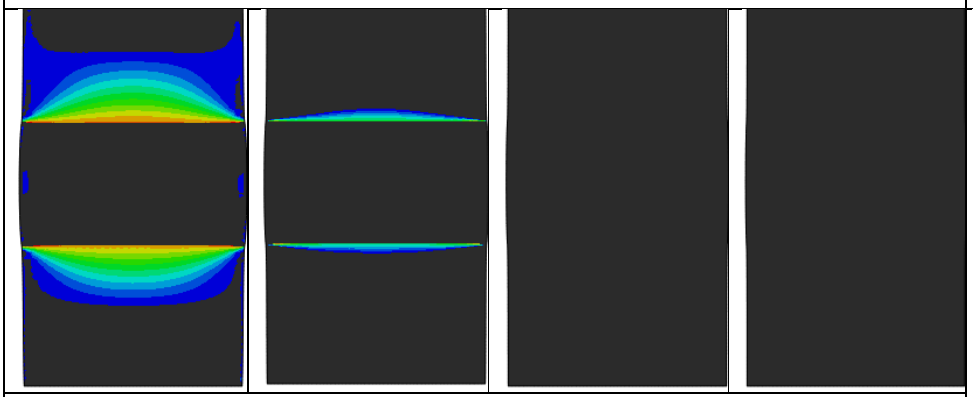 | | | | 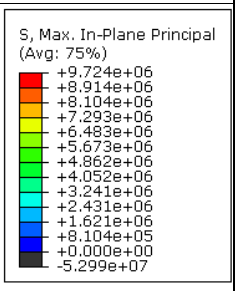 |
| Mechanical Contrast: 4.8 | | | | |
| AIN-BNT-AIN | | | | |
| Sigma 3 -8.39 – 9.72 MPa | Sigma 3 -30.2 – 8.52 MPa | Sigma 3 -44.1 – -8.1 MPa | Sigma 3 -53 – -20 MPa | |



*Figure 53. Tensile stresses distribution in Sigma 3 model of the samples with increasing confining pressure. CP is confining pressure, AIN is Ainsa sandstone and BNT is Bentheim sandstone. The tensile stress only presence in figure (a) and (b), which shown in Sigma 3 range at the bottom part of the table.*

| (a) L13 (MC: 1.1) | (b) L15 (MC: 4.8) | (c) L12 (MC: 5.2) | (d) L32 (MC: 7.1) | Colorbar |
|---|---|---|---|---|
| Increasing mechanical contrast | | | | |
| 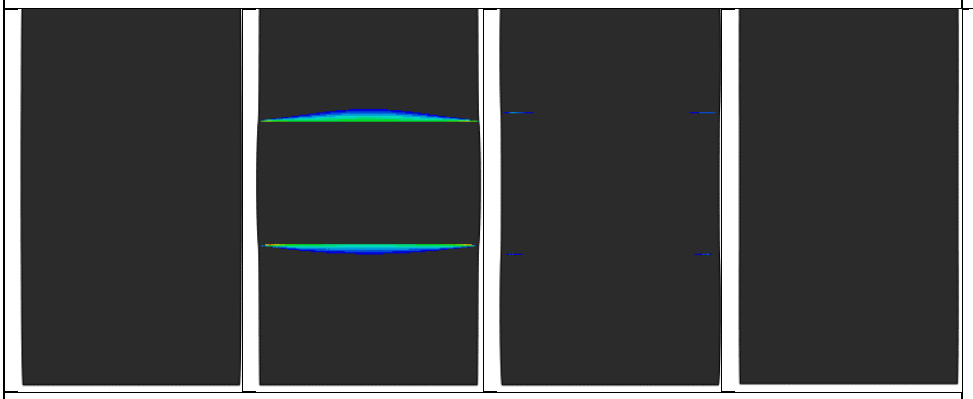 | | | | 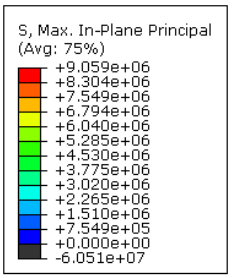 |
| 15 MPa Confining Pressure | | | | |
| AIN-GRA-AIN | AIN-BNT-AIN | BNT-GRA-BNT | RF-GRA-RF | |
| Sigma 3 -60.5 – -0.23MPa | Sigma 3 -30.2 – 8.52 MPa | Sigma 3 -38.4 – 3.41 MPa | Sigma 3 -23.3 – -11.7MPa | |



*Figure 54. Tensile stresses distribution in Sigma 3 model of samples with increasing mechanical contrast. MC is mechanical contrast, AIN is Ainsa sandstone, GRA is Benin granite, BNT is Bentheim sandstone and RF is Red Felser sandstone. The tensile stress only presence in figure (b) and (c), which shown in Sigma 3 range at the bottom part of the table.*

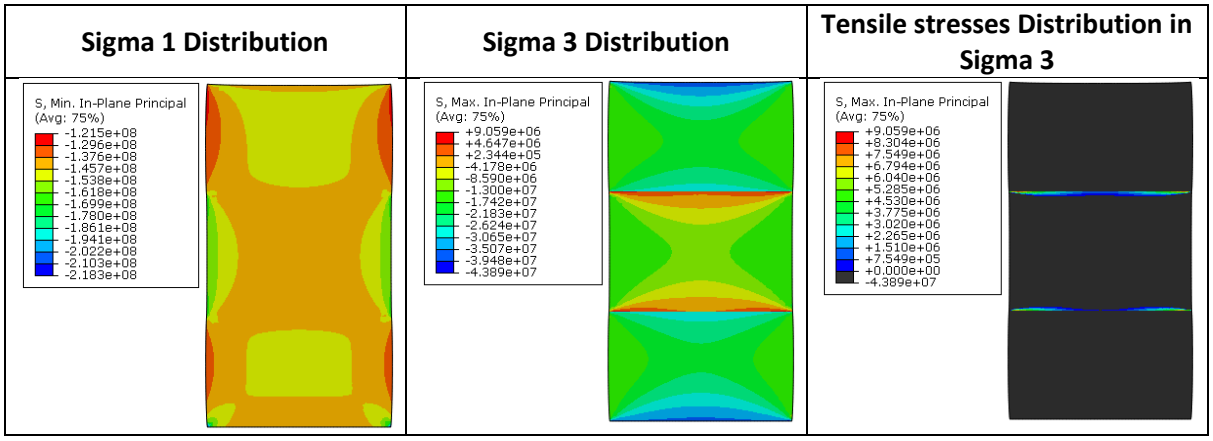


*Figure 55. Reversing the layers order in sample L15 model, consists of Bentheim sandstone (weak layer) – Ainsa sandstone (strong layer) – Bentheim sandstone (weak layer), generating 4.8 mechanical contrast in 15 MPa confining pressure. The tensile stresses still present in the strong layer.*

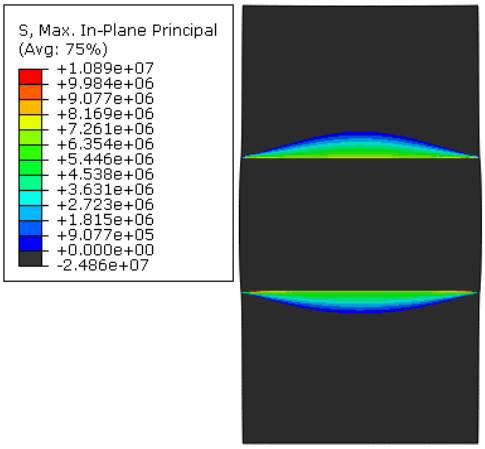


*Figure 56. Sample L17 model for confining pressure sensitivity study. Consists of Ainsa sandstone (strong layer) – Bentheim sandstone (weak layer) – Ainsa sandstone (strong layer), generating 4.8 mechanical contrast in 10 MPa confining pressure.*